MECHANISTIC ANALYSIS OF RADIATION-INDUCED GLIOMAGENESIS

APPROVED BY SUPERVISORY COMMITTEE

Sandeep Burma, Ph.D. (Mentor)
Associate Professor, Radiation Oncology

Robert M. Bachoo M.D, Ph.D. (Chairman)
Associate Professor

Pier P. Scaglioni, M.D
Associate Professor, Internal Medicine

Jerry W. Shay, PhD
Professor, Cell Biology

DEDICATION

To my family, for never letting me be satisfied with my achievements.

MECHANISTIC ANALYSIS OF RADIATION-INDUCED GLIOMAGENESIS

by

PAVLINA KRASIMIROVA TODOROVA

DISSERTATION

Presented to the Faculty of the Graduate School of Biomedical Sciences

The University of Texas Southwestern Medical Center at Dallas

In Partial Fulfillment of the Requirements

For the Degree of

DOCTOR OF PHILOSOPHY

The University of Texas Southwestern Medical Center at Dallas

Dallas, Texas

August, 2017

ACKNOWLEDGEMENTS

First and foremost, I would like to acknowledge my Ph.D. mentor, Dr. Sandeep Burma. My most sincere gratitude for providing me with the space and time to grow as a scientist. Thank you for always keeping me focused and pushing me forward when I lacked direction. I am leaving your lab as a better researcher, writer, public speaker, and team player.

I would like to acknowledge my thesis committee members, Drs. Robert Bachoo, Paolo Scaglioni, and Jerry Shay, who were instrumental in shaping this project. Thank you for your time, mentorship, and continual support throughout the years. I would also like to thank Drs. Ralf Kittler and Michael Story, and their lab members for accommodating my many requests. I am grateful for the support provided by Drs. Peter Guida and Adam Rusek, and the team at the Brookhaven National Laboratory throughout all the runs.

A big thank you to all former and present members of the Burma lab, who have been essential in creating an amazing environment to do science and build friendships. I would like to acknowledge Dr. Cristel Camacho, who laid the foundations, on which this thesis is build, and taught me the skill set to succeed. Thank you also to Dr. Bipasha Mukherjee, for all your help carrying out experiments at BNL, as well as for polishing my written and oral presentation skills.

Finally, I would like to thank all my friends and family who have always supported me and believed in my potential, even when I lacked the confidence.

MECHANISTIC ANALYSIS OF RADIATION-INDUCED GLIOMAGENESIS

Pavlina Krasimirova Todorova, B.A.

The University of Texas Southwestern Medical Center at Dallas, 2017

Supervising Professor: Sandeep Burma, Ph.D.

Glioblastomas (GBM) are devastating brain tumors refractory to any available treatment. Exposure to ionizing radiation (IR) is the only known GBM risk factor. The link between low-linear energy transfer (LET) IR and gliomagenesis has been clearly demonstrated by epidemiological studies of human patients receiving diagnostic or therapeutic radiation. Whether such risk exists with particle radiation exposure, which is more densely ionizing, has not been evaluated. Particle radiation is increasingly used in radiotherapy and is also an occupational hazard for astronauts in space. With no human data

available, animal models mimicking the process of radiation carcinogenesis are essential for risk assessment. Through a large scale systematic interrogation of multi-allele transgenic mice with brain-restricted deletions of GBM-relevant tumor suppressor genes we identified two complementary genotypes ($^{NesCre}Ink4ab^{-/-}Arf^{F/F}$ and $^{NesCre}p53^{+/F};Pten^{+/F}$). We irradiated both models intra-cranially with equal doses of a range of charged particles with different LETs. Interestingly, we found an increase in gliomagenesis with LET until a peak frequency was reached with silicon ions (LET of 79.3 KeV/μm) following which tumor frequencies declined with heavier particles with higher LETs. These radiation-induced mouse tumors phenocopy the histopathological features of human GBM, including infiltrative growth, pseudopalisading necrosis, high mitotic index, and positivity for glial (Gfap, Olig2) and stem/progenitor markers (Sox2). Ex-vivo cultures derived from these tumors showed features of glioma stem-like cells underscoring the undifferentiated nature of the parental tumors. Integrated genomic and functional analyses revealed the driving oncogenic changes in tumors from the $^{NesCre}p53^{+/F};Pten^{+/F}$ model. Regardless of radiation quality, all tumors had genomic deletions of the wild-type alleles of both p53 and Pten. Such concomitant loss signifies the crucial roles that p53 and Pten together play as barriers to radiation-induced transformation. Over-expression of the receptor tyrosine kinase Met following a genomic amplification event harbored by 40% of tumors was similarly observed across all radiation qualities. Met overexpression enhanced the stemness phenotype in the context of p53 loss, and additionally conferred radioresistance. These combinatorial effects illustrate the importance of evaluating GBM drivers as integrated nodes in an oncogenic signaling network. In sum, the identification of two mouse models carrying deletions of independent

TSGs has allowed us to establish the universal role of radiation as a genotoxic agent capable of inducing high grade gliomas. These models and the identified key molecular changes accompanying radiation-induced gliomagenesis can be used in the design of therapeutic strategies for patients with secondary glioma who are currently limited in their options.

TABLE OF CONTENTS

PUBLICATIONS

Camacho, C. V., Todorova, P. K., Hardebeck, M. C., Tomimatsu, N., Gil del Alcazar, C. R., Ilcheva, M., . . . Burma, S. (2015). DNA double-strand breaks cooperate with loss of Ink4 and Arf tumor suppressors to generate glioblastomas with frequent Met amplification. *Oncogene, 34*(8), 1064-1072. doi:10.1038/onc.2014.29

Gil Del Alcazar, C. R., Todorova, P. K., Habib, A. A., Mukherjee, B., & Burma, S. (2016). Augmented HR Repair Mediates Acquired Temozolomide Resistance in Glioblastoma. *Mol Cancer Res, 14*(10), 928-940. doi:10.1158/1541-7786.MCR-16-0125

Mukherjee, B., Todorova, P. K., & Burma, S. (2015). Mouse models of radiation-induced glioblastoma. *Oncoscience, 2*(12), 934-935. doi:10.18632/oncoscience.278

Todorova, P. K., Mukherjee, B., & Burma, S. (2017). MET signaling promotes DNA repair and radiation resistance in glioblastoma stem-like cells. *Ann Transl Med, 5*(3), 61. doi:10.21037/atm.2017.01.67

Todorova, P. K., Fletcher, E. S., Mukherjee, B., Burma, S. Cooperativity between p53 and Pten haplo-insufficiencies in the initiation and progression of radiation-induced glioblastomas. [Manuscript in preparation]

LIST OF FIGURES

LIST OF TABLES

LIST OF APPENDICES

LIST OF ABBREVIATIONS

53BP1- Tumor protein p53 binding protein 1; also TP53BP1

aCGH – Array comparative genomic hybridization

AKT – AKT serine/threonine kinase 1

ALL - acute lymphocytic leukemia

ATM – Ataxia Telangiectasia Mutated, Serine/Threonine kinase

ATR – ATM and Rad3 related protein

BAX – BCL2 Associated X, Apoptosis Regulator

BNL – Brookhaven National Laboratory

bp – base pairs

BRAF – B-Raf proto-oncogene, serine/threonine kinase

C - Carbon

CDK4 – Cyclin dependent kinase 4

CDK6 – Cyclin dependent kinase 6

CDKN2A – Cyclin dependent kinase inhibitor 2A; also $p16^{INK4A}$

CDKN2B – Cyclin Dependent Kinase Inhibitor 2B; also $p15^{INK4B}$

CDKN2C – Cyclin Dependent Kinase Inhibitor 2C; also $p18^{INK4C}$

CHK1 – Checkpoint kinase 1; also CHEK1

CHK2 – Checkpoint kinase 2; also CHEK2

Chr – Chromosome

CT – Computerized tomography

DDR – DNA damage response

DNA – deoxyribonucleic acid

DNA-PK – Protein Kinase, DNA-Activated, Catalytic Polypeptide

ECM – Extracellular matrix

EGFR – Epidermal growth factor receptor

ERK1/2 - Mitogen activated protein kinase; also MAPK

FAK – Focal adhesion kinase

Fe - Iron

FGFR – Fibroblast growth factor receptor

GBM – Glioblastoma multioforme

GCR – Galactic cosmic radiation

GFAP – Glial fibrillary acidic protein

GL – glioma cell line grown as a tumor neurosphere culture

GPSCs – Glioma-propagating stem-like cells

H – hydrogen, also proton

H&E – Hematoxylin and eosin

HR – Homologous recombination

HZE - High charge (Z) and Energy (E)

IDH1 – Isocitrate dehydrogenase 1 (NADP(+)) 1

IHC – Immunohistochemistry

iPS – Induced pluripotent stem (cells)

IR – Ionizing radiation

kV – Kilovolt

LET – Linear energy transfer

Ne - Neon

NF1 – Neurofibromin 1

NHEJ – Non-homologous end joining

MAPK – Mitogen activated protein kinase; also ERK1/2

MDM2 – Murine double minute; also HDM2

MDM4 – Transformed mouse 3T3 cell double minute 4; also MDMX, HDMX

MET – Hepatocyte growth factor receptor

MeV/n – Mega electron-volt per nucleon

MGMT – 6-O-methylguanine-DNA methyltransferase

mRNA – messenger RNA

mTOR – Mammalian target of rapamycin

NOXA - Phorbol-12-Myristate-13-Acetate-Induced Protein 1; also PMAIP1

$p14^{ARF}$ – Alternative reading frame; $p19^{Arf}$ in the mouse

p21 - Cyclin Dependent Kinase Inhibitor 1A; also CDKN1A

PCR – Polymerase chain reaction

PDGFRA – Platelet derived growth factor receptor alpha

PI3K – Phosphatidylinositol 3-kinase

PIP2 – Phosphatidylinositol-4,5-biphosphate

PIP3 – Phosphatidylinositol-3,4,5-triphosphate

PTB – phospho-tyrosine binding

PTEN – Phosphatase and tensin homolog

PUMA – BCL2 binding component 3; also BBC3

qPCR – Quantitative PCR; also real-time PCR

RAS – Rat sarcoma virus oncogene

RB – Retinoblastoma

RB1 – RB transcriptional corepressor 1

RIG – Radiation induced glioma

RNA – ribonucleic acid

RT – Radiotherapy

RT-PCR – Reverse transcription PCR

RTK – receptor tyrosine kinase

S6 – Ribosomal protein S6, also RPS6

SD – Standard deviation

SH2 – Src homology 2

Si - Silicon

SPE – Solar particle event

STATs – Signal transducers and activators of transcription

TCGA – The Cancer Genome Atlas Network

Ti - Titanium

TP53 – Tumor protein 53; also p53, Trp53 (mus musculus)

TSG – Tumor suppressor gene

Z – Atomic number

CHAPTER I

Introduction

Glioblastoma multiforme is the most aggressive primary brain tumor

Malignant gliomas are the most common primary tumors of the adult central nervous system. The annual incidence of malignant glioma in the USA is approximately 6 per 100,000 individuals (Ostrom et al., 2015; Reifenberger, Wirsching, Knobbe-Thomsen, & Weller, 2016) Although the median age at diagnosis is 64 years, these aggressive, therapy-resistant tumors also occur in children, making them a leading cause of cancer-related deaths in both adult and pediatric patients (International Cancer Genome Consortium PedBrain Tumor, 2016; Stiles & Rowitch, 2008). Grade IV glioma, also known as glioblastoma multioforme (GBM), is classified histopathologically by the presence of mitotic figures, cellular atypia, pseudopalisading necrosis, and diffuse infiltration into the surrounding brain parenchyma (Aldape, Zadeh, Mansouri, Reifenberger, & von Deimling, 2015; David N. Louis et al., 2014). The majority of GBMs (90%) occur "de novo", in the absence of clinical, radiological, or histopathological evidence of a low-grade precursor tumor (Ohgaki & Kleihues, 2007). Most patients have a clinical history of less than 3 months, and an average survival of less than 2 years, despite aggressive therapy regimens. Very little is known about the pathological progression of these cancers or what causes them. The remaining 10% of cases represent "secondary" GBMs developing from less malignant lesions over the course of 5-7 years (Ohgaki & Kleihues, 2007). Regardless of clinical presentation, however, GBM remains incurable, and thus presents a major challenge for basic and translational science.

GBMs share a common genomic landscape

Traditionally, glial tumors have been classified based on a set of histopathological characteristics and cell morphology (e.g. astrocytoma versus oligodendroglioma). The recent onco-omics revolution, commenced by the comprehensive sequencing of the glioma genome by The Cancer Genome Atlas Network (TCGA), has revealed distinct mutational landscapes for all major types of adult and pediatric gliomas (Reifenberger et al., 2016). These genome and transcriptome studies have identified common, non-overlapping patterns of abnormalities, leading to the classification of high-grade glioma into molecular subtypes with distinct clinical relevance (Frattini et al., 2013) (Brennan et al., 2013; Cancer Genome Atlas Research, 2008; Verhaak et al., 2010). For example, although most Grade III/IV gliomas have consistent aberrations in the receptor tyrosine kinase (RTK), TP53, and retinoblastoma (RB) pathways **(Fig. 1.1)**, the specific genes affected stratify them as Proneural (*PDGFRA/IDH1*), Classical (*EGFR/CDKN2A*), Mesenchymal (*NF1*), or Neural (expressing neuronal markers) (Cancer Genome Atlas Research, 2008; Parsons et al., 2008; Verhaak et al., 2010). Additional biomarkers, like *IDH1/2* mutations or *MGMT*-promoter methylation have been shown to correlate with disease progression and response to alkylating therapy (Wick et al., 2014; Yan et al., 2009). Based on their proven reproducibility and predictive value, the most recent report by the World Health Organization strongly recommends the inclusion these omics features in an "integrated diagnosis" of diffuse glioma (D. N. Louis et al., 2016; Phillips et al., 2006).

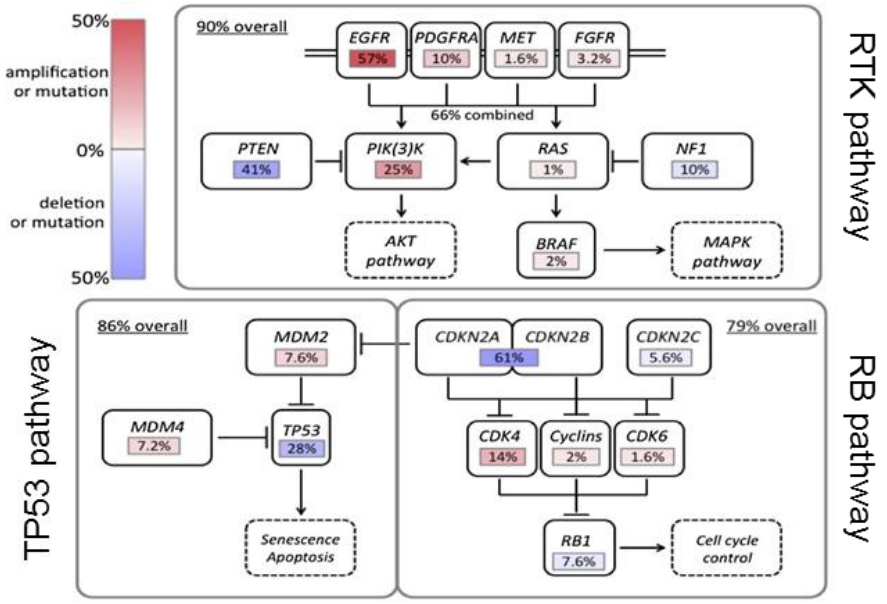

Figure 1.1. Oncogenes and tumor suppressors most commonly abrogated in GBM. Sequencing data from 251 human GBMs reveal consistent aberrations in the RTK, TP53, and RB pathways. Copy number gains are shown in red; deletions are shown in blue (Image modified from Brennan et al., 2013)

Receptor tyrosine kinases are the most frequently amplified genes in GBM

The comprehensive analysis of more than 500 glioma samples by the TCGA led to the identification of the most commonly abrogated proto-oncogenes: genes with pro-proliferative functions, hijacked by the cancer to drive uncontrolled growth, survival, and migration **(Fig. 1.1)**. Aberrant activation of RTKs plays a crucial role in gliomagenesis through the activation of the Phosphatidylinositol 3-kinase (PI3K) and Mitogen-activated protein kinase (MAPK) pathways (Snuderl et al., 2011). EGFR is the most commonly amplified RTK (57%), followed by PDGFRA (10%), FGFR (4%), and MET (1.6%). In addition to amplifications, these genes are often mutated to express constitutively active kinases (e.g. EGFR vIII mutant) or upregulated at the mRNA or protein level without underlying copy number gains

(e.g. PDGFRA), thus decreasing the dependence on exogenous growth factors (A. P. Patel et al., 2014).

RTKs share a common molecular architecture, with extracellular ligand-binding domain, single transmembrane α helix, and a conserved protein tyrosine kinase domain at the cytosolic side (Schlessinger, 2000). Signaling is initiated by binding of the ligand to an inactive RTK monomer and the subsequent receptor dimerization. This results in intracellular reciprocal tyrosine *trans*-autophosphorylations which activate the receptor (Lemmon & Schlessinger, 2010). Additional cytosolic tyrosines are autophosphorylated and serve as binding sites for SH2 (Src homology 2) or PTB (phosphotyrosine binding) domains of downstream docking or signaling complexes, such as PI3K (Phosphatidylinositol 3-kinase) and RAS (rat sarcoma virus oncogene) **(Fig 1.2)**. Subsequently, PI3K activates AKT serine/threonine kinase and mTOR (mammalian target of rapamycin) through the phosphorylation of phosphatidylinositol-4,5-biphosphate (PIP2) to phosphatidylinositol-3,4,5-triphosphate (PIP3). Activation of RAS initiates signaling through the MAPK pathway. Ultimately, these cascades stimulate cell survival, transcription (also controlled by RTK-mediated activation of STATs), protein synthesis, and proliferation (Schlessinger, 2000). Collectively, these downstream pathways position RTKs at the apex of an interconnected and dynamic signaling network utilized by the majority of GBMs.

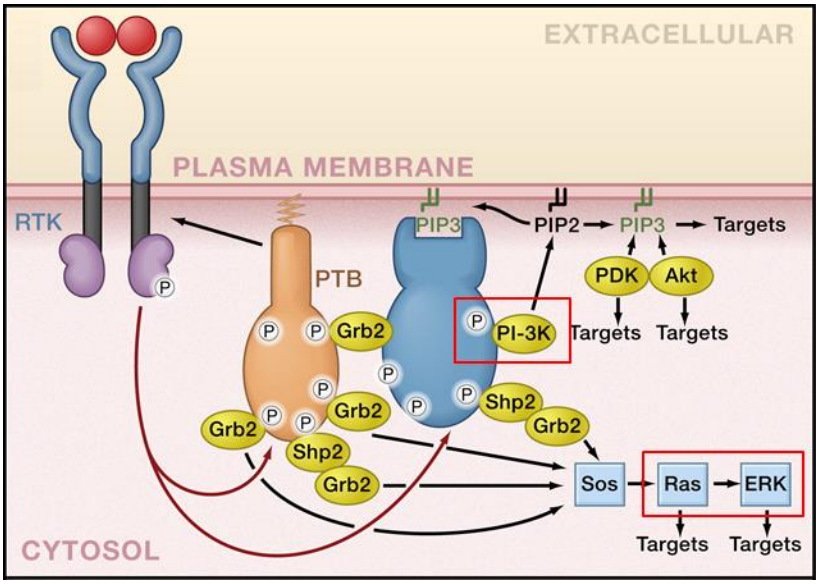

Figure 1.2. Receptor tyrosine kinase signaling pathway. Extracellular ligand binding induces receptor dimerization and subsequent *trans*-autophosphorylations of the protein tyrosine kinase domains. Additional tyrosines are autophosphorylated and bound by docking and signaling complexes through their phosphotyrosine biding domains. These activate a host of downstream signaling molecules including PI3K and RAS. (Image modified from Lemmon & Schlessinger, 2010)

Signaling components of the TP53 and RB pathways (described below) are also amplified, albeit at a lower frequency. MDM2 (7.6%) and MDM4 (7.2%) are negative regulators of TP53. Through direct binding to the N-terminal of TP53, MDM2 and MDM4 inhibit the transcriptional activation function of TP53 (Francoz et al., 2006; Kruse & Gu, 2009). Additionally, MDM2 possesses an E3 ubiquitin ligase activity towards TP53 (Manfredi, 2010). Modification of TP53 by MDM2 targets it for proteasomal degradation, alleviating the cell cycle arrest imposed by active TP53. Progression through the cell cycle is also stimulated by CDK4 (mutated in 14% of GBMs), CDK6 (1.6%), and Cyclin D (2%) - negative regulators of the RB1 (Sherr & McCormick, 2002). The presence of mitogens stimulates the accumulation of CDK-Cyclin complexes which phosphorylate RB1 to induce

the release of the E2F transcription factor. Unbound E2F then stimulates the transcription of genes involved in the transition from G1 to S phase.

PTEN, TP53, and CDKN2A are the most frequently abrogated tumor suppressor genes

PTEN

PTEN (phosphatase and tensin homolog deleted on chromosome 10) is a dual lipid and protein phosphatase. PTEN converts PIP3 to PIP2 by dephoshorylating the 3' position and thus, directly antagonizes PI3K signaling **(Fig 1.3)** (Carracedo, Alimonti, & Pandolfi, 2011). By preventing the unregulated activation of the PI3K pathway (described above), PTEN controls cell proliferation, survival, metabolism, and motility. In addition to growth factor-mediated PI3K signaling, PTEN inhibits integrin-mediated signal transduction upstream of the MAPK pathway (Gu, Tamura, & Yamada, 1998). PTEN dephosphorylates the focal adhesion kinase (FAK) and negatively regulates cell interactions with the extracellular matrix, essential for migration (Tamura et al., 1998). In addition to the phosphatase activity at the cell membrane, PTEN also exerts tumor suppression in the nucleus. Nuclear PTEN activity regulates genomic stability, cell cycle progression, and gene expression (Worby & Dixon, 2014).

The identification of PTEN was the result of a search for a tumor suppressor on chromosome 10q23, which is frequently deleted in advanced cancers (J. Li et al., 1997; Steck et al., 1997). This high frequency of PTEN inactivation may in part be attributed to a lack of functional redundancy in terms of PIP3 dephosphorylation (Chalhoub & Baker, 2009). PTEN is disabled though deletions, mutations, transcriptional silencing, and posttranslational

modifications. In mice PTEN has been shown to be haploinsufficient: one functional allele is not enough to maintain the wild-type condition (Alimonti et al., 2010). GBM patients have PTEN deletions 42% of the time, while loss of one copy of chromosome (chr) 10, which harbors *PTEN* is seen in >70% of cases. Computational analysis of TCGA data identified loss of chr10 (together with gain of chr7) as an initial event in gliomagenesis, regardless of molecular subtype. The primary driver for loss of chr10 is reduced expression of PTEN (Ozawa et al., 2014). Gain of PDGFA (on chr7) and reduced expression of PTEN are sufficient to drive the formation of Proneural GBM in mice. Acquisition of additional mutations can then shift the profile towards the Mesenchymal subtype (Ozawa et al., 2014).

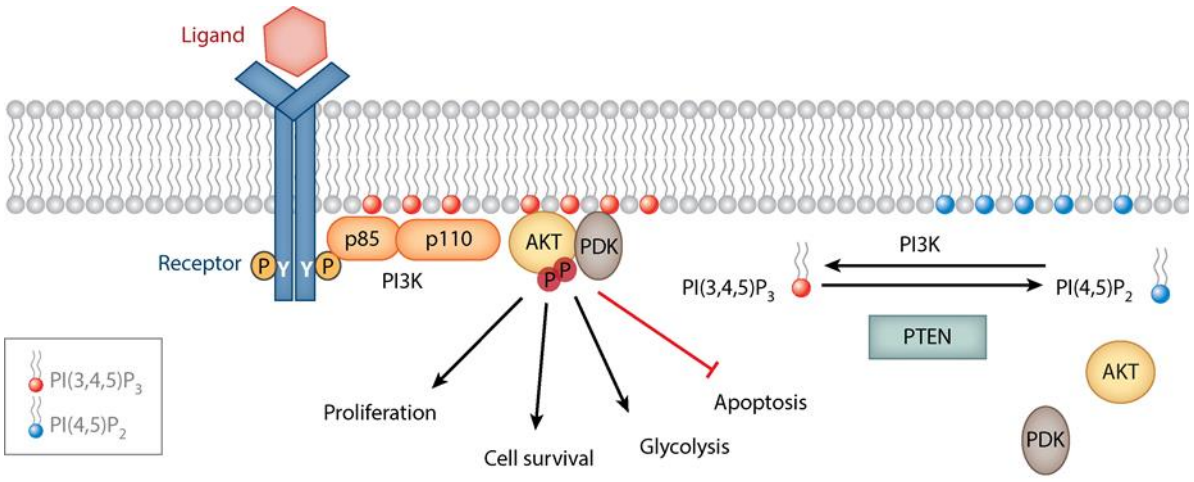

Figure 1.3. PTEN antagonzies PI3K activity. Through its lipid phosphatase activity PTEN converts PIP3 to PIP2, negatively regulating cell proliferation, survival, metabolism, and invasiveness (Image modified from Worby & Dixon, 2014).

TP53

TP53 controls the cellular response to number of stressors (DNA damage, oncogenic signaling, metabolic stress) and thus, serves as a master tumor suppressor gene (TSG). In the absence of stress, TP53 is inhibited by MDM2 and MDM4, and unbiquitinated for proteasomal degradation **(Fig 1.4A)**. Under unfavorable conditions, stress sensors like ATM, ATR, DNA-PK, and CHK1/2 phosphorylate residues at the N-terminus of TP53 which disrupts the inhibitory binding to MDM2. Additionally, in response to oncogenic stress the steady-state level of $p14^{ARF}$ is increased dramatically **(Fig 1.5)**. $p14^{ARF}$ can directly bind to the central domain of MDM2, disrupting the MDM2-TP53 interaction (Kruse & Gu, 2009). The stress response is further enhanced by TP53 acetylation events, which also contribute to target specificity (Brooks & Gu, 2003; Luo, Su, Chen, Shiloh, & Gu, 2000). Post-translationally modified TP53 binds to response elements in the promoters of downstream target genes. The nature of the transcribed TP53 targets determines whether the cell responds to a given assault with cell cycle arrest (*p21)*, senescence, DNA repair, apoptosis (*BAX*, *PUMA, NOXA*), or autophagy **(Fig 1.4B)**. Since MDM2 is a transcriptional target of TP53, once the cellular stress has been resolved, a MDM2-TP53 negative feedback loop decreases TP53 levels back to steady-state. MDM2 and TP53 are part of another regulatory network connecting the TP53 and PI3K pathways. Activated AKT phosphorylates MDM2 and enhances TP53 degradation. PTEN-mediated inhibition of PI3K enables the transcriptional activity of TP53, which can lead to the upregulation of PTEN, as TP53 binds to the promoter region of PTEN (Mayo & Donner, 2002).

Given the central role of TP53 in coordinating transcriptional programs that contribute to tumor suppression it is not surprising that mutations in TP53 or disruptions of the TP53 regulatory network (MDM2, MDM4, $p14^{ARF}$) have been found in more than half of human cancers, and are also linked to familial cancer predisposition syndromes (Kruse & Gu, 2009). Frameshift and nonsense mutations result in loss of protein expression. More frequently, tumor TP53 carries missense mutations, leading to single amino acid substitutions in a stably expressed protein (Muller & Vousden, 2014). The majority of cancer associated substitutions occur in the DNA-binding domain, disrupting the transcriptional activity of TP53 (Hainaut & Hollstein, 2000). Since the protein is a homotetramer in the active state, a monoallelic mutation can exert a dominant-negative effect on the remaining wild-type copy monomers. Furthermore, mutant TP53 has been shown to have novel oncogenic functions. Gain-of-function TP53 mutants have been reported to promote survival, proliferation, and chemo-resistance in glioma cells (Iwadate et al., 1996; Lin, Liang, Zhu, Zhang, & Zhong, 2012). In GBM the protein is mutated/deleted in 28% of the cases, while the pathway is disrupted 85% of the time (Brennan et al., 2013). This leads to loss of oncogene-induced senescence, p21-driven cell cycle arrest, and apoptotic signaling.

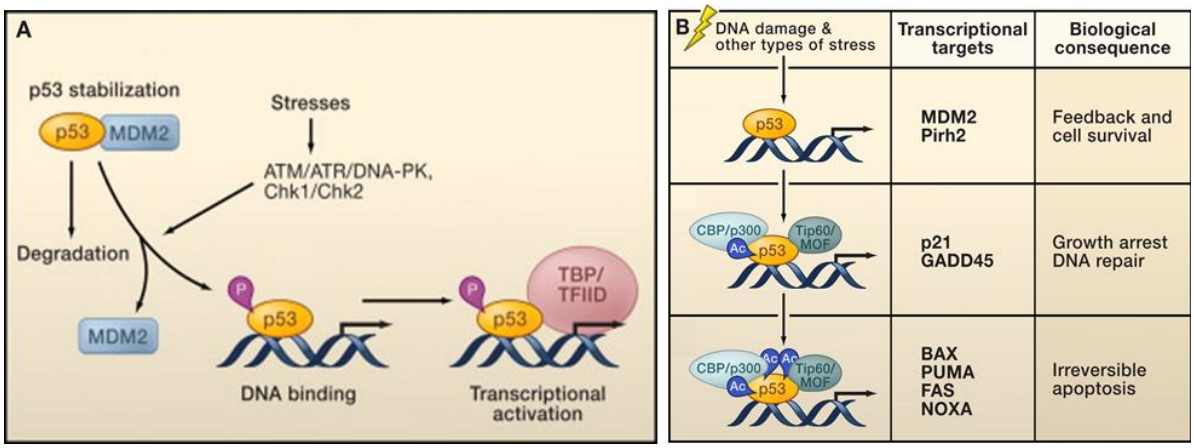

Figure 1.4. Stress-induced activation of TP53. (A) TP53 signaling is initiated by the stress sensors ATM, ATR, DNA-PK, and CHK1/2. Phosphorylation of TP53 causes protein stabilization, DNA binding, and the induction of transcription of TP53 target genes. (B) TP53 target specificity is determined by posttranslational modifications and transcription cofactors (Image modified from Kruse & Gu, 2009).

RB1 and CDKN2A

The RB pathway is another barrier to uncontrolled growth that glioma cells must overcome (Hanahan & Weinberg, 2011). Whereas p53 enforces control over the cell cycle based on intracellular stress signals, RB imposes a G1 arrest largely based on extracellular cues. In the absence of environmental mitogens RB is hypophosphorylated (active state). Hypophosphorylated RB binds to the transcription factor E2F and imposes repression on E2F targets - genes required for DNA replication and mitosis. Sustained mitogen signaling, indicating growth-favorable conditions, allows for the assembly of CDK-Cyclin complexes which exert an inhibitory phosphorylation of RB (Sage, 2012). This leads to the release of E2F from the inhibitory complex with RB and the subsequent transition to S phase. CDK-Cyclin complexes are under the control of the INK4 family of CDK inhibitors. The $p16^{INK4A}$, $p15^{INK4B}$, $p18^{INK4C}$, and $p19^{INK4D}$ CDK inhibitors can disrupt the binding of CDKs to Cyclins, prevent mitogen-induced cell-cycle progression, and induce senescence (Knudsen & Knudsen, 2008). INK4 proteins exert strong tumor suppression and loss of one component of the INK4 family can be ameliorated by the compensatory action of another member (Camacho et al., 2010; Krimpenfort et al., 2007). However, deletion of $p16^{INK4A}$ (seen in 62% of GBM cases) is particularly advantageous for malignant growth, as $p14^{ARF}$ is transcribed from an alternative reading frame of the $p16^{INK4A}$ gene (also known as *CDKN2A* locus) resulting in the loss of two critical tumor suppressors (Quelle, Zindy, Ashmun, &

Sherr, 1995). Additionally, *p15*^{INK4B} is located in close proximity to *CDKN2A* and is often deleted in tandem with *p16*^{INK4A} and *p14*^{ARF} (Krimpenfort et al., 2007). Thus, a focal homozygous deletion can amount to the combined loss of TP53- and RB-mediated oncogene-induced cell-cycle arrest (**Fig. 1.5**).

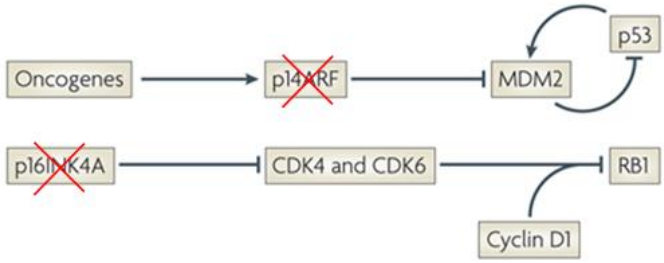

Figure 1.5. Deletion of the *CDKN2A* locus results in the simultaneous loss of *p14*^{ARF} and *p16*^{INK4A} (Image modified from Negrini, Gorgoulis, & Halazonetis, 2010).

Mutual exclusivity among alterations affecting components of the same pathway

Another important result from the sequencing of the glioma genome is the recognition that there is a mutual exclusivity among alterations affecting the same pathway. PI3K mutations were found to be mutually exclusive of PTEN mutations/deletions. In the TP53 pathway TP53 deletions/mutations were mutually exclusive with amplifications of MDM2 or MDM4, or deletions of p14^{ARF} (Negrini, Gorgoulis, & Halazonetis, 2010; Shchors et al., 2013). Similarly, in the RB pathway, mutation or deletion of CDKN2A did not co-occur with CDK4/6 amplification or RB1 deletion (Brennan et al., 2013; Sherr & McCormick, 2002; Verhaak et al., 2010; Vitucci, Hayes, & Miller, 2011). Thus, although there is a selection pressure to disable all three pathways, there appears to be no advantage in altering multiple nodes within the same signaling cascade.

GBMs are characterized by intratumoral heterogeneity

The malignancy and therapy resistance of glioma is attributed to intratumoral heterogeneity - the presence of clonal populations with distinct mutational profiles, differentiation states, and biological properties. Studies examining different regions within individual tumors by genome sequencing, fluorescence in situ hybridization, and single-cell RNA sequencing have revealed a spatial mosaicism of genomic alterations and transcriptome profiles (A. P. Patel et al., 2014; Snuderl et al., 2011). Existence of intermingled clones bearing different focal RTK amplifications (*EGFR, PDGFRA, MET)* or cell populations with multiple RTK co-amplifications has been shown to render tumor cultures resistant to single-RTK inhibition, providing a possible explanation for the therapeutic failure of small molecule inhibitors (Stommel et al., 2007; Szerlip et al., 2012). RTK co-activation reduces the tumor dependence on any single upstream activator of the PI3K and MAPK pathways and allows it to adapt rapidly to a dynamic microenvironment and pharmacological challenge.

In addition to this lateral heterogeneity, there appears to be heterogeneity in terms of differentiation state. A tumor hierarchy, where a small set of glioma-propagating stem-like cells (GPSCs) are responsible for tumor repopulation after therapy has been proposed (Bao et al., 2006; Baumann, Krause, & Hill, 2008; Bleau et al., 2009). Such cells can be isolated from resected tumors and grown in serum-free culture conditions as tumor neurospheres. These tumor neurospheres preserve the parental tumor genetic content more faithfully than conventional monolayer cultures (Lee et al., 2006). Like neural stem cells, GPSCs have unlimited replicative potential and diversity of progeny, giving rise to the heterogeneous bulk

of non-GPSCs differentiated cells and recapitulating the histology and global gene expression patterns when injected in immunocompromised mice (Alcantara Llaguno et al., 2009; Chen, McKay, & Parada, 2012; Lathia, Mack, Mulkearns-Hubert, Valentim, & Rich, 2015). Poorly differentiated tumors, which have a worse prognosis, have transcriptional profiles resembling those of human embryonic stem cells (ESCs). Similar to ESCs GBM samples show under-expression of Polycomb target genes (responsible for differentiation) and over-expression of ES genes (Sox2, Nanog, Oct3/4) and targets of IPS factors (Ben-Porath et al., 2008). Whether these GSCs originate from the normal neural stem cells, oligodendrocyte progenitor cells, or mature astrocytes undergoing de-differentiation remains a question of debate (Bachoo et al., 2002; Dunn et al., 2012; Liu et al., 2011)

RTK amplifications and TSG deletions drive gliomagenesis in mouse models

Although *in vitro* experiments have greatly enhanced our understanding of tumor biology, as a systems disease, cancer is most accurately modeled *in vivo*. Immunocompromised mice have been used as a tool to propagate patient derived xenografts, avoiding any confounding effects of cell culture. Alternatively, the genes most commonly altered in GBM **(Fig. 1.1)** have been utilized to develop genetically engineered mouse models. Majority of these employ a conditional expression of oncogenes or deletion of TSGs using the Cre-Lox system. This tool allows for Cre recombinase-mediated excision of target genes flanked by loxP sequences. The use of cell type-specific Cre promoters has furthered our understanding of glioma cell of origin. Nestin-mediated expression of Cre targets neural stem and progenitor cells, while GFAP-Cre (glial fibrillary acidic protein) targets mature

astrocytes and progenitor cells in the sub-ventricular zone (SVZ) (Mignone, Kukekov, Chiang, Steindler, & Enikolopov, 2004; Zhuo et al., 2001). The fusion of Cre to a mutated estrogen receptor ligand binding domain (Cre-ER) has added a temporal control of Cre induction via the administration of tamoxifen. Variations in the genetic configurations of tumor suppressor allele deletions and oncogene activation including TP53, PTEN, NF1, CDKN2A, RB1, RAS, and EGFR/EGFRvIII, have generated mouse models that faithfully recapitulate human gliomas (Alcantara Llaguno et al., 2009; Chow et al., 2011; Kwon et al., 2008; Zheng et al., 2008; H. Zhu et al., 2009). These mice have been extensively adopted for preclinical testing of potential chemotherapy drugs. However, these models merely recapitulate the genomic landscape of a grade IV disease. There is an urgent need for the development of additional models and tools to evaluate GBM predisposition, initiation, and risk factors.

The standard of care combines surgery with chemoradiotherapy

Unfortunately, high-grade glioma remains a terminal disease, as our improved understanding of the molecular landscape is yet to be translated effectively into personalized treatment. Current targeted therapies have had a marginal effect and the 5-year survival of GBM patients still falls under 10% (Bondy et al., 2008; Cloughesy, Cavenee, & Mischel, 2014). The mainstay of glioma therapy remains a combination of de-bulking surgery and radiotherapy (RT), with adjuvant Temozolomide (TMZ) as a chemotherapeutic agent (Stupp et al., 2009). Gross total resection is followed by chemoradiotherapy consisting of up to 60 Gy of ionizing radiation (IR) and daily TMZ. Additional six cycles of TMZ are administered

as maintenance therapy (Weller et al., 2014). Nonetheless, tumors invariably recur, oftentimes presenting with a different molecular landscape and acquired resistance to therapy, attributed to a population of glioma stem cells and the selection pressure exerted by TMZ and IR (Cloughesy et al., 2014; Negrini et al., 2010; Phillips et al., 2006; J. Wang et al., 2016)

Ionizing radiation is the only known cause of sporadic GBM

Although a lot has been discovered about the genomics of GBM, the etiology of the disease remains poorly understood. IR, which is received by a majority of glioma patients, is paradoxically the only known risk factor for sporadic gliomagenesis (Bondy et al., 2008; Pearce et al., 2012). The role of IR as a carcinogen is most strongly supported by the Life Span Study, the largest epidemiology study on the effects of radiation exposure on human health (Kamiya et al., 2015). The study has followed over 100,000 atomic bomb survivors from the Hiroshima and Nagasaki bombings. Key findings show that survivors have a clear radiation-related excess risk of cancer (including brain) throughout life, which becomes statistically significant at doses above 0.1 Gy.

Radiation induced malignant gliomas (RIGs) develop in non-human primates exposed to electromagnetic or particle radiation (Kent & Pickering, 1957; Krupp, 1976; Lonser et al., 2002). In humans, exposure to radiation for medical diagnostics (e.g. CT scans) increases the relative risk of de novo brain tumors, while adult and pediatric patients undergoing radiation treatment for non-related malignancies present with therapy-induced gliomas later in life (Elsamadicy, Babu, Kirkpatrick, & Adamson, 2015; Pearce et al., 2012; Salvati et al., 2008;

Ward, DeSantis, Robbins, Kohler, & Jemal, 2014; Yamanaka, Hayano, & Kanayama, 2016). Doses received during treatment of the initial condition are in the vicinity of 30-60 Gy but patients irradiated with as little as 3 Gy for tinea capitis treatment also present with RIG (Paulino, Mai, Chintagumpala, Taher, & Teh, 2008; Salvati et al., 2008). Stereotactic radiosurgery, while better preserving the surrounding normal tissue, has been linked to the development of radiation-induced neoplasms, of which gliomas are the most common (T. R. Patel & Chiang, 2014; Shamisa et al., 2001). The advent of particle therapy further necessitates the evaluation of effect of radiation quality on gliomagenesis. Particle therapy, unlike conventional X-rays therapy, utilizes accelerated charged proton (H) and carbon (C) nuclei capable of delivering the dose precisely to the tumor while sparing the surrounding normal tissue (Durante & Loeffler, 2010). Although promising, particle therapy should be approached with caution, as very little is known about the organismal effects of exposure to charged nuclei. The use of IR in modern medicine is steadily growing and now comprises 48% of all sources of human exposure (Fig. 1.6). This warrants a critical evaluation of the cancer risks associated with IR.

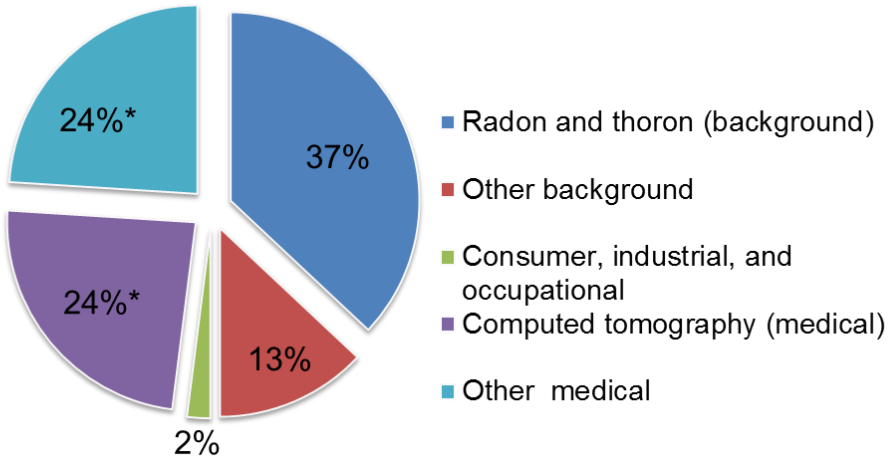

Figure 1.6. Sources of radiation exposure. Radiation for medical purposes amounts to 48% of the pie chart.

Ionizing radiation is a genotoxic agent

Radiation is widely used as for cancer treatment due to its cytotoxic and mutagenic properties. The efficacy in cell killing has made it a standard treatment modality and high doses are received by majority of cancer patients irrespective of malignancy type or demographics. However, cells that undergo IR-induced sub-lethal mutagenic DNA damage are a detriment to secondary cancer-free survival (discussed above).

Radiation is considered "ionizing" if it has sufficient energy to eject orbital electrons. Based on physical properties IR is classified as electromagnetic (X-rays and gamma-rays) and particulate. The extent of DNA damage and subsequent genomic instability depend on the ionization density of the type of radiation, with more densely ionizing radiation causing more damage per unit absorbed dose (Kamiya et al., 2015). The distribution of energy

deposited per distance traveled is also known as linear-energy transfer (LET). Electromagnetic photons are mostly absorbed by outer shell electrons in the ionized tissue. Expulsed electrons can react with surrounding water molecules and create reactive oxygen species that attack DNA, generating simple, uniformly distributed DSBs. Charged particles, by virtue of size (Z), can directly collide with the DNA molecule causing clustered double strand breaks as they transverse the cell (Desai, Durante, Lin, Cucinotta, & Wu, 2005; Moore, Stanley, & Goodarzi, 2014). Clustered DNA damage is defined as a DSB accompanied by another DBS, a single-strand break, or base damage within several base pair distance (Asaithamby & Chen, 2011; Durante & Loeffler, 2010; Mladenov & Iliakis, 2011). Even a single heavy particle radiation track can induce such clustered DNA damage **(Fig. 1.7)** (Hada & Georgakilas, 2008b). Heavy particles are encountered in space, where the radiation environment consist of high-LET protons (85%), alpha particles (14%), and high atomic number, high energy (HZE) nuclei. The exposure of astronauts to HZE radiation was realized during the Apollo missions as crew members reported seeing flashes of light with their eyes closed (Fazio, Jelley, & Charman, 1970). These flashes were caused by the passage of heavy cosmic ray nuclei through the astronauts' eyes. Due to their high energy, such particles cannot be shielded by current spacecraft materials and present an occupational radiation hazard. More recently, a radiation detector aboard the Curiosity Rover measured the cumulative dose of radiation from galactic cosmic radiation (GCR) and solar particle events (SPEs) an astronaut will receive inside the spacecraft during a trip to Mars (~0.5 Gy) (Zeitlin et al., 2013).

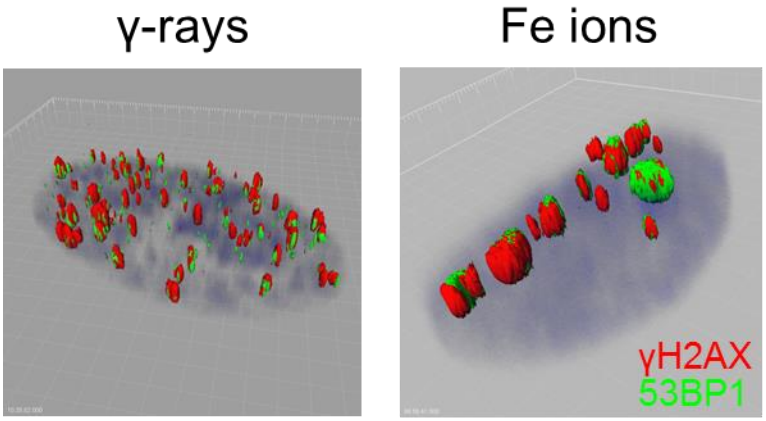

Figure 1.7. DNA damage resulting from exposure to ionizing radiation. 3D reconstruction of 53BP1 and γ-H2AX foci (surrogate markers of DSBs) in cells irradiated with gamma-rays (left) or Fe ions (right) 0.5 h following exposure. (Image modified from Mukherjee et al., 2008)

The complexity of IR-induced damage and the inability of the cell to fully repair its DNA increases directly with LET (the amount of energy deposited) and the atomic number (the cross-sectional ionization pattern) due to the confined nature of energy deposition and the proximity of the lesions (Desai, Durante, et al., 2005; Little, 2000) **(Fig 1.8)**. The longitudinal track structure (the map of ionization events along the trajectory) of heavier particles is further complicated by the generation of energetic secondary electrons projecting tens of micrometers radially from the core (Ballarini, Alloni, Facoetti, & Ottolenghi, 2008). Although the same type of lesions results from low-LET radiation, the sparse nature of the damage allows for more efficient repair and lower frequency of long term effects. Animal studies have corroborated the differential biological effects of low- and high-LET radiation seen *in vitro*. Elevated cancer incidence following exposure to HZE compared to reference electromagnetic radiation has been demonstrated in mice or rats for skin tumors, Harderian and mammary gland tumors, hepatocellular carcinoma, and malignant glioma (Alpen,

Powers-Risius, Curtis, & DeGuzman, 1993; Camacho et al., 2015; Dicello et al., 2004; Weil et al., 2009).

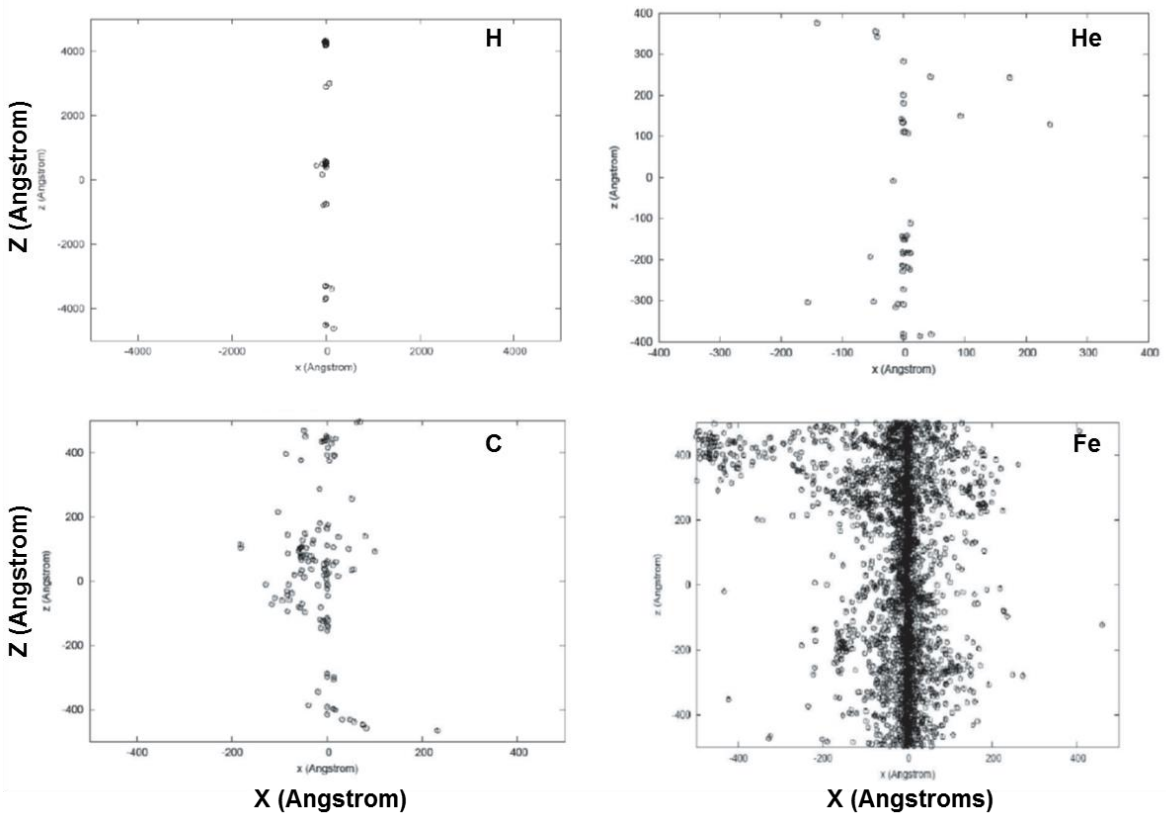

Figure 1.8. 2D projections of track structures (longitudinal ionization events along the trajectory) of H, He, C, and Fe ions traveling in water. (Image modified from Ballarini et al., 2008)

Knowledge gap

Although the underlying mechanisms have not been elucidated, a clear link between exposure to IR and gliomagenesis exists. Given the increased use of IR for medical diagnostics, the rise in cancer incidence (and correspondingly in radiotherapy use), and the existence of unmitigated occupational radiation hazards (including space travel), there is an imperative, yet unaddressed need for animal models of RIGs. The goal of this project is to evaluate the risk of developing RIG, and examine what role radiation quality (atomic size, ionization density, biological effectiveness) plays in gliomagenesis. This task requires appropriate model systems that can faithfully recapitulate the process *in vivo*. The only such mouse model currently in existence was developed by our group (Camacho et al., 2015). By comparing tumorigenesis after X-rays and iron ions exposure we presented the first experimental evidence showing that HZE radiation is more gliomagenic. The effects of protons and carbon ions on gliomagenesis have never been evaluated, and yet, there is a growing number of people undergoing hadron therapy. This project aims to advance our knowledge of radiation-induced gliomagenesis, and has the following aims:

1. To identify a second, independent RIG mouse model (Chapter III)
2. To evaluate the effect of radiation quality on gliomagenesis using two complementary mouse models (Chapter III)
3. To determine the molecular changes driving the process of radiation-induced gliomagenesis (Chapter IV)

Our first mouse model elucidated the role Cdkn2a and Cdkn2b loss plays in radiation-induced gliomagenesis. For the second model we chose to employ deletions of p53 and Pten, collectively exploring all major TSG pathways implicated in GBM by the TCGA **(Fig 1.1)**. To maximize the clinical relevance of this study we compared conventional RT electromagnetic radiation (250 kV X-rays), therapy grade proton (150 MeV/n ^{2}H) and carbon (290 MeV/n ^{12}C), and space-exploration pertinent heavy particles such as silicon and iron (238 MeV/n ^{32}Si and 600 MeV/n ^{56}Fe). Integrated multi-dimensional analysis of tumor samples shed light on the major barriers of transformation and oncogenic events important for the process of radiation-induced gliomagenesis. The results described in the following chapters present an important contribution to the field of heavy particle radiobiology with potential implications to hadron therapy and astronaut safety during space exploration.

CHAPTER II

Methodology

Irradiation

Particle beams of hydrogen, carbon, neon silicon, titanium, and iron were provided by the National Aeronautics and Space Administration (NASA) Space Radiation Laboratory at Brookhaven National Laboratory (BNL) as described (La Tessa, Sivertz, Chiang, Lowenstein, & Rusek, 2016; Mukherjee, Camacho, Tomimatsu, Miller, & Burma, 2008). Briefly, particles are accelerated in the AGS Booster synchrotron, extracted and transported to an irradiation station on which dose monitoring and beam characterization devices and experimental samples are mounted **(Fig 2.1)**. The dose is measured by ionization chambers and monitored by a computer-controlled dosimetry system that automatically cuts off the beam when the specified dose is reached. For these experiments, the LET spectrum of radiation incident on the targets is measured by silicon solid-state detectors with areas similar to that of the biological samples. Low-LET reference radiation was delivered at the University of Texas Southwestern Medical Center (UTSW): for γ-ray irradiation, a ^{137}Cs source was used (JL Shepherd and Associates, San Fernando, CA); X-ray irradiation was performed using an X-RAD 320 device (Precision X-ray, North Branford, CT). Radiation energy and LET values are shown in **Table 2.1**. We used conventional RT electromagnetic radiation (250 kV X-rays), therapy grade proton (150 MeV/n ^{2}H) and carbon (290 MeV/n ^{12}C), and space-exploration pertinent heavy silicon and iron particles (238 MeV/n ^{32}Si and 600 MeV/n ^{56}Fe). This choice allowed for the investigation of a range of sizes (Z from 1 to 26) and LETs (0.5 to 174 keV/μm).

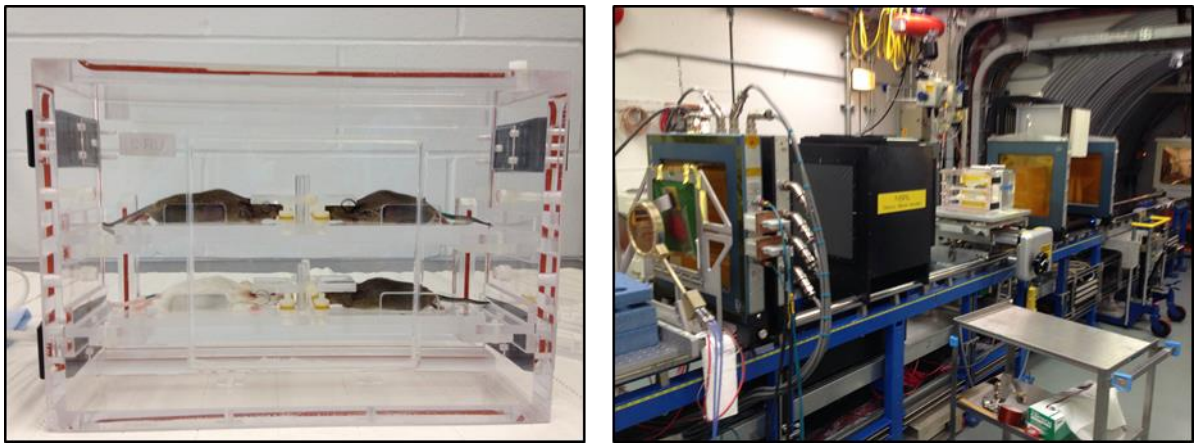

Figure 2.1. Particle beam irradiation station at the NASA Space Radiation Laboratory at Brookhaven National Laboratory. Prior irradiation mice placed in a head-only irradiation box (left panel). The box is mounted at the beam line where the delivered dose is measured by ionization chambers and monitored by a computer-controlled dosimetry system.

Table 2.1. Radiation type, energy, LET, and dose used in Chapter III.

0.5 Gt IR	X-rays	H	C	Ne	Si	Ti	Fe
Z	NA	1	6	10	14	22	26
Energy	250 kV	150 MeV/n	293 MeV/n	255 MeV/n	238 MeV/n	664 MeV/n	600 MeV/n
LET(keV/µm)	2	0.5	13	39	79	120	174

Animal studies

All animal studies were performed under protocols approved by the Institutional Animal Care and Use Committees of UTSW and BNL. Cohorts of 4-8 weeks old mixed gender, mixed strain of mice (FVB/NJ and C57BL6 mixed background) with brain-specific Nestin-Cre (^{NesCre}) driven LoxP-excision of *p53* (exons 2-10) and *Pten* (exon 5) alleles were irradiated at BNL (particle beams) and UTSW (X-rays beam). A second complimentary mouse model with germline deletions of Ink4a and Ink4b, and brain-specific Nestin-Cre driven LoxP-excision of Arf (designated $^{NesCre}Ink4ab^{-/-}Arf^{F/F}$) was used for radiation quality

effects assessment. This model was published by our group and is described elsewhere (Camacho et al., 2015). All animals received a single intracranial dose of 0.5 Gy of the corresponding radiation **(Fig. 2.1)**. Following irradiation, the mice were monitored daily for neurological morbidity. Symptomatic mice were euthanized and the tumors were harvested for histopathological, immunological and molecular analyses. Hematoxylin and eosin (H&E) stained sections of gliomas were examined by the study neuropathologist for tumor grade assessment; tumor grade was assigned based on the World Health Organization (WHO) criteria (D. N. Louis et al., 2007). All surviving mice were euthanized 9 ($^{NesCre}Ink4ab^{-/-}Arf^{F/F}$) or 15 (p53/Pten cohorts) months post-irradiation; serial brain sections were examined to determine the presence of asymptomatic disease.

PCR

Genomic DNA was extracted from tail snips using Direct PCR Lysis Reagent (Viagen Biotechnology) or flash-frozen kidney, pancreas, brain, and tumor tissues using the DNeasy Blood and Tissue Kit (Qiagen). Polymerase Chain Reactions (PCR) were performed using the DreamTaq Green PCR Master Mix (2X) (Thermo Scientific). Each sample was amplified with primers to synthetize the wild-type (WT) and floxed (F) variants of *p53* and *Pten*. Total RNA was extracted from flash-frozen tissue or cultured cells using the RNeasy Mini Kit (Qiagen). Reverse Transcription Polymerase Chain Reactions (RT-PCR) were performed using the Superscript III 1st Strand Kit (Thermo Fisher) and Quantitative Polymerase Chain Reaction (qPCR) was performed with a Bio-Rad CFX 96 Touch Real-Time PCR Detection system (Bio-Rad) using the SYBR Green detection system (Applied

Biosystems). All samples were amplified in triplicate. Relative expression of each gene was normalized to 18s mRNA. All primers are listed in **Table 2.2**.

Table 2.2. Primers used for PCR and quantitative real-time PCR

List of primers			
Method	Gene	Primer direction	Primer sequence
PCR	Cre	Fw	atttgcctgcattaccggtc
		Rv	atcaacgttttcttttcgg
	p53	Fw	cacaaaaacaggttaaacccag
		Rv	agcacataggaggcagagac
	Pten	Fw	aagcactctgcgaactgagc
		Rv	ttgccagacatgctccgaag
RT-PCR	NeuN	Fw	ttttatggtgctgagatttatgga
		Rv	cagcggcatagactctacca
	Gfap	Fw	acagactttctccaacctccag
		Rv	ccttctgacacggatttggt
	Olig2	Fw	tacagaccgagccaacacc
		Rv	gctctcgaatgatccttcttttt
	Sox2	Fw	tgctgcctctttaagactaggg
		Rv	cgggctccaaacttctctc
	p21	Fw	gtacttcctctgccctgc
		Rv	agagtgcaagacagcgacaa
	Mdm2	Fw	agggcacgagctctcagat
		Rv	tctccttcaaaagagtctgtatcg
	Pten	Fw	tgaagaccataacccaccaca
		Rv	tcattacaccagtccgtccgtccct
	18s	Fw	aaacggctaccacatccaag
		Rv	cctccaatggatcctcgtta

Fw = Forward
Rv = Reverse

Adherent cell culture and colony formation assay

Primary murine astrocytes were isolated from 2-day old ^{NesCre}Ink4ab$^{-/-}$Arf$^{F/F}$ and ^{NesCre}p53$^{+/F}$;Pten$^{+/F}$pups and maintained in DMEM containing 10% fetal bovine serum in a humidified incubator at 37°C in the presence of 5% CO_2. For colony formation assays, 300 cells were plated in triplicate T25 flasks and irradiated with graded doses of radiation (0-4 Gy of γ-rays, P, C, Si, and Fe). Surviving colonies were stained with crystal violet 11-12 days post-irradiation and quantified as described (Mukherjee et al., 2008). For repair kinetics studies, cells received a dose of 1 Gy of γ-rays, P, C, Si, or Fe and were fixed at set time-points throughout the course of 24h. DNA damage was detected by 53BP1 staining and quantified. To visualize track of DNA damage along the trajectories of traversing nuclei, cells were irradiated parallel to the beam. DAPI counterstain (Vector Labs) was used to visualize nuclei.

Tumor neurosphere cell cultures

Brains of tumor-bearing mice were micro-dissected and glioma tissue was mechanically and chemically digested for the generation of ex-vivo cultures. The cultures were plated as single cells in DMEM/F-12 1:1 media (Life Technologies) supplemented with B27 without Vitamin A (Life Technologies), 10 ng/mL EGF, and 10 ng/mL basic FGF (Peprotech), and grown as non-adherent spherical clusters. Every 4-6 days the cells were dissociated by titrating in Accutase (Sigma-Aldrich) and sub-cultured (Gil del Alcazar et al., 2014). For serum-induced differentiation studies the spherical cultures were dissociated into single cells and the growth media was switched to DMEM supplemented with 10% FBS. The cells were grown under these conditions for 7 days and assessed for differentiation markers.

For sphere formation and radioresistance assays cells were dissociated and plated at 1.5 cells/well density in Nunclon Sphera Surface ultra-low adhesion 96-well plates (Thermo Fisher) in DMEM/F-12 1:1 media. Sphere number per 96-well plate was quantified after 12 days. All sphere formation assays were performed in triplicates and represented as mean and SD values.

Subcutaneous injections

Cells (as indicated) were suspended in equal volumes of phosphate buffered saline (PBS, Fisher Scientific) and Matrigel (Corning) and injected subcutaneously into the flanks of six- week old Nu/Nu nude mice (Charles River Laboratories International). Mice were monitored daily for tumor formation and measured with digital calipers to establish growth curves. Tumor volume was calculated as follows: length x width x height x 0.5. All animal studies were performed under protocols approved by the Institutional Animal Care and Use Committee (IACUC) of UT Southwestern Medical Center.

Immunohistochemistry and immunofluorescence

Following mouse cardiac perfusion with cold PBS, brain and tumor tissues were dissected and fixed in 4% paraformaldehyde overnight, embedded in paraffin, and sectioned at 5 μm thickness. Tumor tissue sections were de-paraffinized, rehydrated, and stained using standard immunohistochemistry and immunofluorescence protocols. The following antibodies were used: phospho-Erk (Thr202/Tyr204), Ki67/Mib-1, Met, phospho-Met (Tyr1234/1235), Pten, phospho-S6 ribosomal protein (Ser235/236) (Cell Signaling Technology), GFAP (Biocare Medical), Sox2 (Abcam), 53BP1 (Santa Cruz Biotechnology), and γH2AX, Olig2, NeuN (Millipore). For immunofluorescence, DAPI counterstain (Vector

Labs) was used to visualize nuclei. Ki67 indices were quantified by manually counting at least 500 nuclei in the regions of greatest staining.

Immunoblotting

Whole-cell SDS extracts were prepared and assayed as previously described (Mukherjee et al., 2006). The following antibodies were used: Actin (Sigma-Aldrich); Akt, phospho-Akt (Ser473), Met, phospho-Met (Tyr1234/1235), p53, phospho-p53 (Ser15), Pten (Cell Signaling Technology); p19Arf (A kind gift from Dr. David Kirsch), Sox2 (Abcam); V5 (Thermo Fisher); and horseradish peroxidase (HRP)-conjugated secondary antibodies (Bio-Rad).

Array comparative genomic hybridization

Genomic DNA was extracted from flash-frozen normal brain or glioma tissue from $^{NesCre}p53^{+/F};Pten^{+/F}$ animals using the DNeasy Blood and Tissue Kit (Qiagen). Tumor and control DNA samples were hybridized to Sure Print G3 Mouse CGH Microarray 1 X 1M (Agilent); the probes were annotated against the NBCI Build 37 (USSC mm9). Hybridization was automated using an Agilent Hybridization SureHyb chamber kit and gasket slide kit (Agilent), and the arrays were scanned at 2 µm resolution using a fluorescence scanner (Tecan). Feature extraction of raw signals was performed using the ImaGene 9.0 program. Raw signals were imported in Partek (Partek Inc.) and raw copy number calls from Partek were used as input for cghFlasso R package. cghFlassso uses fused lasso regression method to smoothen the raw calls and defines hotspots within the data. This CNV data was merged into segments using circular binary segmentation (CBS) algorithm. Regions of the genome that were significantly amplified or deleted, and the likely gene targets within those regions

were identified by the GISTIC2.0 module (q value< 0.05 and G-score > 1.5). The raw CN calls were visualized using circos (v. 0.69.3).

Whole genome sequencing

Genomic DNA was extracted from flash-frozen normal brain or glioma tissue using the DNeasy Blood and Tissue Kit (Qiagen). Whole genome sequencing was carried out by the Next Generation Sequencing Core at the McDermott Center at UTSW. Sequencing reads were aligned to mm10 build using BWA (v0.7.15) and aligned reads were sorted and filtered for low quality reads using samtools (v.0.0.19). Duplicates were removed using picard tools (v 1.131). Read depth values per 10000 bp were calculated by in house perl script using Bio::DB::Sam perl module and plotted using circos (v.0.69.3). CNV calls were made on this WGS data using Cnvnator (v0.3.3). The minimum length of each predicted CNV should be >=5000bp.

Lentiviral transduction

Human Met cDNA was obtained from Addgene (gift from Joan Brugge; Addgene, Cambridge, MA, USA; plasmid no. 17493) and sequentially cloned into pLenti6.3/V5-DEST using the Gateway Cloning system (Invitrogen). Virus production was carried out using ViraPower Lentiviral Packaging Mix (Invitrogen), as specified by the manufacturer. Cells were infected with viral particles at a multiplicity of infection (MOI) of 10 with 4 μg/ml polybrene. Cells were maintained under selection with 5 μg/ml blasticidin and screened for expression of Met-V5 by Western blotting.

Statistical Analysis

Kaplan-Meier analyses were used to illustrate glioma-free survival. Glioma frequencies were compared using a chi-square test. Sphere formation assays were analyzed by unpaired, 2-tailed t tests with Welch correction. The p21 and Mdm2 induction and tumor neurosphere radioresistance assays were analyzed by multiple t-tests. A p-value ≤ 0.05 was considered to statistically significant. Significance was indicated as follows: $*P \leq 0.05$, $** P \leq 0.005$, $*** P \leq 0.0005$. All statistical analyses were performed with GraphPad Prism Version 7.

CHAPTER III

Effect of radiation quality on gliomagenesis

3.1 INTRODUCTION

The link between exposure to low LET radiation (X-rays and gamma-rays) and carcinogenesis is evident from human epidemiological data from Hiroshima and Nagasaki and various nuclear accidents, as well as from patients exposed to diagnostic or therapeutic radiation (Abboud et al., 2015; Braganza et al., 2012; Christodouleas et al., 2011; Pearce et al., 2012; Preston, Shimizu, Pierce, Suyama, & Mabuchi, 2003). Since there is no epidemiological data on human populations exposed to HZE particle radiation, cancer patients undergoing hadron therapy suffer an unevaluated and potentially heightened risk of secondary cancers. Occupational hazards for astronauts – another population exposed to high LET radiation, are currently extrapolated from low-LET data. However, due to the different physical properties and biological effects of space radiation such extrapolations are ridden with a considerable uncertainty (Cucinotta et al., 2001; Zeitlin et al., 2013)

Unlike gamma rays, HZE particles are directly ionizing, causing clustered double strand breaks (DSBs) in the DNA molecule (Blakely & Chang, 2009; Tabocchini, Campa, & Dini, 2012). The complexity of this damage and the inability of the cell to fully repair its genome are due to the confined nature of energy deposition and the proximity of the DSBs. Consequently, in cell-based studies, HZE particles have been shown to be more clastogenic and more efficient in transformation in comparison to low-LET radiation (Camacho et al., 2010; Durante & Cucinotta, 2008; Loucas, Durante, Bailey, & Cornforth, 2013; Maalouf, Durante, & Foray, 2011; Mukherjee et al., 2008). Complimentary animal studies have shown that the differential biological effects of low- and high-LET radiation result in a difference in their tumorigenic potential, with HZE nuclei having a higher carcinogenic effect (Blakely &

Chang, 2009). This increased tumor incidence with HZE radiation renders risk-assessment approaches based on human epidemiological data from X-ray and gamma-ray exposure insufficient and emphasizes the need for further-finessed animal models. Moreover, individual HZE particles produce quantitatively different cellular effects depending on their LETs (the amount of energy deposited) and the atomic number (the cross-sectional ionization pattern), further contributing to the uncertainty (Ding et al., 2013; Tabocchini et al., 2012).

This chapter provides empirical evidence on the differential *in vivo* effects of HZE radiation. We have identified the first two mouse models that faithfully capture the process of radiation-induced gliomagenesis. The characterization of the first model is described in detail here. The second model was published recently and will only be used in **Sections 3.2.3** and on (Camacho et al., 2015). Using a comprehensive set of electromagnetic and particulate radiation we sought to determine a relationship between LET and transformation and improve our understanding of the risks from exposure.

3.2 RESULTS

3.2.1 Mice deficient in one copy of p53 and one copy of Pten are highly susceptible to iron ion-induced tumorigenesis

In order to identify an optimal RIG *in vivo* model, we examined transgenic mice bearing floxes alleles of one or both copies of *p53* and/or *Pten* genes. We crossed these mice with a Nestin-Cre mouse (Isaka et al) to achieve Cre-mediated excision of floxed alleles during early embryonal development in all CNS lineages, including glia, neurons, and adult neural stem cells. Cohorts of 40 Nestin-Cre positive (NesCre) mice with combinations of *p53*

and *Pten* allele deletions were irradiated intracranially and monitored for tumor development. All experimental p53/Pten genotypes and the corresponding glioma frequencies are listed in **Table 3.1.**

Table 3.1. List of experimental genotypes with cumulative deletions of p53 and Pten alleles

Glioma frequency	WT	p53+/-	Pten+/-	p53+/-;Pten+/-	p53-/-;Pten+/-
Mock IR (%)	0	0	0	2.5	>50
Fe ions IR (%)	0	8.1	2.5	27.5	ND*

*ND = not determined

For brevity "-" denotes floxed alleles excised by Cre recombinase

For this experiment, we used 0.5 Gy of iron ions beam (^{56}Fe 600 MeV/u), as we previously showed that iron radiation is a potent inducer of RIGs (Camacho et al., 2015). Although WT mice ($^{NesCre}p53^{+/+};Pten^{+/+}$) did not form brain tumors following irradiation, mono-allelic deletion of either tumor suppressor, in combination with iron irradiation, was sufficient to drive tumorigenesis (8.1% and 2.5% in the $^{NesCre}p53^{+/F}$ and $^{NesCre}Pten^{+/F}$ cohorts respectively). The frequency of radiogenic malignancies was enhanced to 27.5% upon excision of one copy each of both tumor suppressors, with the other allele still intact ($^{NesCre}p53^{+/F};Pten^{+/F}$) **(Fig. 3.1A)**. Importantly, only one non-irradiated control $^{NesCre}p53^{+/F};Pten^{+/F}$ animal developed brain tumor spontaneously (2.5%) at 15 months post mock-IR , underscoring that this genotype is indeed relevant, but the transforming effect of radiation is a necessary driver of tumorigenesis **(Fig. 3.1B)**. Targeted Cre-mediated excision of floxed *p53* and *Pten* alleles was achieved in the brain, but not in the kidney and pancreas **(Fig. 3.1C)**. H&E sections of $^{NesCre}p53^{+/F};Pten^{+/F}$ animals revealed enlarged brains bearing extensive cortical lesions, the mass effect of which distorted normal anatomical structures **(Fig. 3.1D)**. In our most TSG- depleted genotype the complete loss of *p53* resulted in the

frequent formation of spontaneous tumors, as previously reported (Zheng et al., 2008). Therefore, the $^{NesCre}p53^{F/F};Pten^{+/F}$ genotype was excluded from further analysis and the $^{NesCre}p53^{+/F};Pten^{+/F}$ model was chosen for all subsequent studies.

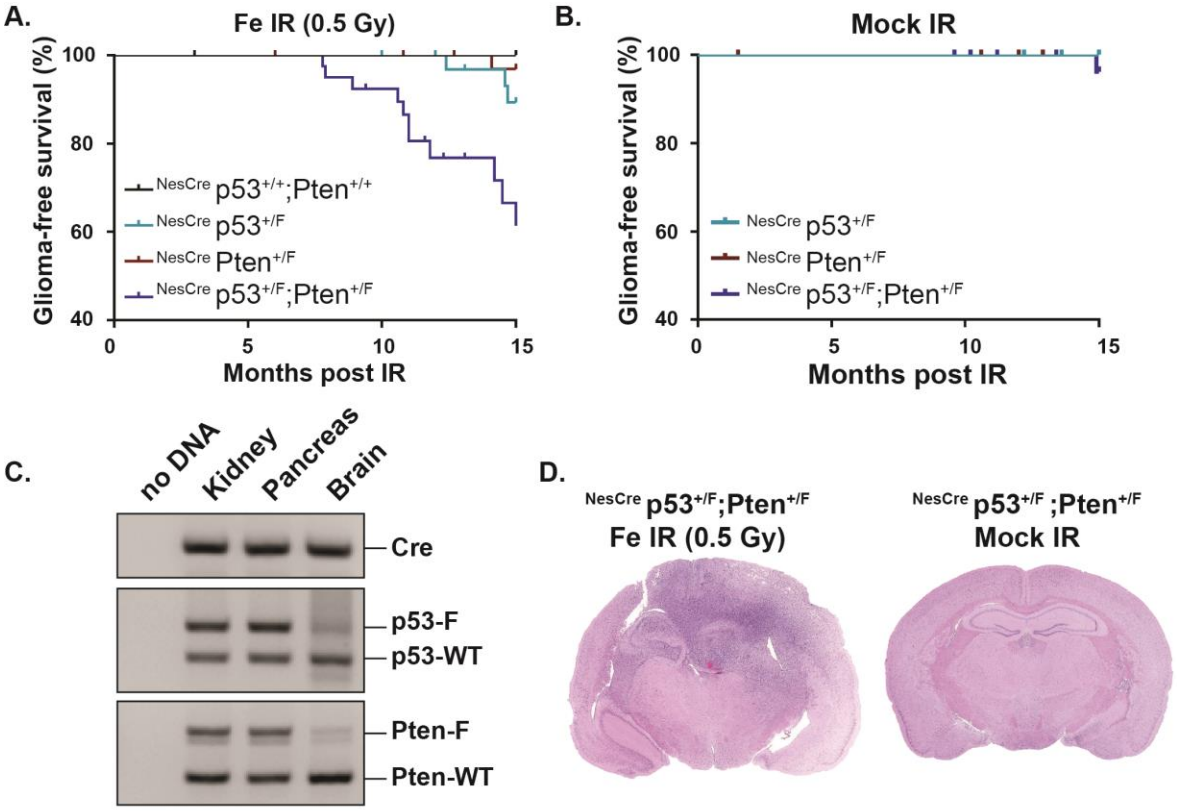

Figure 3.1. Frequent induction of brain tumors in $^{NesCre}p53^{+/F};Pten^{+/F}$ mice exposed to iron ions. A. Kaplan-Meier curves showing glioma-free survival of mice with different combinations of *p53* and *Pten* allelic deletions exposed to 0.5 Gy of Fe ions. Per genotype, 40 mice were irradiated. B. Kaplan-Meier curves showing glioma-free survival of control mice that were not irradiated. C. Genomic PCR on kidney, pancreas, and brain DNA extracted from $^{NesCre}p53^{+/F};Pten^{+/F}$ mice was performed to confirm the brain-targeted deletion of floxed alleles. D. Panoramic views of H&E sections of tumor bearing and control $^{NesCre}p53^{+/F};Pten^{+/F}$ brains.

3.2.2 Murine astrocytes irradiated with heavier, more energetic particles are more susceptible to cell killing

We next wanted to use the $^{NesCre}p53^{F/F};Pten^{+/F}$ model to evaluate the transforming effects of a range of charge particles relevant to hadron therapy and space exploration. Before carrying out these studies, we first determined the effects of these ions in vitro on primary murine astrocyte cultures derived from pups. Astrocytes derived from $^{NesCre}p53^{+/F};Pten^{+/F}$ mice grow for only 2-3 passages and cannot be used effectively in a colony formation assay – a standard tool to evaluate cell survival (Mukherjee et al., 2008). Instead, we used $p53^{-/-}$ and $Ink4ab^{-/-}Arf^{-/-}$ immortalized astrocytes. Since Nestin is expressed during embryonal development, the Cre-mediated excision of floxed alleles occurs *in utero* (Dahlstrand, Lardelli, & Lendahl, 1995; Mignone et al., 2004). We irradiated astrocytes cultures grown in monolayer with 0.5 Gy of γ-rays or H, C, Si, and Fe ions and fixed them 0.5h post IR. The resulting DSBs were visualized by 53BP1 staining. Gamma-rays and lighter particles (H, C) induced multiple punctate foci of damage, while transversal by Si and Fe left clustered "tracks" of DSB along their trajectories (**Fig. 3.2A)**. Colony survival assays showed increased cell killing with increasing Z, iron ions being most efficient (**Fig. 3.2B)**. The same dependency between Z/LET and survival was demonstrated with both genotypes, suggesting a generalized enhanced biological effectiveness of heavy particles.

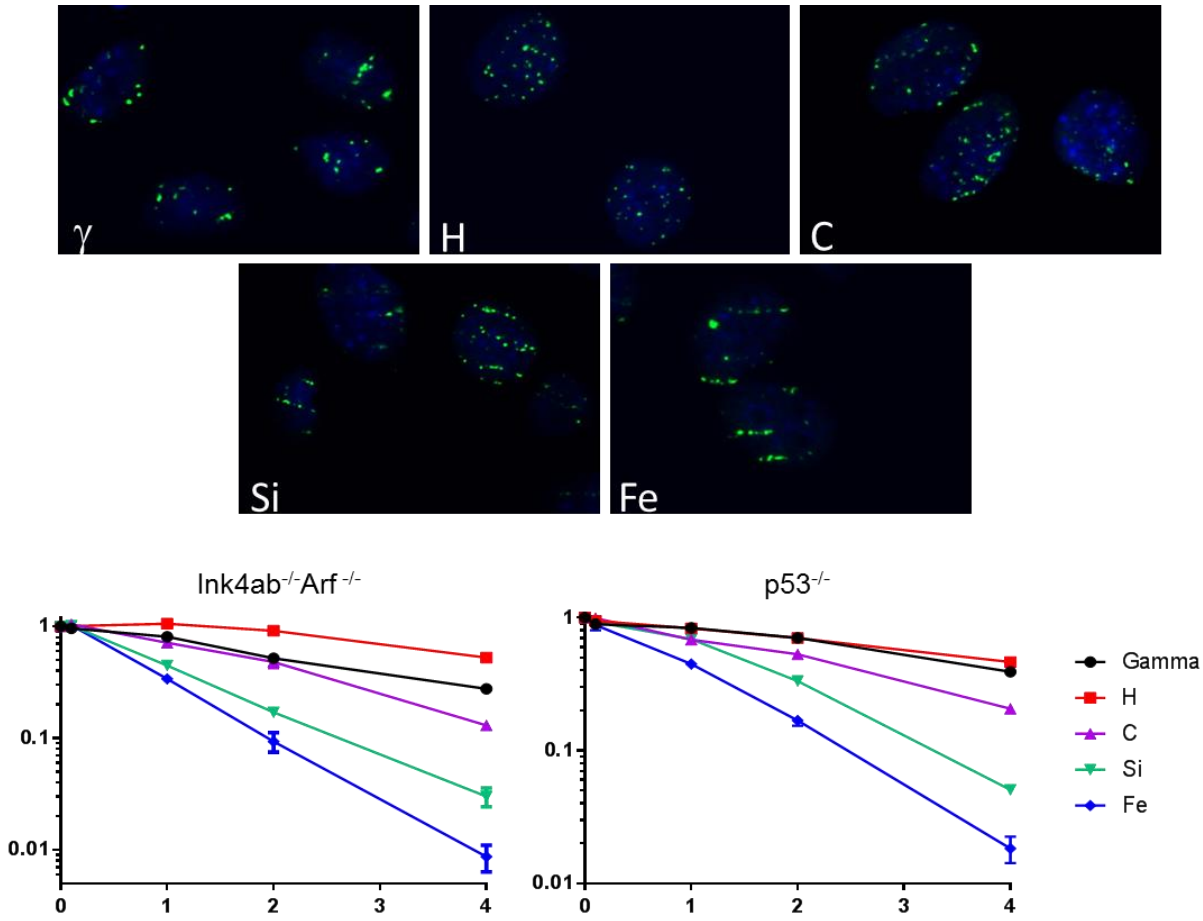

Figure 3.2 Radiation quality effects on murine astrocyte survival. A. Ink4ab$^{-/-}$Arf$^{-/-}$ astrocytes irradiated with 1 Gy of γ-rays or H, C, Si, or Fe ions were fixed at 0.5h post exposure. DSBs were visualized by 53BP1 staining. Nuclei were counterstained with DAPI B. Primary Ink4ab$^{-/-}$Arf$^{-/-}$ and p53$^{-/-}$ astrocytes were irradiated with increasing doses of ionizing radiation. The surviving fraction of cells that formed colonies were quantified and plotted against IR dose.

3.2.3 Silicon ions are more gliomagenic than heavier, more energetic iron ions

Once we had identified an optimal genotype that is independent but complimentary to the ^{NesCre}Ink4ab$^{-/-}$Arf$^{F/F}$ model we wanted establish the effect of radiation quality on gliomagenesis. We exposed cohorts of ^{NesCre}Ink4ab$^{-/-}$Arf$^{F/F}$ and ^{NesCre}p53$^{+/F}$;Pten$^{+/F}$ mice (n=40) to a single intracranial dose of 0.5 Gy of X-rays, hydrogen, carbon, silicon, or iron

ions **(Table 2.1)**. Initial DNA damage was observed in mouse brains 1h following exposure **(Fig. 3.3)**. X-rays and lighter ions (hydrogen and carbon) induced DSBs in a diffused, scattered manner. Irradiations with silicon and iron produced track-like patterns of 53BP1 signal resulting from the dense ionization along the trajectories of traversing particles, as captured in vitro **(Fig. 3.2A)**.

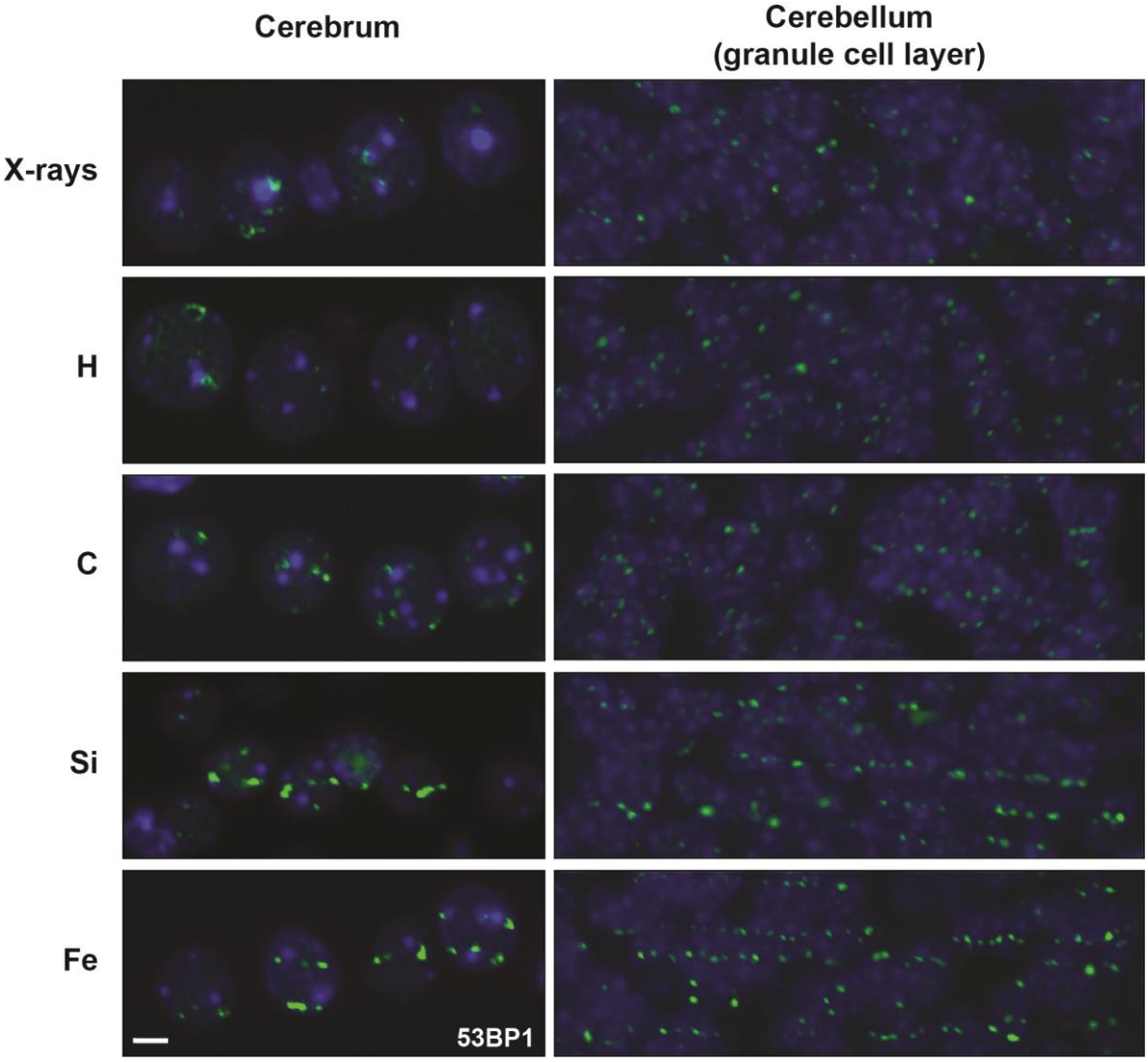

Figure 3.3. DNA DSBs in the mouse brain in response to different types of radiation. DSBs induced by 0.5 Gy of X-rays, H, C, Si, or Fe ions were visualized by 53BP1 staining 1h after exposure. Nuclei were counterstained with DAPI. Representative images of neurons in the cerebrum and the granule cell layer of the cerebellum are shown. Scale bar = 50 μm.

RIGs were observed in all 10 experimental cohorts **(Fig 3.4A).** Chi-square tests performed on the frequencies of each genotype yielded highly significant p-values (0.0013 and <0.0001 for the $^{NesCre}p53^{+/F}$;$Pten^{+/}F$ and $^{NesCre}Ink4ab^{-/-}Arf^{F/F}$ models respectively). Overall, the $^{NesCre}p53^{+/F}$;$Pten^{+/}F$ mouse appeared to be more susceptible to transformation, however, the same trends were observed regardless of genotype. While the tumorigenic potential of hydrogen was similar to that of X-rays, we observed an increase of brain tumor incidence with increasing Z and LET **(Fig 3.4B)**. In the case of the $^{NesCre}Ink4ab^{-/-}Arf^{F/F}$ model the maximum RIG frequency was observed with Si and plateaued at higher LET (Si vs Fe p-value=0.478) **Fig 3.4C)**. The RIG frequency in the more sensitive $^{NesCre}p53^{+/F}$;$Pten^{+/F}$ model actually decreased significantly between the Si and Fe cohorts (p-value=0.0389) indicating that a Z of 14 and an LET of 79 keV/µm may have the worst biological outcomes, at least in terms of carcinogenesis.

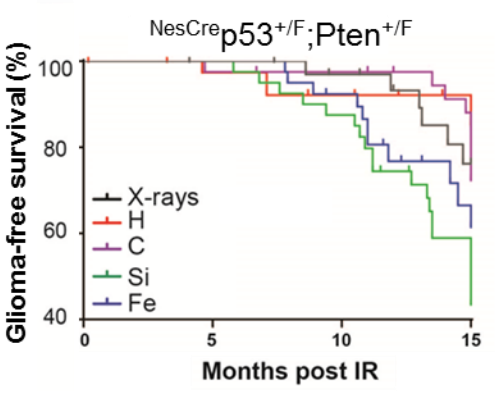

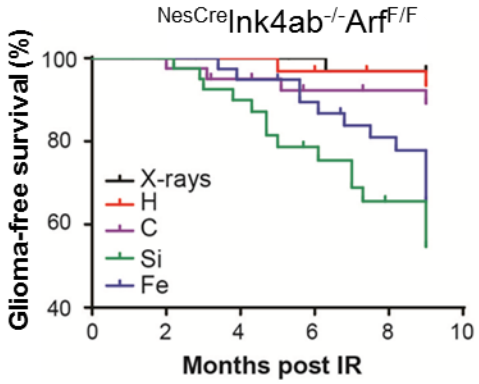

NesCre p53+/F;Pten+/F	Tumor frequency
X-rays	16.2%
H	12.5%
C	22.5%
Si	50%
Fe	27.5%

NesCre Ink4ab-/- ArfF/F	Tumor frequency
X-rays	2.6%
H	5.6%
C	10%
Si	37.5%
Fe	30%

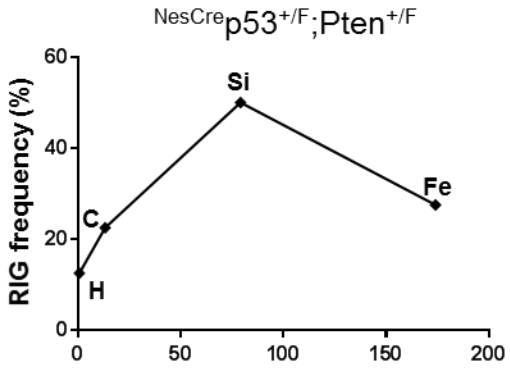

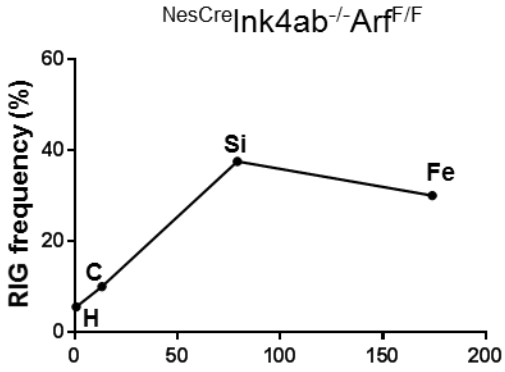

Figure 3.4. Gliomagenesis following exposure to IR. A. Kaplan-Meier curves showing glioma-free survival after exposure to 0.5 Gy of IR. B. Tabulated frequencies of RIG formation in the $^{NesCre}Ink4ab^{-/-}Arf^{F/F}$ and $^{NesCre}p53^{+/F};Pten^{+/F}$ models. C. Relationship between LET and RIG frequency. Maximal frequency was observed with Si (LET=79 MeV/n) regardless of model genotype.

3.2.4 Further evaluation of the relation between LET and gliomagenesis confirms Si as the most tumorigenic ion

Although the same results in terms of peak gliomagenesis were obtained with both models, there was a substantial gap in the Z and LET values between Si and the other species we tested. Thus, additional ions with Z and LET values that fall in between C and Si and between Si and Fe were selected to determine if Si with LET of ~79 keV/μm is one of the most detrimental ions in terms of cancer risk. We exposed two cohorts of $^{NesCre}Ink4ab^{-/-}Arf^{F/F}$ mice to neon (Ne; Z=10; LET=39 keV/μm) and titanium (Ti; Z=22; LET=120 keV/μm) **(Table 2.1)**. The glioma frequency following exposure to Ne was 27.5%, which was comparable to the frequencies observed with Si and Fe ions. This result suggest that the glioma frequency may start to plateau at LET lower than 79 keV/μm. Data collection from the Ti cohort is currently ongoing.

3.2.5 All RIGs phenocopy the histopathological features of high-grade human glioma

Grade IV gliomas (GBM) are defined by the presence of mitotic figures, cellular atypia, pseudopalisading necrosis, and diffuse infiltration into the surrounding brain parenchyma (Aldape et al., 2015; David N. Louis et al., 2014). After examining serial sections of all irradiated brains we found no histological evidence of less malignant tumors or precursor lesions, suggesting that this model recapitulates primary GBM (Ohgaki & Kleihues, 2007). H&E staining revealed single unilateral masses in the forebrain with no distinct borders, oftentimes infiltrating through the corpus callosum **(Fig. 3.5A).** Microscopically, the tumors showed pseudopalisading necrosis **(Fig. 3.5B)** and profound

nuclear atypia **(Fig. 3.5C)**. All mouse RIGs were highly proliferative (Ki67 index >25%). There was no significant difference in the proliferative index between radiation types. Examination of serial coronal sections showed unilateral spread through the subarachnoid space **(Fig. 3.6A),** secondary structures of Scherer (perivascular and perineuronal satellitosis) **(Fig. 3.6B and C)** and prominent mitotic figures **(Fig. 3.6D).** Although invasion was frequent, we did not find brains bearing two or more independent tumors. Collectively, all mouse tumors were histopathologically indistinguishable from human grade III/IV disease regardless of radiation type, Z, or LET.

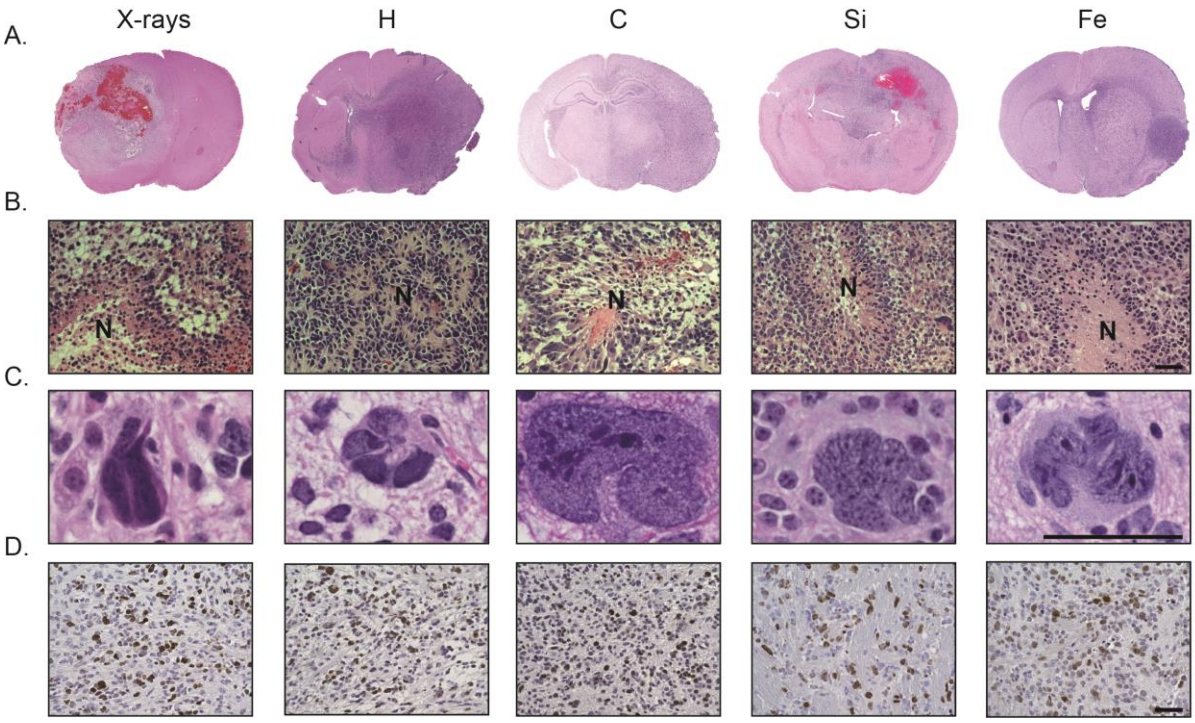

Figure 3.5. IR induces mouse tumors with features of high grade human glioma. A. Coronal brain sections reveal massive unilateral tumors spreading contralaterally through the corpus callosum. Radiation type is indicated above each tumor. B. Examples of GBM-characteristic pseudopalisading necrosis. "N" indicates necrotic area. C. Tumor cells exhibit notable nuclear atypia. D. Ki67 staining demarcates proliferating cells. Scale bar = 50 μm. Representative tumors derived from the $^{NesCre}p53^{+/F}$;$Pten^{+/F}$ model; $^{NesCre}Ink4ab^{-/-}Arf^{F/F}$ tumors display the same histopathology.

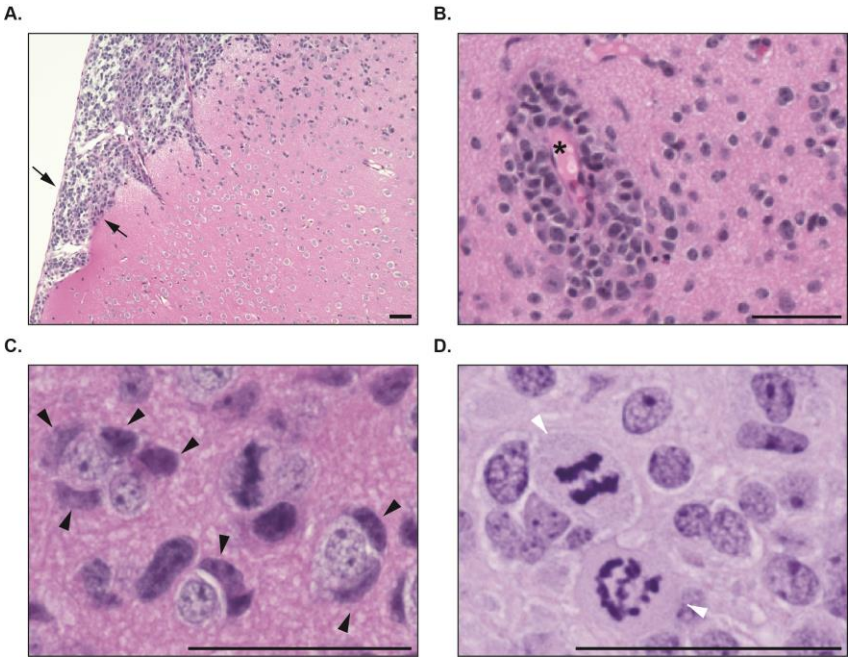

Figure 3.6. Histopathological features of mouse RIGs. A. Tumor cells infiltrating the subarachnoid space is indicated by arrows. B. High density of glioma cells surrounding a blood vessel (*) as an example of perivascular satelitosis. C. Tumor cells growing adjacent to neuronal bodies (perineuronal satelitosis, arrowheads). D. Glioma cells undergoing mitosis. Scale bar = 50 µm.

3.2.6 RIGs express cell lineage markers of glial origin

We used gene expression and immunological assays to further confirm the glial nature of the radiation-induced tumors. In a sample of C-, Si-, and Fe-induced tumors from the $^{NesCre}p53^{+/F}$;Pten$^{+/}$F model we found decreased expression of *NeuN* (a neuronal marker), and elevated mRNA levels of the classical glial markers *Gfap* and *Olig2*, and the progenitor cell marker *Sox2* (a transcription factor important for induction of pluripotency and glioma cell de-differentiation) (Singh et al., 2017; Suva et al., 2014), as compared to control $^{NesCre}p53^{+/F}$;Pten$^{+/F}$ brain tissue **(Fig 3.7)**. Accordingly, the tumors were non-reactive for NeuN, but stained positive for Gfap and, particularly, for Olig2 and Sox2, as determined by

IHC staining **(Fig 3.8)**. Tumors originating from the ^{NesCre}Ink4ab$^{-/-}$Arf$^{F/F}$ model showed an identical pattern of cell lineage marker immunoreactivity (data not shown).

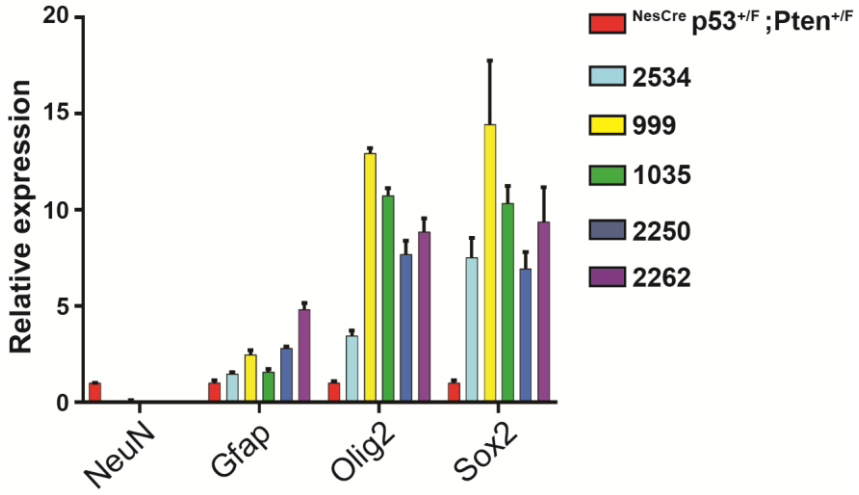

Figure 3.7. Expression of cell lineage markers in RIGs. The relative expression levels of NeuN, Gfap, Olig2, and Sox2 mRNA were determined by qPCR in five RIGs (one C-, two Fe-, and two Si-induced tumors) and compared to expression in ^{NesCre}p53$^{+/F}$;Pten$^{+/F}$ normal brain. All measurements were normalized to 18s mRNA levels. Error bars represent technical triplicates.

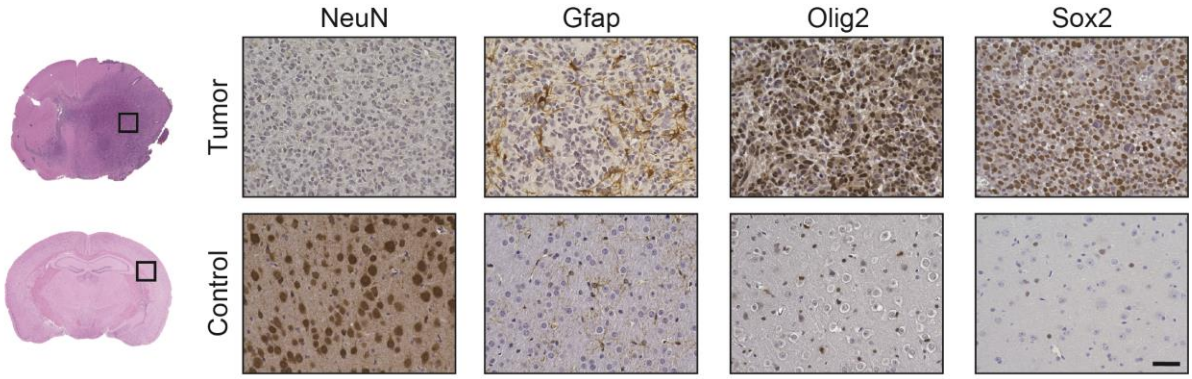

Figure 3.8. Immunoreactivity of RIGs for cell lineage markers. RIGs were negative for NeuN, showed patchy expression of Gfap, and ubiquitous staining for Olig2 and Sox2. Representative images are shown. Nuclei were counterstained with hematoxylin. Scale bar = 50 µm. Representative tumors derived from the ^{NesCre}p53$^{+/F}$;Pten$^{+/F}$ model; ^{NesCre}Ink4ab$^{-/-}$Arf$^{F/F}$ tumors display the same immunoreactivity pattern.

3.2.7 Tumor neurospheres from RIGs possess glioma-propagating stem-like cell (GPSC) qualities

Consistent with the expression on the stem/progenitor marker Sox2, freshly resected $^{NesCre}p53^{+/F};Pten^{+/F}$ tumors were capable of growing in serum-free media as tumor neurospheres. These glioma lines (GLs) maintained Sox2 expression, as determined by IF staining and immunoblotting **(Fig 3.9A and B)**. To test whether the tumor neurospheres contained cells with cancer stem-like cell properties we assessed self-renewal, lineage differentiation, and tumor reconstitution *in vivo*. In vitro experiments confirmed the ability of RIG cultures to self-renew, as shown by single cell sphere formation assay. Over 35% of the single cells plated in 96-well plates were capable of forming secondary tumor neurospheres **(Fig. 3.9C).** Following a short exposure to serum the GLs switched to adherent growth, exhibited a morphology change, and underwent differentiation programs giving rise to heterogeneous lineages of cancer cells **(Fig. 3.10)**. Lastly, upon subcutaneous injections in immunocompromised mice, as few as 500 tumor neurosphere cells were capable of reconstituting tumors (data not shown). All these properties are attributed to human GPSC, and therefore support the conclusion that RIGs contain a population of Sox2-positive cancer stem-like cells (Chen et al., 2012).

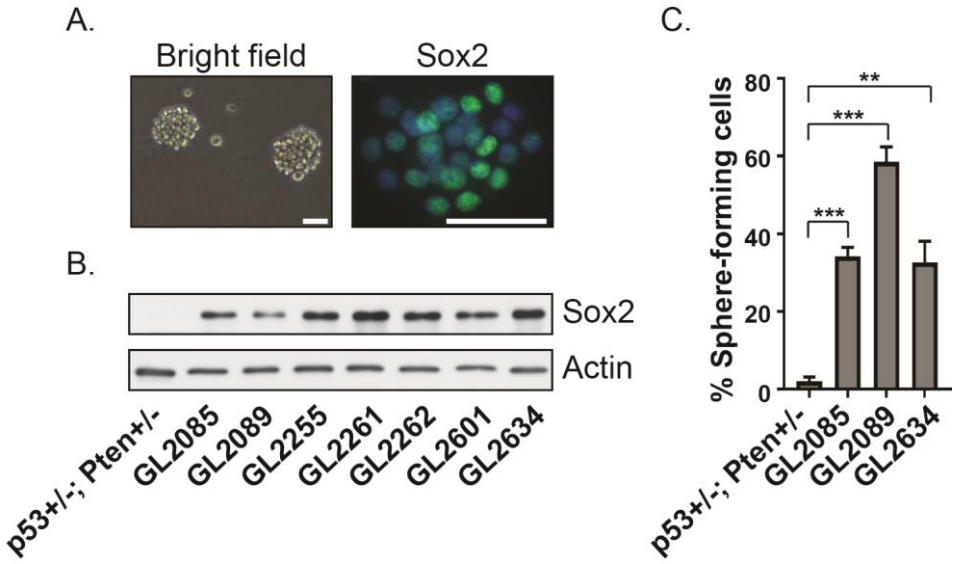

Figure 3.9. Populations of glioma-propagating stem-like cells in RIGs. A. Resected RIGs were cultured as tumor neurospheres that maintained Sox2 expression. Nuclei were counterstained with DAPI. Scale bar = 50 µm. B. Expression of Sox2 was confirmed in a panel of mouse radiation-induced glioma lines (GLs). The self-renewing capacity of GLs was confirmed by a sphere formation assay. Three representative lines are shown. Error bars represent SD from three independent experiments.

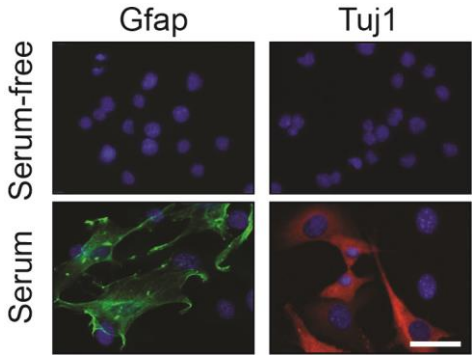

Figure 3.10. Serum-induced differentiation of RIG stem-like cells. GLs established from resected RIGs have a limited capacity to differentiated into astrocytic and neuronal lineages. Upon exposure to serum tumor neurosphere cells exhibited a marked morphology change and expressed Gfap (astrocyte lineage marker) and Tuj1 (neuronal lineage marker). Nuclei were counterstained with DAPI. Scale bar = 50 µm.

3.3 Discussion

Before hadron therapy can be adopted widely and manned deep-space exploration can be executed safely, outstanding questions about the connection between radiation quality and tumorigenesis, including the individual contribution of specific HZE particles, the effect of LET, and the frequency and grade of radiation induced tumors need to be answered. To elucidate the process of IR-induced gliomagenesis we developed two mouse models, which, in the absence of confounding occurrence of spontaneous tumors, are readily transformed by IR. The high prevalence of p53, Pten, and CDKN2A alterations in GBM patients (Cancer Genome Atlas Research, 2008; Parsons et al., 2008; Verhaak et al., 2010) makes both the $^{NesCre}p53^{+/F}$;$Pten^{+/F}$ and $^{NesCre}Ink4ab^{-/-}Arf^{F/F}$ models highly clinically relevant.

Our studies aiming to determine the transforming potential of an array of HZE particles demonstrated gliomagenesis following exposure to iron, silicon, carbon, and hydrogen (and X-rays). We used both models to exclude the possibility of genotype-specific effects and better understand the risk of radiation-induced gliomagenesis. Mice exposed to low-LET radiation (0.5 Gy of protons or carbon) formed tumors 5-20% of the time. This frequency increased to 37.5% ($^{NesCre}Ink4ab^{-/-}Arf^{F/F}$) and 50% ($^{NesCre}p53^{+/F}$;$Pten^{+/F}$) following exposure to silicon but then decreased with further increases in Z and LET. The observed tumorigenesis frequencies are suggestive of a positive association between atomic number and transforming potential for a Z of up to 14 and an LET of up to 79 KeV/μm. Our findings indicate that Si is the most detrimental with respect to carcinogenesis out of all the ions we tested. The observed plateau ($^{NesCre}Ink4ab^{-/-}Arf^{F/F}$) or even decrease ($^{NesCre}p53^{+/F}$;$Pten^{+/F}$) in frequency with LETs higher than 79 keV/μm may reflect a balance between mutagenesis

(transformation) and cytotoxicity occurring at very high LET. As reported here and elsewhere, there is an increase in cell killing with increasing LET *in vitro* (Asaithamby et al., 2008; X. Wang et al., 2015). The fraction of surviving (colony-forming) cells decreases by orders of magnitude following exposure to Fe ions compared to silicon. Additionally, Fe ions have been shown to induce more apoptosis in 3D human vessel models and mouse bone marrow, compared to protons or equitoxic doses of gamma-rays, respectively (Datta et al., 2012; Grabham, Hu, Sharma, & Geard, 2011), suggesting that the increase in cell killing with increasing LET may be relevant *in vivo*. Thus Fe-induced apoptosis in genetically unstable cells following exposure may serve an anti-carcinogenic effect, ultimately diminishing the transforming effect of very high LET by decreasing the possibility of carcinogenic mutations being passed on. Importantly, the results with Si are in agreement with recent acute myeloid leukemia and lung carcinogenesis (X. Wang et al., 2015; Weil et al., 2014) as well as CNS studies (Raber, Marzulla, Stewart, Kronenberg, & Turker, 2015) and certainly warrant further investigation into the mechanistic reasons for the peak observed with Si.

In addition to direct DNA damage, the effects of IR may be exacerbated by ensuing changes in the extracellular matrix (ECM). Irradiated mammary ECM has been shown to be pro-tumorigenic (Illa-Bochaca et al., 2014; Nguyen et al., 2011). In the breast, IR, and in particular HZE radiation has been shown to cause extracellular matrix remodeling that persists over 14 days (Ehrhart, Gillette, & Barcellos-Hoff, 1996). Thus, it is possible that an irradiated cell that has suffered complex but sub-lethal damage can re-enter the cell cycle in the context of an altered ECM environment.

An intriguing conclusion of the work presented in this chapter is that all radiation induced mouse tumors were high grade – corresponding to human grade III/IV disease. None of the 51 tumors arising from all ten cohorts of irradiated mice were classified as grade I or II. The majority of human IR-induced gliomas also present as grade IV, with no radiological evidence of precursor lesions (Broniscer et al., 2004; Yamanaka et al., 2016). Further, clinical studies which compared human RIGs to spontaneous GBMs failed to determine a distinctive histopathology (Brat et al., 1999; Donson et al., 2007; Kleinschmidt-Demasters, Kang, & Lillehei, 2006). Similarly, the mouse RIGs described here are histopathologically indistinguishable from published grade III/IV glioma mouse models employing RTKs overexpression and/or TSG deletions (Alcantara Llaguno et al., 2009; Kwon et al., 2008; Y. Wang et al., 2009; Zheng et al., 2008; H. Zhu et al., 2009). Although X-rays and protons induced tumors less frequently than silicon, their pathological presentations were identical. This suggests that radiation quality affects frequency but not glioma malignancy. One potential explanation for this quantitative difference may stem from the differential kinetics and degree of DSB repair after exposure to low- and high-LET radiation. It has been shown that an inability to faithfully repair DSBs leads to genomic instability, which promotes carcinogenesis (Khanna & Jackson, 2001; Pierce et al., 2001). In this context, Si- or Fe-induced complex breaks which persist longer and are repaired poorly, can contribute to gliomagenesis through the induction of genomic instability (Asaithamby et al., 2011; Asaithamby et al., 2008; Costes et al., 2006; Desai, Davis, et al., 2005; Hada & Georgakilas, 2008a; Leatherbarrow, Harper, Cucinotta, & O'Neill, 2006; H. Wang, Wang, Zhang, &

Wang, 2008). On the other hand, a smaller fraction of the X-rays- and H-induced damage is complex, decreasing the chance of genomic instability induction.

The identification of two mouse models carrying deletions of independent TSGs has allowed us to confirm the universal role of particle radiation as a genotoxic agent capable of inducing high grade gliomas *in vivo*. These models of RIG can be further used to address radiobiology questions seminal to human space exploration (e.g. about the efficacy of countermeasures, the effects of shielding or the exposure to mixed-beam resulting from nuclear fragmentation) or inform the particle choice in hadron therapy.

CHAPTER IV

The genomic landscape of radiation-induced malignant gliomas derived from the $^{NesCre}p53^{+/F};Pten^{+/F}$ model

4.1 INTRODUCTION

High doses of ionizing radiation are received by the majority of cancer patients irrespective of malignancy type or patient demographics. An unfavorable side effect of radiotherapy is the development of secondary cancers (Diallo et al., 2009; Elsamadicy et al., 2015; Salvati et al., 2008; Yamanaka et al., 2016). The adult and pediatric central nervous systems (CNS) are particularly susceptible to radiation-induced malignancies. Exposure to ionizing radiation (IR) is, in fact, the only known risk factor for the development of malignant gliomas - aggressive, therapy-resistant brain tumors, leading to death within 15 months of diagnosis (Bondy et al., 2008; Pearce et al., 2012; Stupp et al., 2009). Exposure to radiation for medical diagnostics increases the relative risk of de novo brain tumors, while adult and pediatric patients undergoing CNS radiation treatment for non-related malignancies present with radiation-induced malignant gliomas (RIGs) later in life (Elsamadicy et al., 2015; Pearce et al., 2012; Salvati et al., 2008; Ward et al., 2014; Yamanaka et al., 2016). Clinical reports describe cases of RIG after acute lymphocytic leukemia (ALL) and brain tumor treatment, the clinical course of which may be more aggressive than that of "spontaneous" GBM (Broniscer et al., 2004; Carret et al., 2006; Donson et al., 2007; Paulino et al., 2008; Yamanaka et al., 2016). Although several groups have attempted molecular analysis of RIG, conclusive findings remain scant due a small patient population spread over multiple institutions (Brat et al., 1999; Broniscer et al., 2004; Donson et al., 2007). These limitations necessitate the experimental modeling and comprehensive analysis of the process of radiation-induced gliomagenesis.

IR is widely used as an anti-cancer treatment due to its cytotoxic and mutagenic properties. In Chapter III we used sparsely ionizing (low LET) and densely ionizing (high LET) radiation to model RIG in mice and study the effect of radiation quality on gliomagenesis. Mouse models with Nestin-Cre driven brain-targeted deletions of *p53* and *Pten* alleles ($^{NesCre}p53^{+/F};Pten^{+/F}$) were exposed to X ray or particle radiation (hydrogen, carbon, silicon or iron; ions of increasing size and LET). We found that these mice, even in the absence of engineered activating oncogenes, are susceptible to transformation by IR. The resulting RIGs faithfully phenocopied the histopathological features of human high-grade gliomas. By applying multidimensional analysis on tumor tissue and ex vivo cultures generated from this mouse model we sought to determine what the molecular changes are that orchestrate the process of radiation-induced gliomagenesis.

4.2 RESULTS

4.2.1 The wild-type allele of *p53* is lost in RIG

Deletion of a single copy of p53 sensitized mice to iron ion radiation-induced gliomas **(Fig 3.1)**. Tumor frequency was increased from 8.1 to 27.5% (p-value=0.0275) upon additional monoallelic deletion of *Pten*. Since in GBM patients p53 is frequently disabled by mutations or deletions (Brennan et al., 2013; Cancer Genome Atlas Research, 2008) we wanted to determine whether the wild type (WT) p53 allele is retained in the case of mouse RIGs. To test the status of the WT allele we performed PCR analysis on tumor DNA. All six tumors tested (one X-rays, one H, three Si, and one Fe-induced tumors) revealed loss of the *p53* WT amplification product, compared to control $^{NesCre}p53^{+/F};Pten^{+/F}$ pancreas and brain

(Fig. 4.1). As expected, Cre-mediated excision of floxed (F) alleles was observed in gliomas and control brain but not in the pancreas.

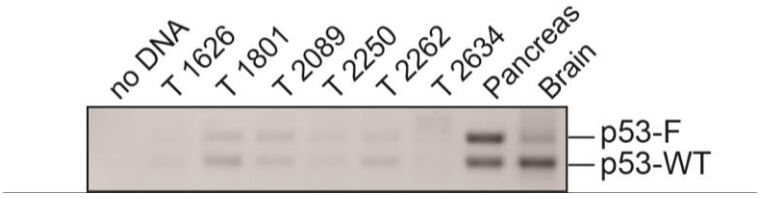

Figure 4.1. RIGs show loss of wild type *p53* allele. Genomic DNA was extracted from tumor tissues and tested for amplification of the WT and floxed *p53* alleles by PCR. Pancreas and brain tissue were included as controls.

4.2.2. Glioma neurospheres are incapable of activating transcriptional targets of p53

The primers used to detect the WT *p53* allele hybridize to a region between exons 1 and 2. To exclude the possibility of a truncated version of p53 being expressed and retaining activity we used assays to assess p53 functionality. DNA damage induced by ionizing radiation is detected by ATM and ATR, which phosphorylate p53 at serine 15 to induce its transcriptional activity (Kruse & Gu, 2009). Exposure of glioma neurosphere cultures to 10 Gy of gamma-rays failed to induce p53 phosphorylation **(Fig. 4.2A)**. While irradiation triggered stabilization of p53 in $p53^{+/-}$;$Pten^{+/-}$ control cells, evident by the increase of total p53 signal, no protein was detected in the GLs or the $p53^{-/-}$ cells. Additionally, no DNA damage-mediated induction of p21 and Mdm2 (transcriptional targets of p53) was observed at 2 and 4 hours post IR, confirming the abrogation of the p53 signaling pathway (Fig. 4.2B and C) (Harris & Levine, 2005; Macleod et al., 1995; Millau, Bastien, Bouchard, & Drouin, 2009).

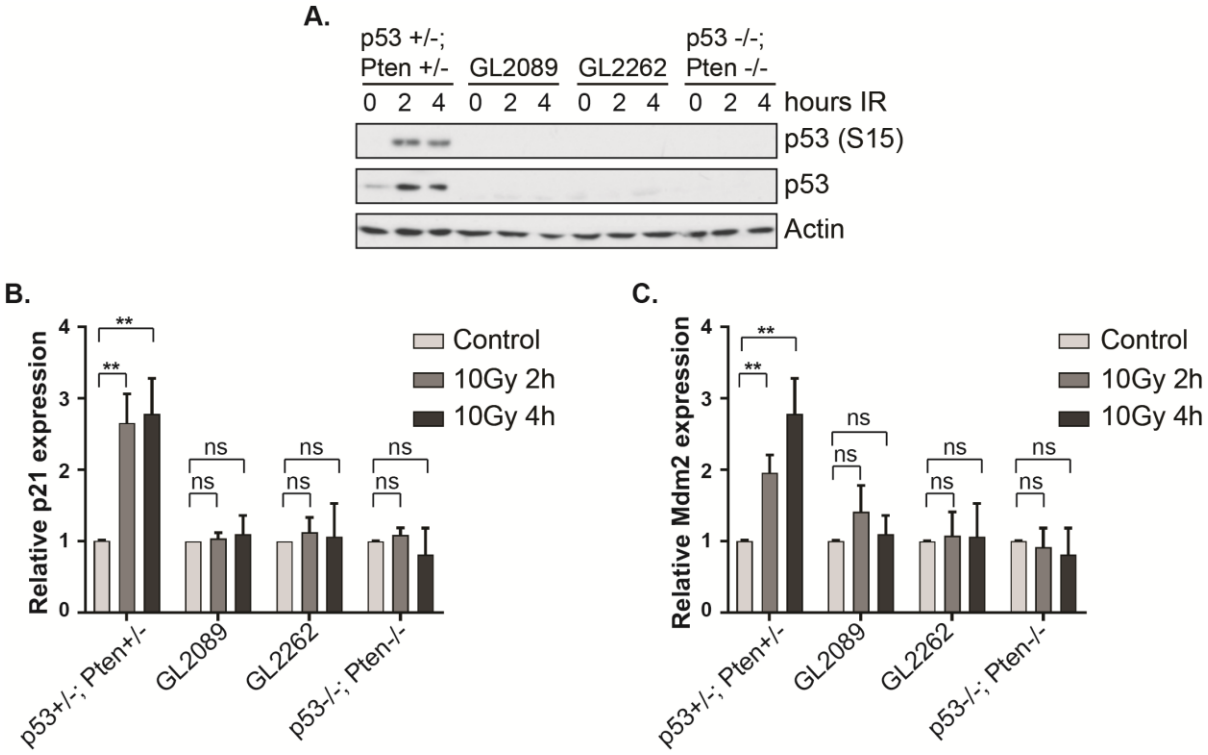

Figure 4.2. Functional inactivation of the p53 pathway in RIGs. A. Protein lysates extracted from RIG GLs at 2 and 4h after exposure to 10 Gy of gamma-rays were probed for total and phosphorylated p53. Actin was used as a loading control. B. Relative levels of p21 mRNA following exposure to 10 Gy of gamma rays. C. Relative expression of *Mdm2* following exposure to 10 Gy of gamma rays. All measurements were normalized to 18s mRNA levels. Error bars represent SD from three independent experiments.

4.2.3 Loss of Pten is observed in all RIGs

In GBM patients the most common route to PTEN inactivation is through deletion (Brennan et al., 2013). To determine the status of the WT *Pten* allele we performed PCR analysis on tumor DNA extracted from the same six tumors tested for *p53* **(Fig. 4.1)**. A PCR assay identified the loss of WT *Pten* allele **(Fig. 4.3A)**. Cre-mediated excision of floxed (F) alleles was observed in gliomas and control brain but not in the pancreas. The observed loss of WT *Pten* was further validated by looking at Pten mRNA expression in five tumors **(Fig 4.3B)**. Further, immunohistochemical analysis of a comprehensive panel of 33 RIG induced

by low- or high-LET radiation showed that all tumors tested were non-reactive for Pten protein **(Appendix A)**. A limited number of RIGs arising in the $^{NesCre}p53^{+/F}$ mice irradiated with Fe ions were also found to be negative for Pten by IHC (data not shown). Pten loss was accompanied by activation of ribosomal protein S6 kinase, Erk, and Akt – downstream components of signaling pathways, inhibited by functional Pten **(Fig. 4.4)** (Gu et al., 1998; Worby & Dixon, 2014). In summary, we demonstrated a concomitant loss of Pten and p53 in all tumors tested, across all radiation qualities. The ubiquitous nature of these events suggests that Pten and p53 may function independently as barriers to radiation-induced gliomagenesis, and that there is a selective advantage for the concurrent loss of both wild-type alleles.

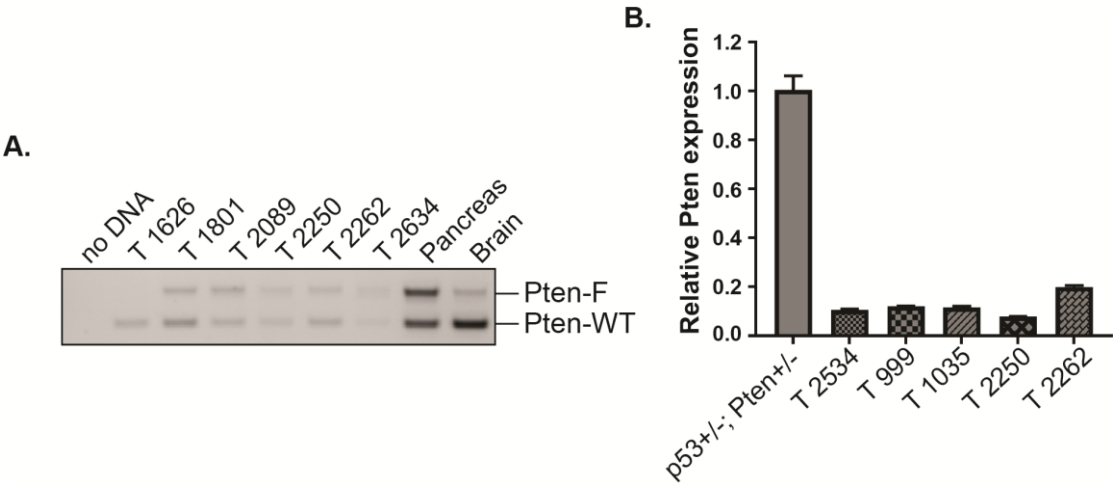

Figure 4.3. Loss of Pten in radiation-induced gliomas. A. Genomic DNA from tumor tissues was tested for amplification of the WT and floxed *Pten* alleles by PCR. Pancreas and brain DNA were included as controls.

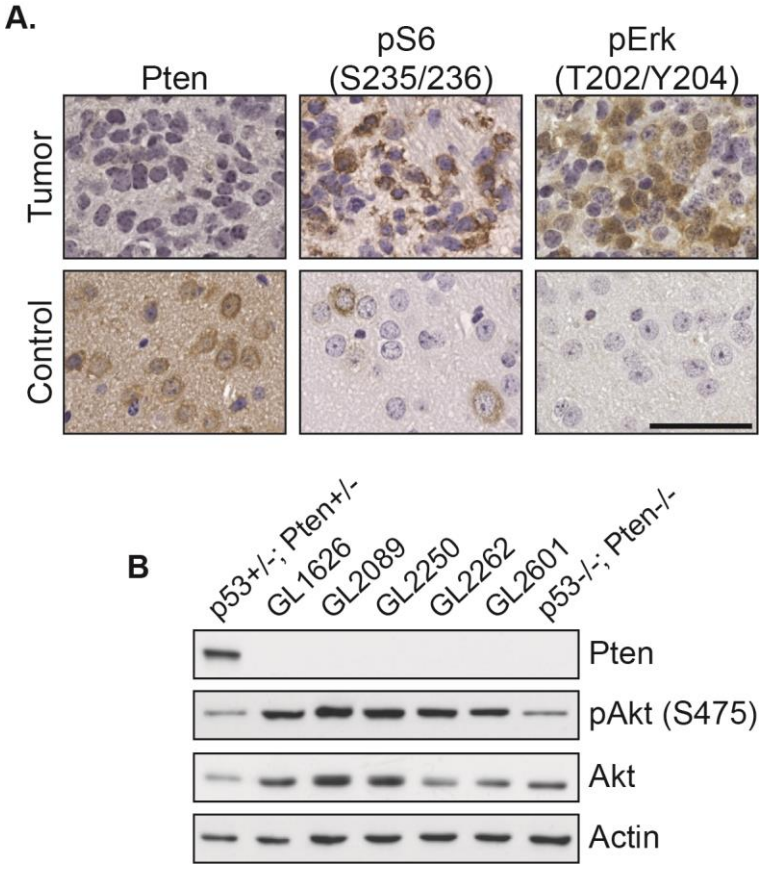

Figure 4.4. Activation of signaling pathways downstream of Pten. A. Immunoreacitivity of tumor and normal brain tissues from $^{NesCre}p53^{+/F};Pten^{+/F}$ animals for Pten, phospho-S6, and phospho-Erk. Scale bar = 50 µm. B. Protein lysates extracted from RIG GLs were probed for Pten and total and phosphorylated Akt. Actin was used as a loading control.

4.2.4 The genomic region containing the Met RTK is commonly amplified in RIG

Having established the concomitant loss of p53 and Pten, we wanted to determine whether there were additional oncogenic changes in the mouse RIGs. Human gliomas bear multiple copy number alterations in the PI3K, p53, and RB pathways, and amplification of RTKs is collectively observed in over 70% of cases (Brennan et al., 2013). We analyzed the genomes of 7 HZE-induced tumors by array comparative genomic hybridization (aCGH) **(Fig 4.5A; Appendix B)**. To detect significantly reoccurring focal and broad copy number

(CN) changes we used the Genomic Identification of Significant Targets in Cancer (GISTIC2.0) algorithm (Mermel et al., 2011). Events with q-value <0.05 were considered significant. This cut-off generated a list of 35 genes falling within the narrow GISTIC peaks **(Appendix C)**. A small region on Chr6 containing the RTK Met (q-value=$1.15x10^{-5}$) was present in 43% (3/7) of tumors tested **(Fig 4.5A&B)**. The homologous region containing human MET is located on chr7 and is amplified focally in 1.6% of GBM patients (Brennan et al., 2013). One mouse sample had a single copy gain, while the remaining two samples had high CN gain (approximately 6 and 50 copies). Met amplification correlated with robust protein expression and activation, as observed in matched tumor sections **(Fig 4.6)**. Met/pMet IHC analysis was extended to a panel of 33 RIG induced by low- or high-LET radiation **(Appendix A)**. Met positivity was found in 48.5% of samples, while the protein was phosphorylated in 36.4%.

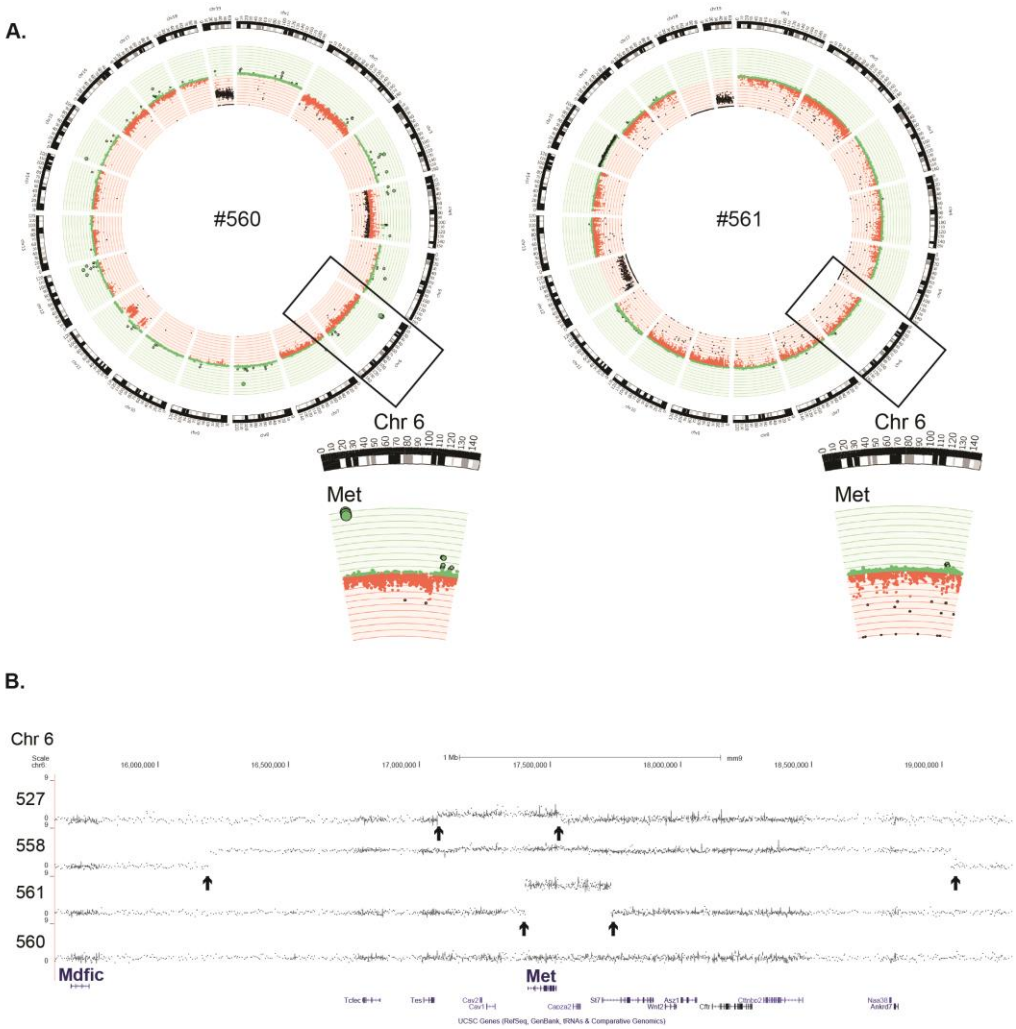

Figure 4.5. Regions of genomic amplifications or deletions in RIGs. A. Circos plots of the genomes of two RIG samples. Green color represents gain of CN and red represents CN loss. A black border indicates a CN change of 1 or more. Magnified views of the boxed regions containing chromosome 6 are shown below each circos plot. B. Genomic tracks of the Met-containing region on chr6. The three samples with CN gain are shown together with one non-amplified sample. Arrows indicate the borders of the amplified regions. Log2 ratios of CN are plotted on the y-axis.

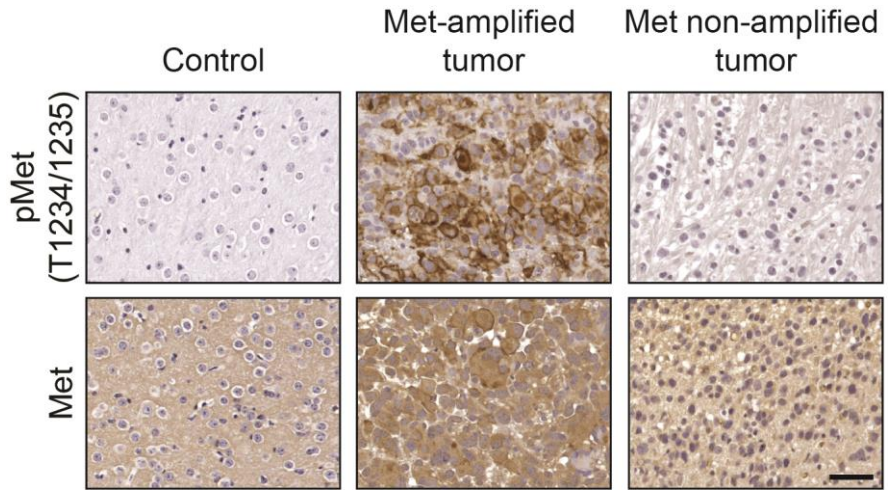

Figure 4.6. Expression of Met in RIGs with or without focal amplification of chr6. The same tumors (560 amplified, 561 non-amplified) shown in **Figure 4.5** were stained for phospho- and total Met. Scale bar = 50 μm.

The region containing the Met locus was the only CN gain event considered significant by GISTIC. *Egfr* amplification, occurring in 60% of GBM patients, was present in one sample, where a single-copy gain had occurred (Brennan et al., 2013). *Pdgfr-α* amplifications were not detected. However, as previously reported in $p53^{-/-}$;$Pten^{-/-}$ mouse GBM, all RIGs over-expressed Pdgfr-α **(Appendix A)** suggesting that Pdgfr-α signaling is common in p53/Pten-mediated gliomagenesis, (Chow et al., 2011; Y. Wang et al., 2009). Similarly, transgenic mouse models and human GBM patients often overexpress PDGFR-α without an underlying genomic amplification (Chow et al., 2011; Furnari et al., 2007; Zheng et al., 2008).

4.2.5 Ectopic expression of Met in $p53^{-/-}$;$Pten^{-/-}$ astrocytes confers the ability to grow under serum-free conditions

Besides orchestrating growth factor-mediated proliferative signaling, the Met RTK has also been linked to the induction and maintenance of a "stemness" phenotype in glioma

cells (Camacho et al., 2015; Kyeung Min Joo et al., 2012; Y. Li et al., 2011). To determine the effect of Met in the context of p53 and Pten losses (as seen in the RIGs), $p53^{-/-}$;$Pten^{-/-}$ primary astrocytes were transfected with lentiviral vectors expressing V5-tagged β-Gal (control) or human MET. The presence of V5-tagged proteins was confirmed in protein lysates **(Fig 4.7 A)**. Expression of MET did not confer additional growth advantage, as these cells are already rapidly proliferating (data not shown). However, $p53^{-/-}$;$Pten^{-/-}$ MET cells were able to grow in serum-free conditions as neurospheres. The ability of these cells to self-renew was assessed via single cell sphere formation assay; more than half of the single cells had formed spheres 12 days after plating **(Fig 4.7 B)**. β-Gal transfected cells were incapable of forming spheres or self-renew under these conditions (p-value=0.0002). The functionality of MET in the generated neurospheres was confirmed by the ability of HGF supplementation to the growth media to induce phosphorylation **(Fig 4.7 C)**.

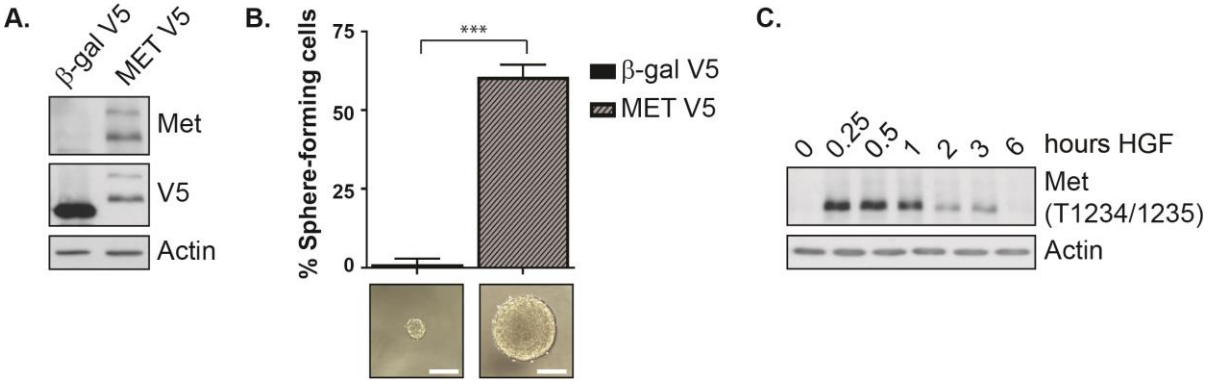

Figure 4.7. Ectopic expression of MET in $p53^{-/-}$;$Pten^{-/-}$ astrocytes. A. Expression of V5-tagged proteins was assessed by immunoblotting. Whole-cell lysates were probed for Met and V5. Actin served as a loading control. B. Expression of MET conferred the ability to form neurospheres from single cells. Images below the graph show representative spheres 12 days after plating. Error bars derived from standard deviation from three independent experiments are shown. Scale bar = 200 μm. C. Supplementation of the growth medium with HGF induced robust phosphorylation of MET. Cell lysates were generated at indicated time-points following treatment with 50 ng/mL HGF and probed for phospho-MET. Actin served as a loading control.

4.2.6 Ectopic expression of MET in a tumor neurosphere culture confers radioresistance

Through its role in GBM stem-like cell maintenance Met may be contributing to the therapeutic resistance ascribed to this subpopulation (Bao et al., 2006; Baumann et al., 2008; Bleau et al., 2009). Stem-like cells extracted from GBM patients have been shown to be more radioresistant compared to bulk tumor cells, and the status of MET expression has been linked to the observed survival benefit (Bao et al., 2006; De Bacco et al., 2016; Kyeung Min Joo et al., 2012). To determine whether Met expression would confer radioresistance to GLs generated from RIGs we expressed human MET or β-Gal in a tumor neurosphere culture **(Fig. 4.8A).** Similar to the $p53^{-/-}$;$Pten^{-/-}$ astrocytes, the tumor cells expressing ectopic MET did not gain a proliferative advantage (data not shown). Self-renewal was also unaffected by MET expression (**Fig 4.8B** 0 Gy dose). However, the self-renewing capacity was significantly increased in MET-positive cells exposed to 2 of 4 Gy of IR, compared to the isogenic β-Gal groups. Even at the highest dose (6 Gy) more spheres were observed in the MET-expressing cells although the trend did not reach statistical significance.

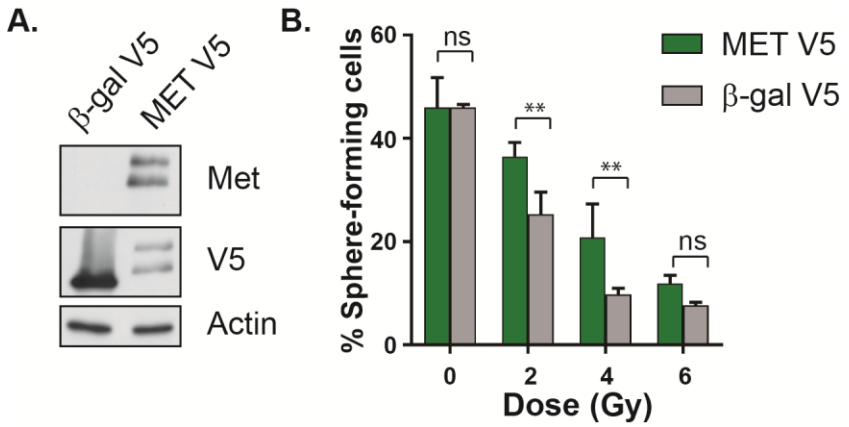

Figure 4.8. Ectopic expression of MET in a RIG neurosphere culture. A. Expression of V5-tagged proteins was confirmed by immunoblotting. Whole-cell lysates were probed for Met and V5. Actin served as a loading control. B. The self-renewing capacity of MET- and β-Gal-expressing GL2089 cells following exposure to gamma-rays was assessed by single sphere formation assay. Error bars represent standard deviation from three independent experiments.

4.2.7 Radiation quality dictates a distinct mutational signature

Ionizing radiation has been shown to generate distinctive mutational signatures in secondary non-CNS cancers (Behjati et al., 2016). Whole genome sequencing of 12 radiation-associated secondary tumors revealed a highly significant enrichment of small-scale deletions. Similarly, we wanted to determine whether radiation quality could contribute to a distinction in the mutational signatures of mouse RIGs derived from different LETs. Using whole genome sequencing we analyzed 2 X-rays (low-LET electromagnetic radiation), 2 H (low-LET particulate radiation) and 2 Si (high-LET particulate radiation) –induced tumors. A non-tumor genome was included to control for mouse strain-specific genomic variation. The majority of significant events detected in all tumors regardless of radiation quality were deletions. Genome-wide there was a qualitative difference in the scale of deletions between electromagnetic and particulate radiation-induced GBMs **(Fig. 4.9A)**. The median event lengths in the X-ray tumors were in the range of 5000-10 000 base pairs (bp).

In contrast, the lengths of significant events in the particle-induced tumors ranged from 65 000 to $20x10^6$ bp, often resulting in whole chromosome monosomies **(Fig. 4.9A&B)**. Further, X-rays tumors carried a higher number of non-contiguous significant events **(Fig. 4.B)**.

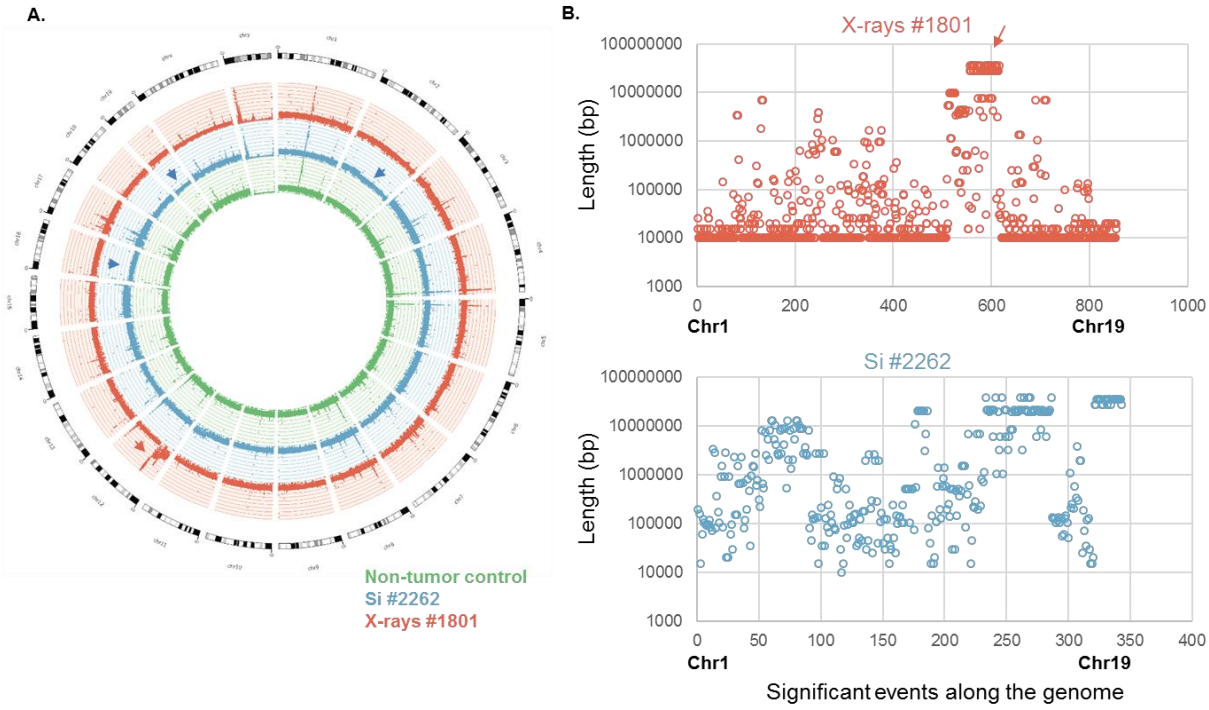

Figure 4.9. Whole-genome sequencing RIGs. A. A circos plot comparing the genomes of representative Si (blue) and an X-rays (red) induced RIGs. A non-tumor genotype-matched control genome is shown in green. Blue arrows indicate large-scale deletions in the Si tumor; red arrow indicates a region of focal amplification on chr12 in the X-ray tumor. B. The length of all significantly deleted or amplified regions (y-axis) was plotted along the genome (x-axis). Each open circle represents an event. Red arrow indicates the region of focal amplification on chr12 in the X-ray tumor. Please note the difference in scale along the x-axis.

4.3 DISCUSSION

As the success rate of managing malignancies increases, the need to understand and prevent RIGs becomes pressing, particularly for childhood cancer survivors with long life expectancy. The 5-year survival rate of "standard risk" pediatric patients with brain and CNS tumors and acute lymphocytic leukemia (ALL), which together amount to 47% of all childhood cancers, is 75% and 90% respectively (Hunger & Mullighan, 2015; Ward et al., 2014). Although these numbers are very encouraging, the successful treatment frequently involves irradiation of the CNS, which is particularly susceptible to secondary, radiation induced malignancies (Crawford, MacDonald, & Packer, 2007; Massimino et al., 2016; Ward et al., 2014). Existing reports describing cases of RIG after brain and CNS tumor and ALL treatment are suggestive of a more aggressive phenotype with average survival of only few months (Donson et al., 2007; Paulino et al., 2008; Yamanaka et al., 2016). A comprehensive genomic landscape of RIG has not been obtained due to a limited availability of patient samples distributed over multiple institutions (Broniscer et al., 2004; Donson et al., 2007). Past studies have mostly focused on examining a small set of GBM-relevant genes including *TP53* and *EGFR* through IHC or exon-targeted sequencing. Thus far, somatic p53 mutations resulting in single amino acid substitutions have been identified in human RIGs (Brat et al., 1999; Gessi et al., 2008; Tada, Sawamura, Abe, & Iggo, 1997; Yang et al., 2005). A PubMed database search on clinical cases points to a lower frequency of EGFR amplification and immunoreactivity compared to spontaneous GBM (Alexiou et al., 2010; Brat et al., 1999; Gessi et al., 2008; Yang et al., 2005). The most in-depth molecular analysis of RIG published

up to date examined 5 samples from pediatric patients by genome-wide gene expression microarray (Donson et al., 2007). The authors identified a higher number of conserved signature genes with more tightly defined gene expression profiles within the RIGs as compared to de novo pediatric GBMs. Among the highest-expressed genes were PDGFR-α, OLIG1, and OLIG2. None of the RIG cases reported displayed unique mutations not seen in spontaneous GBMs.

In the absence of sufficient human samples, our ultimate goal behind identifying animal RIG models was to elucidate the genomic changes accompanying the process of radiation-induced tumorigenesis. The experiments described in this chapter utilized a set of RIGs, driven by different radiation qualities, in mice with monoallelic deletions of floxed *p53* and *Pten* copies. Through genomic and functional assays, we established the universal loss of the remaining wild-type alleles. Unlike the mutual exclusivity of events targeting genes converging on the same downstream pathway observed in GBM, losses of p53 and Pten were concomitant. This signifies the crucial role p53 and Pten together play as barriers to radiation-induced transformation. The importance of combined tumor suppressor loss was further demonstrated in tumors arising in Pten-wild type $^{NesCre}p53^{+/F};Pten^{+/+}$ mice irradiated with Fe ions where Pten was not detected immunologically.

Overall, the molecular events we identified (Pten loss, Met amplification, Pdgfr-α over-expression) match known abrogations occurring in human RT-induced and spontaneous GBMs, establishing the clinical utility of the $^{NesCre}p53^{+/F};Pten^{+/F}$ model. One discrepancy between our results and the limited human RIG molecular data was the ubiquitous occurrence of p53 deletions rather than mutations. Germline missense mutations in *TP53* are

the cause of a cancer predisposition syndrome called Li-Fraumeni (McBride et al., 2014). Among other malignancies, Li-Fraumeni patients present with gliomas, underscoring the importance of p53 in the epidemiology of familial GBM. In sporadic cancers missense mutations constitute 80% of the p53 mutations (Royds & Iacopetta, 2006). Such alterations usually affect the DNA-binding domain and lead to the synthesis of a full-length stable protein monomers (Muller & Vousden, 2014). Since the activity of p53 requires the assembly of a homotetramer, a mutated monomer in a complex with three wild-type units can exert a dominant-negative effect. Thus, a single amino acid substitution can effectively result in p53 functional nullizygosity and be more tumorigenic than a heterozygous deletion. In primary and radiation-induced human gliomas *TP53* missense mutations are more common than deletions (Cancer Genome Atlas Research, 2008). This is in stark contrast with the observed genomic loss in the $^{NesCre}p53^{+/F}$;$Pten^{+/F}$ RIGs. One possible explanation for this discrepancy may stem from the fact that the cells of origin in the mouse model have only one functional *p53* copy. Therefore, a monoallelic deletion is sufficient to disable the p53 pathway. This preponderance of allelic deletion over mutation is seen in another transgenic mouse model of glioma. Zhu et al., utilized a Cre-mediated deletion of *NF1* using the hGFAP promoter in a germline heterozygous p53 background (Y. Zhu et al., 2005). hGFAP-Cre drives embryonal excision of floxed alleles leading to recombinase-mediated deletions in adult neural progenitor cells, neurons, astrocytes, and oligodendrocytes - populations targeted by the Nestin-Cre model used in our study. These mice formed spontaneous tumors which recapitulated human GBM and lost WT p53 by means of genomic deletion.

Additional mouse models with embryonic (all CNS lineages) or inducible (astrocytes and neural precursor cells) targeted homozygous deletions further validate the gliomagenic effect of compound p53 and Pten loss (Chow et al., 2011; Jacques et al., 2010; Zheng et al., 2008). Nullizigosity of p53 combined with Pten heterozygosity (or homozygosity when utilizing the Cre-ER recombinase) is sufficient to generate a penetrant acute-onset high grade malignant glioma phenotype which recapitulates human primary GBM. Interestingly, Chow et al., subjected GFAP-CreER^{T2} p53$^{F/F}$;Pten$^{F/F}$ tumors to aCGH analysis and found the Met-containing region on chr6 to be the most common focal amplification (24%) (Chow et al., 2011). Compared to their results, we found higher frequency of Met amplification (43%). Although our aCGH sample size was small, existing evidence suggest that Met overexpression correlates with gene amplification, and Met immunolabeling has been used successfully as a predictive tool for gene amplification in GBM (Burel-Vandenbos et al., 2017; Ohshima et al., 2017; Santarius, Shipley, Brewer, Stratton, & Cooper, 2010). Thus, based on the panel of 33 samples stained for phospho- and total Met it is plausible to assume the frequency of Met amplification in RIG approximates 40% **(Appendix A)**. The elevated frequency of chr6 amplification in RIG may indicate a direct or an indirect, (DNA damage-induced) genomic instability-mediated effect of IR, combined with positive selection pressure for clones expressing Met.

MET signaling activates the PI3K-AKT and RAS-MAPK pathways and affects gene expression and cell cycle progression through the action of downstream transcription factors, such as the ETS family members **(Fig. 1.2)** (Gherardi, Birchmeier, Birchmeier, & Vande Woude, 2012). Physiologically, MET is important for epithelial-to-mesenchymal transition

and cell migration during embryogenesis, tissue regeneration, and wound healing (Trusolino, Bertotti, & Comoglio, 2010). These roles are hijacked by cancer cells, in which aberrant MET activation is key for cell survival, invasion, and metastasis (Gherardi et al., 2012). MET has been implicated in renal, hepatocellular, gastric, and colorectal carcinomas, and basal-like breast cancer. In GBM, *MET* is focally amplified in 1.6% of cases. Despite relative rarity, overexpression of MET has been associated to a shorter survival and poorer response to treatment (Kong et al., 2009). Several laboratories have shown expression of MET in GBM ex-vivo cultures, where it plays a role in the maintenance of a stemness phenotype, possibly through the indirect induction of reprogramming transcription factors (Bazzoli et al., 2012; De Bacco et al., 2012; K. M. Joo et al., 2012; Laterra et al., 1997). Additionally, a role in radioresistance mediated by the activation of the DNA damage response (DDR) machinery has been ascribed to MET expressed at high levels in GBM stem-like cells (De Bacco et al., 2016). MET could also contribute to radioresistance indirectly through the induction and maintenance of cancer stem-like cells which are inherently more radioresistant (Bao et al., 2006; Baumann et al., 2008). Importantly, inhibition of MET has been shown to have clinical benefits, providing a viable therapeutic target in GBM patients with MET amplifications (Chi et al., 2012; International Cancer Genome Consortium PedBrain Tumor, 2016).

In accordance with a role in stemness phenotype maintenance, ectopic MET expressed in $p53^{-/-}$;$Pten^{-/-}$ murine astrocytes conferred the ability to grow in serum free conditions and propagate spheres from single cells. The high efficiency with which self-renewing tumor neurospheres were generated may have been driven by a synergistic effect of MET expression and p53 loss. Established de-differentiation paradigms involve the forced

expression of the Sox2, cMyc, Oct3/4, and Klf4 transcription factors (Takahashi & Yamanaka, 2006). The efficacy of induced pluripotent stem (iPS) cell induction is limited by p53 which exerts inhibition in a dose-dependent manner (Hong et al., 2009; Kawamura et al., 2009). Complete loss of p53 increases iPS cell induction efficiency significantly. Expression of two out of the four factors (Sox2 and Oct4) in $p53^{-/-}$ mouse and human embryonic fibroblasts is sufficient for reprogramming (Kawamura et al., 2009). MET, which is not a *bona fide* iPS factor, has been linked to induction of stemness through the upregulation of such factors (Y. Li et al., 2011). Thus, ectopic expression of MET in murine astrocytes which are "primed" for reprogramming by p53 deletion could be sufficient to drive the reported acquisition of tumor neurosphere phenotype. Such cooperativity between p53 and Met in the induction of stemness was recently described in a mouse model of basal-like breast cancer (Chiche et al., 2017). Patients with basal-like breast cancer, which is characteristically poorly differentiated and contains breast cancer stem-like cells, present with TP53 abrogation 80% of the time (Sorlie et al., 2001). Such TP53-mutated cancers often overexpress MET. p53 deletion in a Wnt/β-Catenin-driven mouse model of basal-like breast cancer resulted in the expansion of a cell population with stem-like properties. The functionality of these stem-like cells was enhanced by HGF and decreased by volitinib, a Met-specific inhibitor (Chiche et al., 2017).

Not all tumorsphere cultures described here were derived from Met upregulating tumors, as determined by aCGH and IHC. It is possible that in those cases alternative oncogenes collaborate with the loss of p53 to induce stemness. In addition to Met, RIG showed overexpression of Pdgfr-α, another RTK also expressed in patients and mouse

models of GBM (Chow et al., 2011; Furnari et al., 2007; Zheng et al., 2008). Pdgfr-α signaling impinges on many of the pathways activated by Met and thus may serve a synonymous function in the induction of stemness in the context of p53 loss. Alternatively, Myc signaling may also collaborate with p53 loss. Myc is a known oncogene and one of the four Yamanaka factors used in the somatic reprogramming of iPS cells. Zgeng et al., reported a p53/Pten nullizygosity-driven activation of Myc in a hGFAP-Cre $p53^{F/F}$;$Pten^{+/F}$ GBM model. Accordingly, we also observed an upregulation of Myc in tumor neurosphere cultures in the context of p53 and Pten loss (data not shown).

Finally, we showed that a tumor neurosphere culture expressing MET ectopically acquired resistance to gamma radiation. Since these cells possessed a stem cell-like phenotype prior to transduction, it is likely that ectopic MET contributed to resistance through upregulation of the DDR signaling, as recently proposed by De Bacco et al., (De Bacco et al., 2016). Preliminary experiments demonstrated that cell lysates from tumor neurosphere cultures had increased levels of DDR proteins compared to serum-differentiated matched glioma lines. However, additional assays are required to elucidate the exact contribution of MET to radioresistance with the goal of designing multi-pronged treatment approaches eliminating the GBM bulk and stem cell populations simultaneously and permanently.

The identification of distinct mutational signatures in the electromagnetic and particulate radiation-induced tumors is of interest, as it could conceivably be attributed to the initial DNA damage and repair (extensively discussed in Section **3.3**), and could represent a radiation quality effect. A recent effort to distinguish a mutational signature of IR in

secondary tumors utilized whole-genome sequencing of 12 radiation-associated secondary malignancies of four different types (osteosarcoma, spindle cell sarcoma, angiosarcoma, and breast cancer) (Behjati et al., 2016). Although the observed driver mutations were similar between matched spontaneous and radiation-associated tumors, the authors identified two radiation-specific signatures that transcended tumor type: excess small deletions and balanced inversions. Although we have not examined our data for the presence of balanced inversions, in the X-rays induced tumors we observed abundant, uniformly distributed small deletions, reminiscent of the reported mutational signatures of human radiation-associated tumors. Interestingly, deletions in the particulate radiation induced tumors were longer but fewer in number. The validity of this result may be limited by the number of tumors sequenced; additional studies would be required to establish if a radiation-quality mutational signature exists. However, given the clustered nature of ionization (and subsequent DNA damage, **Figs. 1.7 and 1.8**) characteristic of particulate radiation, our results certainly warrant further investigation.

CHAPTER V

Conclusions and future directions

Knowledge gap narrowed

The work presented in this dissertation establishes the role of both terrestrial and space radiation in gliomagenesis. Through the use of animal models validated in the course of this dissertation (^{NesCre}Ink4ab$^{-/-}$Arf$^{F/F}$ and ^{NesCre}p53$^{+/F}$;Pten$^{+/F}$) we have provided evidence of the potent ability of IR to induce high grade GBMs in specific mouse model susceptible to glioma initiation. Further, using these two complimentary but independent models which faithfully recapitulate the process of radiation-induced gliomagenesis we have established a relationship between LET and glioma frequency. Following a systematic analysis of large mouse cohorts, we determined the carcinogenic effects of conventional RT electromagnetic radiation (250 kV X-rays), therapy grade proton (150 MeV/n ^{2}H) and carbon (290 MeV/n ^{12}C), as well as space-exploration pertinent heavy silicon and iron particles (238 MeV/n ^{32}Si and 600 MeV/n ^{56}Fe). Data on the effects of particle size and LET on radiation induced glioma (RIG) frequency illustrate the importance of using animal models in the evaluation of the carcinogenic effects of IR. The shape of the LET versus gliomagenesis curve **(Fig 3.4)**, with a peak at Si (Z of 14 and an LET of 79 keV/μm) and subsequent plateau, differs from the linearity observed between LET and biological effects *in vitro*, likely reflecting a balance in mutagenesis and cytotoxicity required for maximal glioma induction.

All radiogenic gliomas, regardless of radiation quality recapitulated the clinical course of primary GBM. Tumors presented classical GBM histopathological features and cell lineage markers. The observed driver mutations in the RIGs followed the pattern seen in spontaneous mouse GBM models and human patients. Similar with published data we observed abrogations in the GBM-relevant PI3K and TP53 pathways (Brennan et al., 2013).

This establishes the clinical utility of our models and suggests a broader use of radiation in glioma pre-clinical modeling. We did, however, observe certain events (Met amplification, concomitant loss of p53 and Pten) that are not typically seen in human tumor formation, while other frequently targeted genes were generally unaffected (*EGFR, CDKN2a*) (discussed in Section **4.3**). These observations may be interpreted to suggest that some aspects of radiation-induced glioma may be considered a separate pathological entity with distinct clinical progression, requiring tailored treatment (Brat et al., 1999; Donson et al., 2007; Prasad & Haas-Kogan, 2009).

Our complementary *in vitro* assays emphasize the importance of evaluating GBM drivers as integrated nodes in an oncogenic signaling network, rather than simply targets for monotherapy. For example, expression of MET in the context of p53 loss was sufficient to confer a stemness phenotype to adherent murine astrocytes. Similarly, the observed enhanced radioresistance of p53-negative MET-overexpressing tumor neurospheres could have been mediated by the simultaneous effects of MET on stemness and on DDR-mediated IR damage resolution as postulated by De Bacco et al., (discussed in Section **4.3)**. All these findings should be taken into consideration if we are to develop treatment approaches eliminating GBM bulk and stem cell populations simultaneously and permanently.

Future directions

To further estimate the transforming potential of charged particles in terms of their atomic numbers, LETs, and dose

As demonstrated, our transgenic model systems are "primed" to be tumorigenic and are ideal for rapidly and quantifiably evaluating the tumorigenic potential of HZE particle radiation. Through systematic analysis we observed an increase of gliomagenesis with increasing Z and LET, with a peak at Si, past which lower frequencies were seen. The ions we chose provided incremental increases in nuclear size and ionization potential. Going forward, additional experiments can be designed to further dissect the individual contributions of Z and LET. This can be achieved in at least two complementary ways. First, by keeping Z constant, while manipulating the energy (the speed with which the ions will pass through the brain), we can expose mouse cohorts to Si ions of different LET. Alternatively, we can manipulate the energy of three different particles (e.g. C, Si, and Fe) to achieve constant LET, and then compare the relationship between atomic size and gliomagenesis.

The fact that both models developed RIGs with high frequency provides a window of opportunity to evaluate the effect of dose on GBM risk. Although risk estimates based on epidemiological studies on human populations exposed to high doses of IR are dependable, it is harder to distinguish between radiation-induced and spontaneous tumors when the absorbed doses are low. By using large cohorts of $^{NesCre}Ink4ab^{-/-}Arf^{F/F}$ and $^{NesCre}p53^{+/F};Pten^{+/F}$ mice we may be able to determine if there is a safe dose that does not contribute to extra

cancer risk, or whether the relationship between absorbed dose and carcinogenesis is truly linear.

To understand how specific DNA repair pathways act as barriers to HZE-induced carcinogenesis

As discussed in Chapter II, the observed variation in RIG frequency with radiation quality may be attributed to the nature of the underlying radiogenic damage, and to how proficient the cell is in DSB repair. Two major pathways have evolved to repair these breaks – non-homologous end joining (NHEJ) and homologous recombination (HR) (Heyer, Ehmsen, & Liu, 2010; Lieber, 2010; Wyman & Kanaar, 2006). A number of studies have investigated the relative usage of these pathways in the repair of complex DSBs induced by particle radiation *in vitro*. An emerging consensus is that HR may be more critical in the cellular response to particle radiation, as NHEJ may not be able to repair clustered DSBs inflicted by high LET radiation (Moore et al., 2014). Since our mouse models are "primed" for radiation-induced gliomagenesis by the deletion of key TSGs, we can evaluate the importance of DNA repair pathway at the organismal level, by incorporating deletions of DDR genes, and selectively disabling HR or NHEJ. A comparison of the gliomagenesis frequency between these models will elucidate the relative importance of each pathway in the brain and potentially inform mitigation strategies.

Conclusion

The work presented here is timely, given the increased use of IR for medical diagnostics, the rise in cancer incidence (and correspondingly in RT use), the diversification of both low and high LET treatment modalities, and the concerted push for prolonged space missions. By identifying and validating two mouse models of RIG we have provided the tools needed for the development of effective therapeutic strategies for radiation-induced and sporadic malignant glioma treatment. We hope that this work will contribute to the increased understanding of radiation carcinogenesis, the beneficiaries of which would be countless cancer patients and their families. Additionally, we are confident that the knowledge we have provided on the effects of LET on gliomagenesis will have broad implications for space exploration and the design of a safer work environment for astronauts. The two approaches described above exemplify some of the many potential uses of the mouse models characterized in this dissertation. Further applications in the fields of radioprotection, drug testing, and tumor biomarkers can be envisioned. The unique features of these models (readily inducible GBMs in a tumor-free background, short latency of tumor formation, low burden of engineered genetic modifications) position them as versatile tools that can be further modified to serve the ever-evolving needs of the scientific community.

APPENDIX

APPENDIX A
IHC staining on a panel of 33 RIG samples

IR	Sample ID	Pten	Met	pMet	Pdgfra
X-rays	p53#1808	Neg	Neg	Neg	Pos
	p53#1804	Neg	Neg	Neg	Pos
	p53#2378	Neg	Neg	Neg	Pos
H	p53#2601	Neg	Neg	Neg	Pos
	p53#2634	Neg	Pos	Pos	Pos
	p53#2668	Neg	Pos	Pos	Pos
C	p53#1361	Neg	Pos	Neg	Pos
	p53#2534	Neg	Neg	Neg	Pos
	p53#2556	Neg	Neg	Neg	Pos
	p53#2686	Neg	Neg	Pos	Pos
	p53#2694	Neg	Pos	Pos	Pos
Si	p53#2108	Neg	Neg	Neg	Pos
	p53#2160	Neg	Pos	Pos	Pos
	p53#2090	Neg	Pos	Pos	Pos
	p53#2085	Neg	Neg	Neg	Pos
	p53#2089	Neg	Neg	Neg	Pos
	p53#2103	Neg	Neg	Neg	Pos
	p53#2262	Neg	Pos	Pos	Pos
	p53#2267	Neg	Pos	Pos	Pos
	p53#2271	Neg	Neg	Neg	Pos
	p53#2274	Neg	Pos	Pos	Pos
	p53#2290	Neg	Neg	Neg	Pos
	p53#2300	Neg	Pos	Neg	Pos
Fe	p53#124	Neg	Neg	Neg	Pos
	p53#1023	Neg	Pos	Neg	Pos
	p53#961	Neg	Pos	Neg	Pos
	p53#1035	Neg	Neg	Neg	Pos
	p53#966	Neg	Neg	Neg	Pos
	p53#975	Neg	Pos	Pos	Pos
	p53#1022	Neg	Pos	Neg	Pos
	p53#999	Neg	Neg	Neg	Pos
	p53#980	Neg	Pos	Pos	Pos
	p53#1679	Neg	Pos	Pos	Pos

APPENDIX B
Additional circos plots of aCGH data

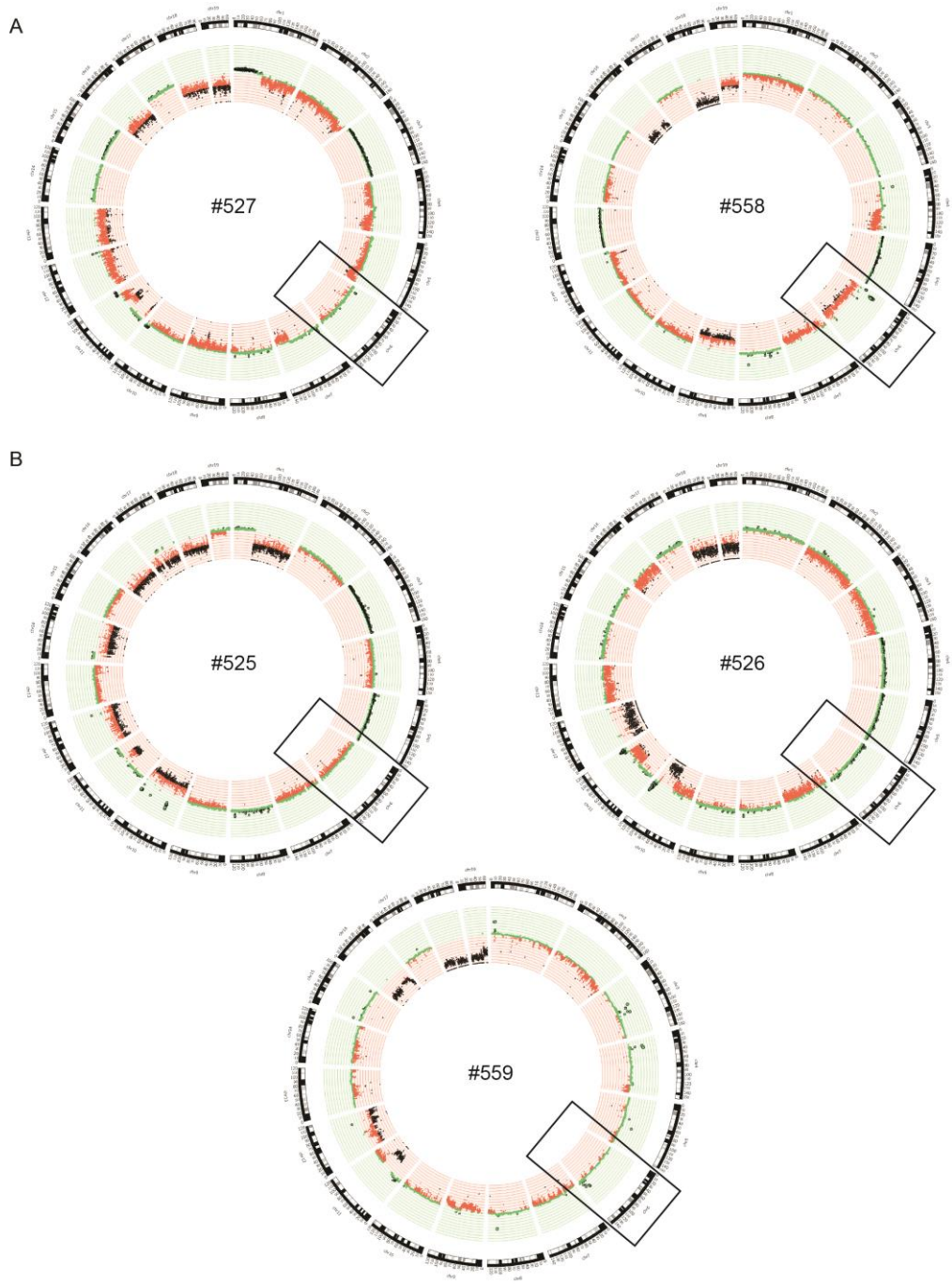

A. Met amplified B. Met non-amplified

APPENDIX C
List of the significant genomic events determined by GISTIC

Chromosome	Type	Q-Bound	G-Score	Gene Symbol	Name
chr11	CN Loss	5.38E-06	3.85920	Nlrp1c-ps	NLR family, pyrin domain containing 1C, pseudogene
chr6	CN Gain	1.15E-05	9.73900	Met	met proto-oncogene
chr18	CN Loss	0.00203	2.93620	1700011I03Rik	RIKEN cDNA 1700011I03 gene
chr16	CN Loss	0.00288	2.66260	Hunk	hormonally upregulated Neu-associated kinase
chr11	CN Loss	0.00288	2.43665	Sfi1	Sfi1 homolog, spindle assembly associated (yeast)
chr6	CN Loss	0.00288	2.28050	Slc4a5	solute carrier family 4, sodium bicarbonate cotransporter, member 5
Chr1	CN Loss	0.00288	2.21793	Kansl1l	KAT8 regulatory NSL complex subunit 1-like
chr7	CN Loss	0.00288	2.19671	Agbl1	ATP/GTP binding protein-like 1
chr19	CN Loss	0.00288	2.12582	Vwa2	von Willebrand factor A domain containing 2
chr19	CN Loss	0.00288	2.12582	Afap1l2	actin filament associated protein 1-like 2
Chr1	CN Loss	0.00408	1.94080	Hhat	hedgehog acyltransferase
chr9	CN Loss	0.01282	1.74398	Npsr1	neuropeptide S receptor 1
chr13	CN Loss	0.01407	1.72735	Phactr1	phosphatase and actin regulator 1
chr12	CN Loss	0.01889	1.67337	Adcy3	adenylate cyclase 3
chr12	CN Loss	0.01889	1.67337	Cenpo	centromere protein O
chr12	CN Loss	0.01889	1.67337	Ptrhd1	peptidyl-tRNA hydrolase domain containing 1
chr14	CN Loss	0.02007	1.66654	Rnase2a	ribonuclease, RNase A family, 2A (liver, eosinophil-derived neurotoxin)
chr7	CN Loss	0.02124	1.65229	1600014C10Rik	RIKEN cDNA 1600014C10 gene
Chr1	CN Loss	0.02251	1.64038	Ugt1a10	UDP glycosyltransferase 1 family, polypeptide A10
Chr1	CN Loss	0.02251	1.64038	Ugt1a9	UDP glucuronosyltransferase 1 family, polypeptide A9
Chr1	CN Loss	0.02251	1.64038	Ugt1a7c	UDP glucuronosyltransferase 1 family, polypeptide A7C
Chr1	CN Loss	0.02251	1.64038	Ugt1a6b	UDP glucuronosyltransferase 1 family, polypeptide A6B
Chr1	CN Loss	0.02251	1.64038	Ugt1a6a	UDP glucuronosyltransferase 1 family, polypeptide A6A
Chr1	CN Loss	0.02251	1.64038	Ugt1a5	UDP glucuronosyltransferase 1 family, polypeptide A5
Chr1	CN Loss	0.02251	1.64038	Ugt1a2	UDP glucuronosyltransferase 1 family, polypeptide A2
Chr1	CN Loss	0.02251	1.64038	Ugt1a1	UDP glucuronosyltransferase 1 family, polypeptide A1
Chr1	CN Loss	0.02251	1.64038	Mroh2a	maestro heat-like repeat family member 2A
Chr1	CN Loss	0.02251	1.64038	6430706D22Rik	RIKEN cDNA 6430706D22 gene
Chr1	CN Loss	0.02251	1.64038	Hjurp	Holliday junction recognition protein
Chr1	CN Loss	0.02251	1.64038	A730008H23Rik	RIKEN cDNA A730008H23 gene
Chr1	CN Loss	0.02251	1.64038	Trpm8	transient receptor potential cation channel, subfamily M, member 8
chr10	CN Loss	0.02874	1.60322	Mir5615-1	microRNA 5615-1
chr10	CN Loss	0.02874	1.60322	Mir5615-2	microRNA 5615-2
chr10	CN Loss	0.02874	1.60322	Map2k2	mitogen-activated protein kinase kinase 2
chr10	CN Loss	0.04512	1.52856	Esr1	estrogen receptor 1 (alpha)

BIBLIOGRAPHY

Abboud, S. E., Wolansky, L. J., Manjila, S. V., Lo, S. S., Arafah, B. M., Selman, W. R., . . . Rogers, L. R. (2015). Histologically Proven Radiation-Induced Brainstem Glioma 93 Months After External Beam Radiotherapy for Pituitary Macroadenoma: Radiation Treatment Dose and Volume Correlation. *Journal of Neuroimaging, 25*(4), 674-676. doi:10.1111/jon.12181

Alcantara Llaguno, S., Chen, J., Kwon, C. H., Jackson, E. L., Li, Y., Burns, D. K., . . . Parada, L. F. (2009). Malignant astrocytomas originate from neural stem/progenitor cells in a somatic tumor suppressor mouse model. *Cancer Cell, 15*(1), 45-56. doi:10.1016/j.ccr.2008.12.006

Aldape, K., Zadeh, G., Mansouri, S., Reifenberger, G., & von Deimling, A. (2015). Glioblastoma: pathology, molecular mechanisms and markers. *Acta Neuropathol, 129*(6), 829-848. doi:10.1007/s00401-015-1432-1

Alexiou, G. A., Moschovi, M., Georgoulis, G., Neroutsou, R., Stefanaki, K., Sfakianos, G., & Prodromou, N. (2010). Anaplastic oligodendrogliomas after treatment of acute lymphoblastic leukemia in children: report of 2 cases. *J Neurosurg Pediatr, 5*(2), 179-183. doi:10.3171/2009.9.PEDS09154

Alimonti, A., Carracedo, A., Clohessy, J. G., Trotman, L. C., Nardella, C., Egia, A., . . . Pandolfi, P. P. (2010). Subtle variations in Pten dose determine cancer susceptibility. *Nat Genet, 42*(5), 454-458. doi:10.1038/ng.556

Alpen, E. L., Powers-Risius, P., Curtis, S. B., & DeGuzman, R. (1993). Tumorigenic potential of high-Z, high-LET charged-particle radiations. *Radiat Res, 136*(3), 382-391.

Asaithamby, A., & Chen, D. J. (2011). Mechanism of cluster DNA damage repair in response to high-atomic number and energy particles radiation. *Mutat Res, 711*(1-2), 87-99. doi:10.1016/j.mrfmmm.2010.11.002

Asaithamby, A., Hu, B., Delgado, O., Ding, L. H., Story, M. D., Minna, J. D., . . . Chen, D. J. (2011). Irreparable complex DNA double-strand breaks induce chromosome breakage in organotypic three-dimensional human lung epithelial cell culture. *Nucleic Acids Res, 39*(13), 5474-5488. doi:gkr149 [pii]
10.1093/nar/gkr149

Asaithamby, A., Uematsu, N., Chatterjee, A., Story, M. D., Burma, S., & Chen, D. J. (2008). Repair of HZE-particle-induced DNA double-strand breaks in normal human fibroblasts. *Radiat Res, 169*(4), 437-446. doi:10.1667/RR1165.1

Bachoo, R. M., Maher, E. A., Ligon, K. L., Sharpless, N. E., Chan, S. S., You, M. J., . . . DePinho, R. A. (2002). Epidermal growth factor receptor and Ink4a/Arf: convergent mechanisms governing terminal differentiation and transformation along the neural stem cell to astrocyte axis. *Cancer Cell, 1*(3), 269-277.

Ballarini, F., Alloni, D., Facoetti, A., & Ottolenghi, A. (2008). Heavy-ion effects: from track structure to DNA and chromosome damage. *New Journal of Physics, 10*. doi:Artn 075008
10.1088/1367-2630/10/7/075008

Bao, S., Wu, Q., McLendon, R. E., Hao, Y., Shi, Q., Hjelmeland, A. B., . . . Rich, J. N. (2006). Glioma stem cells promote radioresistance by preferential activation of the DNA damage response. *Nature, 444*(7120), 756-760. doi:10.1038/nature05236

Baumann, M., Krause, M., & Hill, R. (2008). Exploring the role of cancer stem cells in radioresistance. *Nat Rev Cancer, 8*(7), 545-554. doi:10.1038/nrc2419

Bazzoli, E., Pulvirenti, T., Oberstadt, M. C., Perna, F., Wee, B., Schultz, N., . . . Squatrito, M. (2012). MEF promotes stemness in the pathogenesis of gliomas. *Cell Stem Cell, 11*(6), 836-844. doi:10.1016/j.stem.2012.09.012

Behjati, S., Gundem, G., Wedge, D. C., Roberts, N. D., Tarpey, P. S., Cooke, S. L., . . . Campbell, P. J. (2016). Mutational signatures of ionizing radiation in second malignancies. *Nat Commun, 7*, 12605. doi:10.1038/ncomms12605

Ben-Porath, I., Thomson, M. W., Carey, V. J., Ge, R., Bell, G. W., Regev, A., & Weinberg, R. A. (2008). An embryonic stem cell-like gene expression signature in poorly differentiated aggressive human tumors. *Nat Genet, 40*(5), 499-507. doi:10.1038/ng.127

Blakely, E. A., & Chang, P. Y. (2009). Biology of charged particles. *Cancer J, 15*(4), 271-284. doi:10.1097/PPO.0b013e3181b666c5

Bleau, A. M., Hambardzumyan, D., Ozawa, T., Fomchenko, E. I., Huse, J. T., Brennan, C. W., & Holland, E. C. (2009). PTEN/PI3K/Akt pathway regulates the side population phenotype and ABCG2 activity in glioma tumor stem-like cells. *Cell Stem Cell, 4*(3), 226-235. doi:10.1016/j.stem.2009.01.007

Bondy, M. L., Scheurer, M. E., Malmer, B., Barnholtz-Sloan, J. S., Davis, F. G., Il'yasova, D., . . . Brain Tumor Epidemiology, C. (2008). Brain tumor epidemiology: consensus from the Brain Tumor Epidemiology Consortium. *Cancer, 113*(7 Suppl), 1953-1968. doi:10.1002/cncr.23741

Braganza, M. Z., Kitahara, C. M., Berrington de Gonzalez, A., Inskip, P. D., Johnson, K. J., & Rajaraman, P. (2012). Ionizing radiation and the risk of brain and central nervous system tumors: a systematic review. *Neuro Oncol, 14*(11), 1316-1324. doi:10.1093/neuonc/nos208

Brat, D. J., James, C. D., Jedlicka, A. E., Connolly, D. C., Chang, E., Castellani, R. J., . . . Burger, P. C. (1999). Molecular genetic alterations in radiation-induced astrocytomas. *Am J Pathol, 154*(5), 1431-1438. doi:10.1016/S0002-9440(10)65397-7

Brennan, C. W., Verhaak, R. G., McKenna, A., Campos, B., Noushmehr, H., Salama, S. R., . . . Chin, L. (2013). The somatic genomic landscape of glioblastoma. *Cell, 155*(2), 462-477. doi:10.1016/j.cell.2013.09.034

Broniscer, A., Ke, W., Fuller, C. E., Wu, J., Gajjar, A., & Kun, L. E. (2004). Second neoplasms in pediatric patients with primary central nervous system tumors: the St. Jude Children's Research Hospital experience. *Cancer, 100*(10), 2246-2252. doi:10.1002/cncr.20253

Brooks, C. L., & Gu, W. (2003). Ubiquitination, phosphorylation and acetylation: the molecular basis for p53 regulation. *Curr Opin Cell Biol, 15*(2), 164-171.

Burel-Vandenbos, F., Ngo-Mai, M., Dadone, B., Di Mauro, I., Gimet, S., Saada-Bouzid, E., . . . Pedeutour, F. (2017). MET immunolabelling is a useful predictive tool for MET gene amplification in glioblastoma. *Neuropathol Appl Neurobiol, 43*(3), 252-266. doi:10.1111/nan.12320

Camacho, C. V., Mukherjee, B., McEllin, B., Ding, L. H., Hu, B., Habib, A. A., . . . Burma, S. (2010). Loss of p15/Ink4b accompanies tumorigenesis triggered by complex DNA double-strand breaks. *Carcinogenesis, 31*(10), 1889-1896. doi:10.1093/carcin/bgq153

Camacho, C. V., Todorova, P. K., Hardebeck, M. C., Tomimatsu, N., Gil del Alcazar, C. R., Ilcheva, M., . . . Burma, S. (2015). DNA double-strand breaks cooperate with loss of Ink4 and Arf tumor suppressors to generate glioblastomas with frequent Met amplification. *Oncogene, 34*(8), 1064-1072. doi:10.1038/onc.2014.29

Cancer Genome Atlas Research, N. (2008). Comprehensive genomic characterization defines human glioblastoma genes and core pathways. *Nature, 455*(7216), 1061-1068. doi:10.1038/nature07385

Carracedo, A., Alimonti, A., & Pandolfi, P. P. (2011). PTEN Level in Tumor Suppression: How Much Is Too Little? *Cancer Res, 71*(3), 629-633. doi:10.1158/0008-5472.can-10-2488

Carret, A. S., Tabori, U., Crooks, B., Hukin, J., Odame, I., Johnston, D. L., . . . Canadian Pediatric Brain Tumour, C. (2006). Outcome of secondary high-grade glioma in children previously treated for a malignant condition: a study of the Canadian Pediatric Brain Tumour Consortium. *Radiother Oncol, 81*(1), 33-38. doi:10.1016/j.radonc.2006.08.005

Chalhoub, N., & Baker, S. J. (2009). PTEN and the PI3-kinase pathway in cancer. *Annu Rev Pathol, 4*, 127-150. doi:10.1146/annurev.pathol.4.110807.092311

Chen, J., McKay, R. M., & Parada, L. F. (2012). Malignant glioma: lessons from genomics, mouse models, and stem cells. *Cell, 149*(1), 36-47. doi:10.1016/j.cell.2012.03.009

Chi, A. S., Batchelor, T. T., Kwak, E. L., Clark, J. W., Wang, D. L., Wilner, K. D., . . . Iafrate, A. J. (2012). Rapid radiographic and clinical improvement after treatment of a MET-amplified recurrent glioblastoma with a mesenchymal-epithelial transition inhibitor. *J Clin Oncol, 30*(3), e30-33. doi:10.1200/JCO.2011.38.4586

Chiche, A., Moumen, M., Romagnoli, M., Petit, V., Lasla, H., Jezequel, P., . . . Faraldo, M. M. (2017). p53 deficiency induces cancer stem cell pool expansion in a mouse model of triple-negative breast tumors. *Oncogene, 36*(17), 2355-2365. doi:10.1038/onc.2016.396

Chow, L. M., Endersby, R., Zhu, X., Rankin, S., Qu, C., Zhang, J., . . . Baker, S. J. (2011). Cooperativity within and among Pten, p53, and Rb pathways induces high-grade astrocytoma in adult brain. *Cancer Cell, 19*(3), 305-316. doi:10.1016/j.ccr.2011.01.039

Christodouleas , J. P., Forrest , R. D., Ainsley , C. G., Tochner , Z., Hahn , S. M., & Glatstein , E. (2011). Short-Term and Long-Term Health Risks of Nuclear-Power-Plant Accidents. *New England Journal of Medicine, 364*(24), 2334-2341. doi:10.1056/NEJMra1103676

Cloughesy, T. F., Cavenee, W. K., & Mischel, P. S. (2014). Glioblastoma: from molecular pathology to targeted treatment. *Annu Rev Pathol, 9*, 1-25. doi:10.1146/annurev-pathol-011110-130324

Costes, S. V., Boissiere, A., Ravani, S., Romano, R., Parvin, B., & Barcellos-Hoff, M. H. (2006). Imaging features that discriminate between foci induced by high- and low-LET radiation in human fibroblasts. *Radiat Res, 165*(5), 505-515. doi:RR3538 [pii]
10.1667/RR3538.1

Crawford, J. R., MacDonald, T. J., & Packer, R. J. (2007). Medulloblastoma in childhood: new biological advances. *Lancet Neurol, 6*(12), 1073-1085. doi:10.1016/S1474-4422(07)70289-2

Cucinotta, F. A., Schimmerling, W., Wilson, J. W., Peterson, L. E., Badhwar, G. D., Saganti, P. B., & Dicello, J. F. (2001). Space radiation cancer risks and uncertainties for Mars missions. *Radiat Res, 156*(5 Pt 2), 682-688.

Dahlstrand, J., Lardelli, M., & Lendahl, U. (1995). Nestin mRNA expression correlates with the central nervous system progenitor cell state in many, but not all, regions of developing central nervous system. *Brain Res Dev Brain Res, 84*(1), 109-129.

Datta, K., Suman, S., Trani, D., Doiron, K., Rotolo, J. A., Kallakury, B. V., . . . Fornace, A. J., Jr. (2012). Accelerated hematopoietic toxicity by high energy (56)Fe radiation. *Int J Radiat Biol, 88*(3), 213-222. doi:10.3109/09553002.2012.639434

De Bacco, F., Casanova, E., Medico, E., Pellegatta, S., Orzan, F., Albano, R., . . . Boccaccio, C. (2012). The MET oncogene is a functional marker of a glioblastoma stem cell subtype. *Cancer Res, 72*(17), 4537-4550. doi:10.1158/0008-5472.CAN-11-3490

De Bacco, F., D'Ambrosio, A., Casanova, E., Orzan, F., Neggia, R., Albano, R., . . . Boccaccio, C. (2016). MET inhibition overcomes radiation resistance of glioblastoma stem-like cells. *EMBO Mol Med, 8*(5), 550-568. doi:10.15252/emmm.201505890

Desai, N., Davis, E., O'Neill, P., Durante, M., Cucinotta, F. A., & Wu, H. (2005). Immunofluorescence detection of clustered gamma-H2AX foci induced by HZE-particle radiation. *Radiat Res, 164*(4 Pt 2), 518-522. doi:RR3431 [pii]

Desai, N., Durante, M., Lin, Z. W., Cucinotta, F., & Wu, H. (2005). High LET-induced H2AX phosphorylation around the Bragg curve. *Adv Space Res, 35*(2), 236-242.

Diallo, I., Haddy, N., Adjadj, E., Samand, A., Quiniou, E., Chavaudra, J., . . . de Vathaire, F. (2009). Frequency distribution of second solid cancer locations in relation to the irradiated volume among 115 patients treated for childhood cancer. *Int J Radiat Oncol Biol Phys, 74*(3), 876-883. doi:10.1016/j.ijrobp.2009.01.040

Dicello, J. F., Christian, A., Cucinotta, F. A., Gridley, D. S., Kathirithamby, R., Mann, J., . . . Huso, D. (2004). In vivo mammary tumourigenesis in the Sprague-Dawley rat and microdosimetric correlates. *Phys Med Biol, 49*(16), 3817-3830.

Ding, L. H., Park, S., Peyton, M., Girard, L., Xie, Y., Minna, J. D., & Story, M. D. (2013). Distinct transcriptome profiles identified in normal human bronchial epithelial cells after exposure to gamma-rays and different elemental particles of high Z and energy. *BMC Genomics, 14*, 372. doi:10.1186/1471-2164-14-372

Donson, A. M., Erwin, N. S., Kleinschmidt-DeMasters, B. K., Madden, J. R., Addo-Yobo, S. O., & Foreman, N. K. (2007). Unique molecular characteristics of radiation-induced glioblastoma. *J Neuropathol Exp Neurol, 66*(8), 740-749. doi:10.1097/nen.0b013e3181257190

Dunn, G. P., Rinne, M. L., Wykosky, J., Genovese, G., Quayle, S. N., Dunn, I. F., . . . Hahn, W. C. (2012). Emerging insights into the molecular and cellular basis of glioblastoma. *Genes Dev, 26*(8), 756-784. doi:10.1101/gad.187922.112

Durante, M., & Cucinotta, F. A. (2008). Heavy ion carcinogenesis and human space exploration. *Nat Rev Cancer, 8*(6), 465-472. doi:10.1038/nrc2391

Durante, M., & Loeffler, J. S. (2010). Charged particles in radiation oncology. *Nat Rev Clin Oncol, 7*(1), 37-43. doi:10.1038/nrclinonc.2009.183

Ehrhart, E. J., Gillette, E. L., & Barcellos-Hoff, M. H. (1996). Immunohistochemical evidence of rapid extracellular matrix remodeling after iron-particle irradiation of mouse mammary gland. *Radiat Res, 145*(2), 157-162.

Elsamadicy, A. A., Babu, R., Kirkpatrick, J. P., & Adamson, D. C. (2015). Radiation-induced malignant gliomas: a current review. *World Neurosurg, 83*(4), 530-542. doi:10.1016/j.wneu.2014.12.009

Fazio, G. G., Jelley, J. V., & Charman, W. N. (1970). Generation of Cherenkov light flashes by cosmic radiation within the eyes of the Apollo astronauts. *Nature, 228*(5268), 260-264.

Francoz, S., Froment, P., Bogaerts, S., De Clercq, S., Maetens, M., Doumont, G., . . . Marine, J.-C. (2006). Mdm4 and Mdm2 cooperate to inhibit p53 activity in proliferating and quiescent cells in vivo. *Proc Natl Acad Sci U S A, 103*(9), 3232-3237. doi:10.1073/pnas.0508476103

Frattini, V., Trifonov, V., Chan, J. M., Castano, A., Lia, M., Abate, F., . . . Iavarone, A. (2013). The integrated landscape of driver genomic alterations in glioblastoma. *Nat Genet, 45*(10), 1141-1149. doi:10.1038/ng.2734

Furnari, F. B., Fenton, T., Bachoo, R. M., Mukasa, A., Stommel, J. M., Stegh, A., . . . Cavenee, W. K. (2007). Malignant astrocytic glioma: genetics, biology, and paths to treatment. *Genes Dev, 21*(21), 2683-2710. doi:10.1101/gad.1596707

Gessi, M., Maderna, E., Guzzetti, S., Cefalo, G., Massimino, M., Solero, C. L., . . . Pollo, B. (2008). Radiation-induced glioblastoma in a medulloblastoma patient: a case report with molecular features. *Neuropathology, 28*(6), 633-639. doi:10.1111/j.1440-1789.2008.00900.x

Gherardi, E., Birchmeier, W., Birchmeier, C., & Vande Woude, G. (2012). Targeting MET in cancer: rationale and progress. *Nat Rev Cancer, 12*(2), 89-103. doi:10.1038/nrc3205

Gil del Alcazar, C. R., Hardebeck, M. C., Mukherjee, B., Tomimatsu, N., Gao, X., Yan, J., . . . Burma, S. (2014). Inhibition of DNA double-strand break repair by the dual PI3K/mTOR inhibitor NVP-BEZ235 as a strategy for radiosensitization of glioblastoma. *Clin Cancer Res, 20*(5), 1235-1248. doi:10.1158/1078-0432.CCR-13-1607

Grabham, P., Hu, B., Sharma, P., & Geard, C. (2011). Effects of ionizing radiation on three-dimensional human vessel models: differential effects according to radiation

quality and cellular development. *Radiat Res, 175*(1), 21-28. doi:10.1667/RR2289.1

Gu, J., Tamura, M., & Yamada, K. M. (1998). Tumor suppressor PTEN inhibits integrin- and growth factor-mediated mitogen-activated protein (MAP) kinase signaling pathways. *J Cell Biol, 143*(5), 1375-1383.

Hada, M., & Georgakilas, A. G. (2008a). Formation of clustered DNA damage after high-LET irradiation: a review. *J Radiat Res (Tokyo), 49*(3), 203-210. doi:JST.JSTAGE/jrr/07123 [pii]

Hada, M., & Georgakilas, A. G. (2008b). Formation of clustered DNA damage after high-LET irradiation: a review. *J Radiat Res, 49*(3), 203-210.

Hainaut, P., & Hollstein, M. (2000). p53 and human cancer: the first ten thousand mutations. *Adv Cancer Res, 77*, 81-137.

Hanahan, D., & Weinberg, R. A. (2011). Hallmarks of cancer: the next generation. *Cell, 144*(5), 646-674. doi:10.1016/j.cell.2011.02.013

Harris, S. L., & Levine, A. J. (2005). The p53 pathway: positive and negative feedback loops. *Oncogene, 24*(17), 2899-2908. doi:10.1038/sj.onc.1208615

Heyer, W. D., Ehmsen, K. T., & Liu, J. (2010). Regulation of homologous recombination in eukaryotes. *Annu Rev Genet, 44*, 113-139. doi:10.1146/annurev-genet-051710-150955

Hong, H., Takahashi, K., Ichisaka, T., Aoi, T., Kanagawa, O., Nakagawa, M., . . . Yamanaka, S. (2009). Suppression of induced pluripotent stem cell generation by the p53–p21 pathway. *Nature, 460*(7259), 1132-1135. doi:http://www.nature.com/nature/journal/v460/n7259/suppinfo/nature08235_S1.html

Hunger, S. P., & Mullighan, C. G. (2015). Acute Lymphoblastic Leukemia in Children. *N Engl J Med, 373*(16), 1541-1552. doi:10.1056/NEJMra1400972

Illa-Bochaca, I., Ouyang, H., Tang, J., Sebastiano, C., Mao, J. H., Costes, S. V., . . . Barcellos-Hoff, M. H. (2014). Densely ionizing radiation acts via the microenvironment to promote aggressive Trp53-null mammary carcinomas. *Cancer Res, 74*(23), 7137-7148. doi:10.1158/0008-5472.CAN-14-1212

International Cancer Genome Consortium PedBrain Tumor, P. (2016). Recurrent MET fusion genes represent a drug target in pediatric glioblastoma. *Nat Med*. doi:10.1038/nm.4204

Iwadate, Y., Fujimoto, S., Tagawa, M., Namba, H., Sueyoshi, K., Hirose, M., & Sakiyama, S. (1996). Association of p53 gene mutation with decreased chemosensitivity in human malignant gliomas. *Int J Cancer, 69*(3), 236-240. doi:10.1002/(sici)1097-0215(19960621)69:3<236::aid-ijc14>3.0.co;2-5

Jacques, T. S., Swales, A., Brzozowski, M. J., Henriquez, N. V., Linehan, J. M., Mirzadeh, Z., . . . Brandner, S. (2010). Combinations of genetic mutations in the adult neural stem cell compartment determine brain tumour phenotypes. *EMBO J, 29*(1), 222-235. doi:10.1038/emboj.2009.327

Joo, K. M., Jin, J., Kim, E., Ho Kim, K., Kim, Y., Gu Kang, B., . . . Nam, D.-H. (2012). MET Signaling Regulates Glioblastoma Stem Cells. *Cancer Res, 72*(15), 3828-3838. doi:10.1158/0008-5472.can-11-3760

Joo, K. M., Jin, J., Kim, E., Ho Kim, K., Kim, Y., Gu Kang, B., . . . Nam, D. H. (2012). MET signaling regulates glioblastoma stem cells. *Cancer Res, 72*(15), 3828-3838. doi:10.1158/0008-5472.CAN-11-3760

Kamiya, K., Ozasa, K., Akiba, S., Niwa, O., Kodama, K., Takamura, N., . . . Wakeford, R. (2015). Long-term effects of radiation exposure on health. *Lancet, 386*(9992), 469-478. doi:10.1016/S0140-6736(15)61167-9

Kawamura, T., Suzuki, J., Wang, Y. V., Menendez, S., Morera, L. B., Raya, A., . . . Belmonte, J. C. I. (2009). Linking the p53 tumour suppressor pathway to somatic cell reprogramming. *Nature, 460*(7259), 1140-1144. doi:http://www.nature.com/nature/journal/v460/n7259/suppinfo/nature08311_S1.html

Kent, S. P., & Pickering, J. E. (1957). Neoplasms in Monkeys (Macaca-Mulatta) - Spontaneous and Irradiation Induced. *American Journal of Pathology, 33*(3), 625-626.

Khanna, K. K., & Jackson, S. P. (2001). DNA double-strand breaks: signaling, repair and the cancer connection. *Nat Genet, 27*(3), 247-254. doi:10.1038/85798

Kleinschmidt-Demasters, B. K., Kang, J. S., & Lillehei, K. O. (2006). The burden of radiation-induced central nervous system tumors: a single institution s experience. *J Neuropathol Exp Neurol, 65*(3), 204-216. doi:10.1097/01.jnen.0000205146.62081.29

Knudsen, E. S., & Knudsen, K. E. (2008). Tailoring to RB: tumour suppressor status and therapeutic response. *Nat Rev Cancer, 8*(9), 714-724. doi:10.1038/nrc2401

Kong, D. S., Song, S. Y., Kim, D. H., Joo, K. M., Yoo, J. S., Koh, J. S., . . . Nam, D. H. (2009). Prognostic significance of c-Met expression in glioblastomas. *Cancer, 115*(1), 140-148. doi:10.1002/cncr.23972

Krimpenfort, P., Ijpenberg, A., Song, J. Y., van der Valk, M., Nawijn, M., Zevenhoven, J., & Berns, A. (2007). p15Ink4b is a critical tumour suppressor in the absence of p16Ink4a. *Nature, 448*(7156), 943-946. doi:10.1038/nature06084

Krupp, J. H. (1976). Nine-year mortality experience in proton-exposed Macaca mulatta. *Radiat Res, 67*(2), 244-251.

Kruse, J. P., & Gu, W. (2009). Modes of p53 regulation. *Cell, 137*(4), 609-622. doi:10.1016/j.cell.2009.04.050

Kwon, C. H., Zhao, D., Chen, J., Alcantara, S., Li, Y., Burns, D. K., . . . Parada, L. F. (2008). Pten haploinsufficiency accelerates formation of high-grade astrocytomas. *Cancer Res, 68*(9), 3286-3294. doi:10.1158/0008-5472.CAN-07-6867

La Tessa, C., Sivertz, M., Chiang, I. H., Lowenstein, D., & Rusek, A. (2016). Overview of the NASA space radiation laboratory. *Life Sci Space Res (Amst), 11*, 18-23. doi:10.1016/j.lssr.2016.10.002

Laterra, J., Rosen, E., Nam, M., Ranganathan, S., Fielding, K., & Johnston, P. (1997). Scatter factor/hepatocyte growth factor expression enhances human glioblastoma tumorigenicity and growth. *Biochem Biophys Res Commun, 235*(3), 743-747. doi:10.1006/bbrc.1997.6853

Lathia, J. D., Mack, S. C., Mulkearns-Hubert, E. E., Valentim, C. L., & Rich, J. N. (2015). Cancer stem cells in glioblastoma. *Genes Dev, 29*(12), 1203-1217. doi:10.1101/gad.261982.115

Leatherbarrow, E. L., Harper, J. V., Cucinotta, F. A., & O'Neill, P. (2006). Induction and quantification of gamma-H2AX foci following low and high LET-irradiation. *Int J Radiat Biol, 82*(2), 111-118. doi:X21464J0126X7X76 [pii]
10.1080/09553000600599783

Lee, J., Kotliarova, S., Kotliarov, Y., Li, A., Su, Q., Donin, N. M., . . . Fine, H. A. (2006). Tumor stem cells derived from glioblastomas cultured in bFGF and EGF more closely mirror the phenotype and genotype of primary tumors than do serum-cultured cell lines. *Cancer Cell, 9*(5), 391-403. doi:10.1016/j.ccr.2006.03.030

Lemmon, M. A., & Schlessinger, J. (2010). Cell signaling by receptor tyrosine kinases. *Cell, 141*(7), 1117-1134. doi:10.1016/j.cell.2010.06.011

Li, J., Yen, C., Liaw, D., Podsypanina, K., Bose, S., Wang, S. I., . . . Parsons, R. (1997). PTEN, a Putative Protein Tyrosine Phosphatase Gene Mutated in Human Brain, Breast, and Prostate Cancer. *Science, 275*(5308), 1943-1947. doi:10.1126/science.275.5308.1943

Li, Y., Li, A., Glas, M., Lal, B., Ying, M., Sang, Y., . . . Laterra, J. (2011). c-Met signaling induces a reprogramming network and supports the glioblastoma stem-like phenotype. *Proc Natl Acad Sci U S A, 108*(24), 9951-9956. doi:10.1073/pnas.1016912108

Lieber, M. R. (2010). The mechanism of double-strand DNA break repair by the nonhomologous DNA end-joining pathway. *Annu Rev Biochem, 79*, 181-211. doi:10.1146/annurev.biochem.052308.093131

Lin, C., Liang, Y., Zhu, H., Zhang, J., & Zhong, X. (2012). R280T mutation of p53 gene promotes proliferation of human glioma cells through GSK-3beta/PTEN pathway. *Neurosci Lett, 529*(1), 60-65. doi:10.1016/j.neulet.2012.09.022

Little, J. B. (2000). Radiation carcinogenesis. *Carcinogenesis, 21*(3), 397-404.

Liu, C., Sage, J. C., Miller, M. R., Verhaak, R. G., Hippenmeyer, S., Vogel, H., . . . Zong, H. (2011). Mosaic analysis with double markers reveals tumor cell of origin in glioma. *Cell, 146*(2), 209-221. doi:10.1016/j.cell.2011.06.014

Lonser, R. R., Walbridge, S., Vortmeyer, A. O., Pack, S. D., Nguyen, T. T., Gogate, N., . . . Oldfield, E. H. (2002). Induction of glioblastoma multiforme in nonhuman primates after therapeutic doses of fractionated whole-brain radiation therapy. *J Neurosurg, 97*(6), 1378-1389. doi:10.3171/jns.2002.97.6.1378

Loucas, B. D., Durante, M., Bailey, S. M., & Cornforth, M. N. (2013). Chromosome damage in human cells by gamma rays, alpha particles and heavy ions: track interactions in basic dose-response relationships. *Radiat Res, 179*(1), 9-20. doi:10.1667/RR3089.1

Louis, D. N., Ohgaki, H., Wiestler, O. D., Cavenee, W. K., Burger, P. C., Jouvet, A., . . . Kleihues, P. (2007). The 2007 WHO classification of tumours of the central nervous system. *Acta Neuropathol, 114*(2), 97-109. doi:10.1007/s00401-007-0243-4

Louis, D. N., Perry, A., Burger, P., Ellison, D. W., Reifenberger, G., von Deimling, A., . . . Wesseling, P. (2014). International Society of Neuropathology-Haarlem Consensus Guidelines for Nervous System Tumor Classification and Grading. *Brain Pathology, 24*(5), 429-435. doi:10.1111/bpa.12171

Louis, D. N., Perry, A., Reifenberger, G., von Deimling, A., Figarella-Branger, D., Cavenee, W. K., . . . Ellison, D. W. (2016). The 2016 World Health Organization Classification of Tumors of the Central Nervous System: a summary. *Acta Neuropathol, 131*(6), 803-820. doi:10.1007/s00401-016-1545-1

Luo, J., Su, F., Chen, D., Shiloh, A., & Gu, W. (2000). Deacetylation of p53 modulates its effect on cell growth and apoptosis. *Nature, 408*(6810), 377-381. doi:10.1038/35042612

Maalouf, M., Durante, M., & Foray, N. (2011). Biological effects of space radiation on human cells: history, advances and outcomes. *J Radiat Res, 52*(2), 126-146.

Macleod, K. F., Sherry, N., Hannon, G., Beach, D., Tokino, T., Kinzler, K., . . . Jacks, T. (1995). p53-dependent and independent expression of p21 during cell growth, differentiation, and DNA damage. *Genes Dev, 9*(8), 935-944.

Manfredi, J. J. (2010). The Mdm2-p53 relationship evolves: Mdm2 swings both ways as an oncogene and a tumor suppressor. *Genes Dev, 24*(15), 1580-1589. doi:10.1101/gad.1941710

Massimino, M., Biassoni, V., Gandola, L., Garre, M. L., Gatta, G., Giangaspero, F., . . . Rutkowski, S. (2016). Childhood medulloblastoma. *Crit Rev Oncol Hematol, 105*, 35-51. doi:10.1016/j.critrevonc.2016.05.012

Mayo, L. D., & Donner, D. B. (2002). The PTEN, Mdm2, p53 tumor suppressor-oncoprotein network. *Trends Biochem Sci, 27*(9), 462-467.

McBride, K. A., Ballinger, M. L., Killick, E., Kirk, J., Tattersall, M. H. N., Eeles, R. A., . . . Mitchell, G. (2014). Li-Fraumeni syndrome: cancer risk assessment and clinical management. *Nat Rev Clin Oncol, 11*(5), 260-271. doi:10.1038/nrclinonc.2014.41

Mermel, C. H., Schumacher, S. E., Hill, B., Meyerson, M. L., Beroukhim, R., & Getz, G. (2011). GISTIC2.0 facilitates sensitive and confident localization of the targets of focal somatic copy-number alteration in human cancers. *Genome Biol, 12*(4), R41. doi:10.1186/gb-2011-12-4-r41

Mignone, J. L., Kukekov, V., Chiang, A. S., Steindler, D., & Enikolopov, G. (2004). Neural stem and progenitor cells in nestin-GFP transgenic mice. *J Comp Neurol, 469*(3), 311-324. doi:10.1002/cne.10964

Millau, J. F., Bastien, N., Bouchard, E. F., & Drouin, R. (2009). p53 Pre- and post-binding event theories revisited: stresses reveal specific and dynamic p53-binding patterns on the p21 gene promoter. *Cancer Res, 69*(21), 8463-8471. doi:10.1158/0008-5472.CAN-09-2036

Mladenov, E., & Iliakis, G. (2011). Induction and repair of DNA double strand breaks: the increasing spectrum of non-homologous end joining pathways. *Mutat Res, 711*(1-2), 61-72. doi:10.1016/j.mrfmmm.2011.02.005

Moore, S., Stanley, F. K., & Goodarzi, A. A. (2014). The repair of environmentally relevant DNA double strand breaks caused by high linear energy transfer

irradiation--no simple task. *DNA Repair (Amst), 17*, 64-73. doi:10.1016/j.dnarep.2014.01.014

Mukherjee, B., Camacho, C. V., Tomimatsu, N., Miller, J., & Burma, S. (2008). Modulation of the DNA-damage response to HZE particles by shielding. *DNA Repair (Amst), 7*(10), 1717-1730. doi:10.1016/j.dnarep.2008.06.016

Mukherjee, B., Kessinger, C., Kobayashi, J., Chen, B. P., Chen, D. J., Chatterjee, A., & Burma, S. (2006). DNA-PK phosphorylates histone H2AX during apoptotic DNA fragmentation in mammalian cells. *DNA Repair (Amst), 5*(5), 575-590. doi:10.1016/j.dnarep.2006.01.011

Muller, P. A., & Vousden, K. H. (2014). Mutant p53 in cancer: new functions and therapeutic opportunities. *Cancer Cell, 25*(3), 304-317. doi:10.1016/j.ccr.2014.01.021

Negrini, S., Gorgoulis, V. G., & Halazonetis, T. D. (2010). Genomic instability--an evolving hallmark of cancer. *Nat Rev Mol Cell Biol, 11*(3), 220-228. doi:10.1038/nrm2858

Nguyen, D. H., Oketch-Rabah, H. A., Illa-Bochaca, I., Geyer, F. C., Reis-Filho, J. S., Mao, J. H., . . . Barcellos-Hoff, M. H. (2011). Radiation acts on the microenvironment to affect breast carcinogenesis by distinct mechanisms that decrease cancer latency and affect tumor type. *Cancer Cell, 19*(5), 640-651. doi:10.1016/j.ccr.2011.03.011

Ohgaki, H., & Kleihues, P. (2007). Genetic pathways to primary and secondary glioblastoma. *Am J Pathol, 170*(5), 1445-1453. doi:10.2353/ajpath.2007.070011

Ohshima, K., Hatakeyama, K., Nagashima, T., Watanabe, Y., Kanto, K., Doi, Y., . . . Yamaguchi, K. (2017). Integrated analysis of gene expression and copy number identified potential cancer driver genes with amplification-dependent overexpression in 1,454 solid tumors. *Sci Rep, 7*(1), 641. doi:10.1038/s41598-017-00219-3

Ostrom, Q. T., Gittleman, H., Fulop, J., Liu, M., Blanda, R., Kromer, C., . . . Barnholtz-Sloan, J. S. (2015). CBTRUS Statistical Report: Primary Brain and Central Nervous System Tumors Diagnosed in the United States in 2008-2012. *Neuro Oncol, 17 Suppl 4*, iv1-iv62. doi:10.1093/neuonc/nov189

Ozawa, T., Riester, M., Cheng, Y. K., Huse, J. T., Squatrito, M., Helmy, K., . . . Holland, E. C. (2014). Most human non-GCIMP glioblastoma subtypes evolve from a common proneural-like precursor glioma. *Cancer Cell, 26*(2), 288-300. doi:10.1016/j.ccr.2014.06.005

Parsons, D. W., Jones, S., Zhang, X., Lin, J. C., Leary, R. J., Angenendt, P., . . . Kinzler, K. W. (2008). An integrated genomic analysis of human glioblastoma multiforme. *Science, 321*(5897), 1807-1812. doi:10.1126/science.1164382

Patel, A. P., Tirosh, I., Trombetta, J. J., Shalek, A. K., Gillespie, S. M., Wakimoto, H., . . . Bernstein, B. E. (2014). Single-cell RNA-seq highlights intratumoral heterogeneity in primary glioblastoma. *Science, 344*(6190), 1396-1401. doi:10.1126/science.1254257

Patel, T. R., & Chiang, V. L. (2014). Secondary neoplasms after stereotactic radiosurgery. *World Neurosurg, 81*(3-4), 594-599. doi:10.1016/j.wneu.2013.10.043

Paulino, A. C., Mai, W. Y., Chintagumpala, M., Taher, A., & Teh, B. S. (2008). Radiation-Induced Malignant Gliomas: Is There a Role for Reirradiation? *International Journal of Radiation Oncology*Biology*Physics, 71*(5), 1381-1387. doi:http://dx.doi.org/10.1016/j.ijrobp.2007.12.018

Pearce, M. S., Salotti, J. A., Little, M. P., McHugh, K., Lee, C., Kim, K. P., . . . Berrington de Gonzalez, A. (2012). Radiation exposure from CT scans in childhood and subsequent risk of leukaemia and brain tumours: a retrospective cohort study. *Lancet, 380*(9840), 499-505. doi:10.1016/S0140-6736(12)60815-0

Phillips, H. S., Kharbanda, S., Chen, R., Forrest, W. F., Soriano, R. H., Wu, T. D., . . . Aldape, K. (2006). Molecular subclasses of high-grade glioma predict prognosis, delineate a pattern of disease progression, and resemble stages in neurogenesis. *Cancer Cell, 9*(3), 157-173. doi:10.1016/j.ccr.2006.02.019

Pierce, A. J., Stark, J. M., Araujo, F. D., Moynahan, M. E., Berwick, M., & Jasin, M. (2001). Double-strand breaks and tumorigenesis. *Trends Cell Biol, 11*(11), S52-59. doi:S0962-8924(01)02149-3 [pii]

Prasad, G., & Haas-Kogan, D. A. (2009). Radiation-induced gliomas. *Expert Rev Neurother, 9*(10), 1511-1517. doi:10.1002/pmic.200800802

Preston, D. L., Shimizu, Y., Pierce, D. A., Suyama, A., & Mabuchi, K. (2003). Studies of mortality of atomic bomb survivors. Report 13: Solid cancer and noncancer disease mortality: 1950-1997. *Radiat Res, 160*(4), 381-407.

Quelle, D. E., Zindy, F., Ashmun, R. A., & Sherr, C. J. (1995). Alternative reading frames of the INK4a tumor suppressor gene encode two unrelated proteins capable of inducing cell cycle arrest. *Cell, 83*(6), 993-1000.

Raber, J., Marzulla, T., Stewart, B., Kronenberg, A., & Turker, M. S. (2015). (28)Silicon Irradiation Impairs Contextual Fear Memory in B6D2F1 Mice. *Radiat Res, 183*(6), 708-712.

Reifenberger, G., Wirsching, H.-G., Knobbe-Thomsen, C. B., & Weller, M. (2016). Advances in the molecular genetics of gliomas [mdash] implications for classification and therapy. *Nat Rev Clin Oncol, advance online publication*. doi:10.1038/nrclinonc.2016.204

Royds, J. A., & Iacopetta, B. (2006). p53 and disease: when the guardian angel fails. *Cell Death Differ, 13*(6), 1017-1026.

Sage, J. (2012). The retinoblastoma tumor suppressor and stem cell biology. *Genes Dev, 26*(13), 1409-1420. doi:10.1101/gad.193730.112

Salvati, M., D'Elia, A., Melone, G. A., Brogna, C., Frati, A., Raco, A., & Delfini, R. (2008). Radio-induced gliomas: 20-year experience and critical review of the pathology. *J Neurooncol, 89*(2), 169-177. doi:10.1007/s11060-008-9565-x

Santarius, T., Shipley, J., Brewer, D., Stratton, M. R., & Cooper, C. S. (2010). A census of amplified and overexpressed human cancer genes. *Nat Rev Cancer, 10*(1), 59-64. doi:10.1038/nrc2771

Schlessinger, J. (2000). Cell Signaling by Receptor Tyrosine Kinases. *Cell, 103*(2), 211-225. doi:https://doi.org/10.1016/S0092-8674(00)00114-8

Shamisa, A., Bance, M., Nag, S., Tator, C., Wong, S., Noren, G., & Guha, A. (2001). Glioblastoma multiforme occurring in a patient treated with gamma knife surgery. Case report and review of the literature. *J Neurosurg, 94*(5), 816-821. doi:10.3171/jns.2001.94.5.0816

Shchors, K., Persson, A. I., Rostker, F., Tihan, T., Lyubynska, N., Li, N., . . . Evan, G. I. (2013). Using a preclinical mouse model of high-grade astrocytoma to optimize p53 restoration therapy. *Proceedings of the National Academy of Sciences, 110*(16), E1480-E1489. doi:10.1073/pnas.1219142110

Sherr, C. J., & McCormick, F. (2002). The RB and p53 pathways in cancer. *Cancer Cell, 2*(2), 103-112.

Singh, D. K., Kollipara, R. K., Vemireddy, V., Yang, X. L., Sun, Y., Regmi, N., . . . Bachoo, R. M. (2017). Oncogenes Activate an Autonomous Transcriptional Regulatory Circuit That Drives Glioblastoma. *Cell Rep, 18*(4), 961-976. doi:10.1016/j.celrep.2016.12.064

Snuderl, M., Fazlollahi, L., Le, L. P., Nitta, M., Zhelyazkova, B. H., Davidson, C. J., . . . Iafrate, A. J. (2011). Mosaic amplification of multiple receptor tyrosine kinase genes in glioblastoma. *Cancer Cell, 20*(6), 810-817. doi:10.1016/j.ccr.2011.11.005

Sorlie, T., Perou, C. M., Tibshirani, R., Aas, T., Geisler, S., Johnsen, H., . . . Borresen-Dale, A. L. (2001). Gene expression patterns of breast carcinomas distinguish tumor subclasses with clinical implications. *Proc Natl Acad Sci U S A, 98*(19), 10869-10874. doi:10.1073/pnas.191367098

Steck, P. A., Pershouse, M. A., Jasser, S. A., Yung, W. K., Lin, H., Ligon, A. H., . . . Tavtigian, S. V. (1997). Identification of a candidate tumour suppressor gene, MMAC1, at chromosome 10q23.3 that is mutated in multiple advanced cancers. *Nat Genet, 15*(4), 356-362. doi:10.1038/ng0497-356

Stiles, C. D., & Rowitch, D. H. (2008). Glioma stem cells: a midterm exam. *Neuron, 58*(6), 832-846. doi:10.1016/j.neuron.2008.05.031

Stommel, J. M., Kimmelman, A. C., Ying, H., Nabioullin, R., Ponugoti, A. H., Wiedemeyer, R., . . . DePinho, R. A. (2007). Coactivation of receptor tyrosine kinases affects the response of tumor cells to targeted therapies. *Science, 318*(5848), 287-290. doi:10.1126/science.1142946

Stupp, R., Hegi, M. E., Mason, W. P., van den Bent, M. J., Taphoorn, M. J., Janzer, R. C., . . . National Cancer Institute of Canada Clinical Trials, G. (2009). Effects of radiotherapy with concomitant and adjuvant temozolomide versus radiotherapy alone on survival in glioblastoma in a randomised phase III study: 5-year analysis of the EORTC-NCIC trial. *Lancet Oncol, 10*(5), 459-466. doi:10.1016/S1470-2045(09)70025-7

Suva, M. L., Rheinbay, E., Gillespie, S. M., Patel, A. P., Wakimoto, H., Rabkin, S. D., . . . Bernstein, B. E. (2014). Reconstructing and reprogramming the tumor-propagating potential of glioblastoma stem-like cells. *Cell, 157*(3), 580-594. doi:10.1016/j.cell.2014.02.030

Szerlip, N. J., Pedraza, A., Chakravarty, D., Azim, M., McGuire, J., Fang, Y., . . . Brennan, C. W. (2012). Intratumoral heterogeneity of receptor tyrosine kinases EGFR and PDGFRA amplification in glioblastoma defines subpopulations with distinct growth factor response. *Proc Natl Acad Sci U S A, 109*(8), 3041-3046. doi:10.1073/pnas.1114033109

Tabocchini, M. A., Campa, A., & Dini, V. (2012). DNA and cellular effects of charged particles. *Health Phys, 103*(5), 547-555. doi:10.1097/HP.0b013e3182609a3e

Tada, M., Sawamura, Y., Abe, H., & Iggo, R. (1997). Homozygous p53 gene mutation in a radiation-induced glioblastoma 10 years after treatment for an intracranial germ cell tumor: case report. *Neurosurgery, 40*(2), 393-396.

Takahashi, K., & Yamanaka, S. (2006). Induction of pluripotent stem cells from mouse embryonic and adult fibroblast cultures by defined factors. *Cell, 126*(4), 663-676. doi:10.1016/j.cell.2006.07.024

Tamura, M., Gu, J., Matsumoto, K., Aota, S., Parsons, R., & Yamada, K. M. (1998). Inhibition of cell migration, spreading, and focal adhesions by tumor suppressor PTEN. *Science, 280*(5369), 1614-1617.

Trusolino, L., Bertotti, A., & Comoglio, P. M. (2010). MET signalling: principles and functions in development, organ regeneration and cancer. *Nat Rev Mol Cell Biol, 11*(12), 834-848. doi:10.1038/nrm3012

Verhaak, R. G., Hoadley, K. A., Purdom, E., Wang, V., Qi, Y., Wilkerson, M. D., . . . Cancer Genome Atlas Research, N. (2010). Integrated genomic analysis identifies clinically relevant subtypes of glioblastoma characterized by abnormalities in PDGFRA, IDH1, EGFR, and NF1. *Cancer Cell, 17*(1), 98-110. doi:10.1016/j.ccr.2009.12.020

Vitucci, M., Hayes, D. N., & Miller, C. R. (2011). Gene expression profiling of gliomas: merging genomic and histopathological classification for personalised therapy. *Br J Cancer, 104*(4), 545-553. doi:10.1038/sj.bjc.6606031

Wang, H., Wang, X., Zhang, P., & Wang, Y. (2008). The Ku-dependent non-homologous end-joining but not other repair pathway is inhibited by high linear energy transfer ionizing radiation. *DNA Repair (Amst), 7*(5), 725-733. doi:S1568-7864(08)00015-3 [pii]

10.1016/j.dnarep.2008.01.010

Wang, J., Cazzato, E., Ladewig, E., Frattini, V., Rosenbloom, D. I., Zairis, S., . . . Rabadan, R. (2016). Clonal evolution of glioblastoma under therapy. *Nat Genet, 48*(7), 768-776. doi:10.1038/ng.3590

Wang, X., Farris Iii, A. B., Wang, P., Zhang, X., Wang, H., & Wang, Y. (2015). Relative effectiveness at 1 gy after acute and fractionated exposures of heavy ions with different linear energy transfer for lung tumorigenesis. *Radiat Res, 183*(2), 233-239. doi:10.1667/RR13884.1

Wang, Y., Yang, J., Zheng, H., Tomasek, G. J., Zhang, P., McKeever, P. E., . . . Zhu, Y. (2009). Expression of mutant p53 proteins implicates a lineage relationship between neural stem cells and malignant astrocytic glioma in a murine model. *Cancer Cell, 15*(6), 514-526. doi:10.1016/j.ccr.2009.04.001

Ward, E., DeSantis, C., Robbins, A., Kohler, B., & Jemal, A. (2014). Childhood and adolescent cancer statistics, 2014. *CA Cancer J Clin, 64*(2), 83-103. doi:10.3322/caac.21219

Weil, M. M., Bedford, J. S., Bielefeldt-Ohmann, H., Ray, F. A., Genik, P. C., Ehrhart, E. J., . . . Ullrich, R. L. (2009). Incidence of acute myeloid leukemia and hepatocellular carcinoma in mice irradiated with 1 GeV/nucleon (56)Fe ions. *Radiat Res, 172*(2), 213-219. doi:10.1667/RR1648.1

Weil, M. M., Ray, F. A., Genik, P. C., Yu, Y., McCarthy, M., Fallgren, C. M., & Ullrich, R. L. (2014). Effects of 28Si ions, 56Fe ions, and protons on the induction of murine acute myeloid leukemia and hepatocellular carcinoma. *PLoS One, 9*(7), e104819. doi:10.1371/journal.pone.0104819

Weller, M., van den Bent, M., Hopkins, K., Tonn, J. C., Stupp, R., Falini, A., . . . Wick, W. (2014). EANO guideline for the diagnosis and treatment of anaplastic gliomas and glioblastoma. *The Lancet Oncology, 15*(9), e395-e403. doi:https://doi.org/10.1016/S1470-2045(14)70011-7

Wick, W., Weller, M., van den Bent, M., Sanson, M., Weiler, M., von Deimling, A., . . . Reifenberger, G. (2014). MGMT testing[mdash]the challenges for biomarker-based glioma treatment. *Nat Rev Neurol, 10*(7), 372-385. doi:10.1038/nrneurol.2014.100

Worby, C. A., & Dixon, J. E. (2014). Pten. *Annu Rev Biochem, 83*, 641-669. doi:10.1146/annurev-biochem-082411-113907

Wyman, C., & Kanaar, R. (2006). DNA double-strand break repair: all's well that ends well. *Annu Rev Genet, 40*, 363-383. doi:10.1146/annurev.genet.40.110405.090451

Yamanaka, R., Hayano, A., & Kanayama, T. (2016). Radiation-induced gliomas: a comprehensive review and meta-analysis. *Neurosurg Rev*. doi:10.1007/s10143-016-0786-8

Yan , H., Parsons , D. W., Jin , G., McLendon , R., Rasheed , B. A., Yuan , W., . . . Bigner , D. D. (2009). IDH1 and IDH2 Mutations in Gliomas. *New England Journal of Medicine, 360*(8), 765-773. doi:10.1056/NEJMoa0808710

Yang, S. Y., Wang, K. C., Cho, B. K., Kim, Y. Y., Lim, S. Y., Park, S. H., . . . Kim, S. K. (2005). Radiation-induced cerebellar glioblastoma at the site of a treated medulloblastoma: case report. *J Neurosurg, 102*(4 Suppl), 417-422. doi:10.3171/ped.2005.102.4.0417

Zeitlin, C., Hassler, D. M., Cucinotta, F. A., Ehresmann, B., Wimmer-Schweingruber, R. F., Brinza, D. E., . . . Reitz, G. (2013). Measurements of energetic particle radiation in transit to Mars on the Mars Science Laboratory. *Science, 340*(6136), 1080-1084. doi:10.1126/science.1235989

Zheng, H., Ying, H., Yan, H., Kimmelman, A. C., Hiller, D. J., Chen, A. J., . . . DePinho, R. A. (2008). p53 and Pten control neural and glioma stem/progenitor cell renewal and differentiation. *Nature, 455*(7216), 1129-1133. doi:10.1038/nature07443

Zhu, H., Acquaviva, J., Ramachandran, P., Boskovitz, A., Woolfenden, S., Pfannl, R., . . . Charest, A. (2009). Oncogenic EGFR signaling cooperates with loss of tumor

suppressor gene functions in gliomagenesis. *Proc Natl Acad Sci U S A, 106*(8), 2712-2716. doi:10.1073/pnas.0813314106

Zhu, Y., Guignard, F., Zhao, D., Liu, L., Burns, D. K., Mason, R. P., . . . Parada, L. F. (2005). Early inactivation of p53 tumor suppressor gene cooperating with NF1 loss induces malignant astrocytoma. *Cancer Cell, 8*(2), 119-130. doi:10.1016/j.ccr.2005.07.004

Zhuo, L., Theis, M., Alvarez-Maya, I., Brenner, M., Willecke, K., & Messing, A. (2001). hGFAP-cre transgenic mice for manipulation of glial and neuronal function in vivo. *Genesis, 31*(2), 85-94.